The Journal of Antibiotics (2009) 62, 55–61

www.nature.com/ja

ORIGINAL ARTICLE

Discovery of okilactomycin and congeners from *Streptomyces scabrisporus* by antisense differential sensitivity assay targeting ribosomal protein S4

Chaowei Zhang[1], John G Ondeyka[1], Deborah L Zink[1], Angela Basilio[2], Francisca Vicente[2], Oscar Salazar[2], Olga Genilloud[2], Karen Dorso[1], Mary Motyl[1], Kevin Byrne[1] and Sheo B Singh[1]

Protein synthesis inhibition is a highly successful target for developing clinically effective and safe antibiotics. There are several targets within the ribosomal machinery, and small ribosomal protein S4 (RPSD) is one of the newer targets. Screening of microbial extracts using antisense-sensitized *rpsD Staphylococcus aureus* strain led to isolation of okilactomycin and four new congeners from *Streptomyces scabrisporus*. The major compound, okilactomycin, was the most active, with a minimum detection concentration of 3–12 μg ml^{-1} against antisense assay, and showed an MIC of 4–16 μg ml^{-1} against Gram-positive bacteria, including *S. aureus*. The congeners were significantly less active in all assays, and all compounds showed a slight preferential inhibition of RNA synthesis over DNA and protein synthesis. Antisense technology, due to increased sensitivity, continues to yield new, even though weakly active, antibiotics.
The Journal of Antibiotics (2009) **62,** 55–61; doi:10.1038/ja.2008.8; published online 9 January 2009

Keywords: antisense; natural products; RNA synthesis inhibitors; rpsD

INTRODUCTION

Bacterial resistance to antibiotics continues to increase and is reaching alarming levels for certain organisms, including methicillin-resistant *Staphylococcus aureus* and *Pseudomonas aeruginosa*, and remains a serious threat to human lives.[1] The current clinically used antibiotics target fewer than 25 molecular targets, including a number of proteins of ribosomal targets in the protein synthesis machinery. Inhibition of protein synthesis is one of the most highly effective and proven antibacterial approaches.[2,3] Protein synthesis is catalyzed by a ribosome that is comprised of two asymmetric macromolecular units, the large (50S) and small (30S) subunits. The small subunit is composed of 16S rRNA and 21 r-proteins, S1–S21 (refs 4–6). Ribosomal proteins are known to help the ribosome to maintain its quaternary structure. Most of the clinically used drugs bind not only to rRNA but also to one or more ribosomal proteins, and the inhibition of protein synthesis is the composite result of disturbances due to both interactions. Alteration of rRNA binding to r-proteins inactivates protein synthesis. Therefore, selectively altering the conformation of a particular r-protein, or inhibiting the synthesis of an r-protein, would result in loss of function, and may lead to inhibition of the bacterial protein synthesis. Small ribosomal protein S4 (RPSD) is one of those proteins that seemed to be suitable targets for antibacterial discovery. It is encoded by the *rpsD* gene in both Gram-positive and Gram-negative bacteria, is conserved across bacterial species and is essential for bacterial growth.[7,8]

A *S. aureus*-based antisense two-plate whole-cell differential sensitivity screening assay was designed earlier and developed by us for the discovery of new antibiotics.[9,10] This assay was based on an antisense-sensitized *S. aureus* strain that targeted the *fabF/H* genes, leading to reduced expression and thus reduced production of FabF/H proteins.[9,10] This assay led to the discovery of platensimycin and platencin, two novel and potent inhibitors of FabF and FabF/H enzymes with *in vivo* antibiotic activities.[11–14] A similar two-plate assay, with reduced expression of the *rpsD* gene by antisense and hence reduced expression of the RPSD protein, was developed and used for screening of natural product extracts. This screening strategy led to the identification of lucensimycin A and B[15] from a strain of *Streptomyces lucensis* MA7349, coniothyrione from a fungal strain of *Coniothyrium cerealis* MF7209 (ref. 16), pleosporone from an unidentified ascomycete[17] and phaeosphenone from *Phaeosphaeria* sp.[18] Continued screening of microbial extracts led to the discovery of a *Streptomyces scabrisporus* strain that showed good activity in the two-plate screening assay. The acetone extract of the fermentation broth produced by the strain was subjected to bioassay-guided fractionation, leading to the isolation of okilactomycin (**1**) and four new compounds, named okilactomycin A (**2**), B (**3**), C (**4**) and D (**5**) (Figure 1). The isolation, structure elucidation and biological characterization of these compounds are reported herein.

[1]Merck Research Laboratories, Rahway, NJ, USA and [2]Centro de Investigación Básica (CIBE), Merck Sharp & Dohme de España, SA Josefa Valcárcel, Madrid, Spain
Correspondence: Dr SB Singh, Natural Products Chemistry, Merck Research Laboratories, Rahway, NJ 07065, USA.
E-mail: sheo_singh@merck.com
Received 30 September 2008; accepted 7 November 2008; published online 9 January 2009

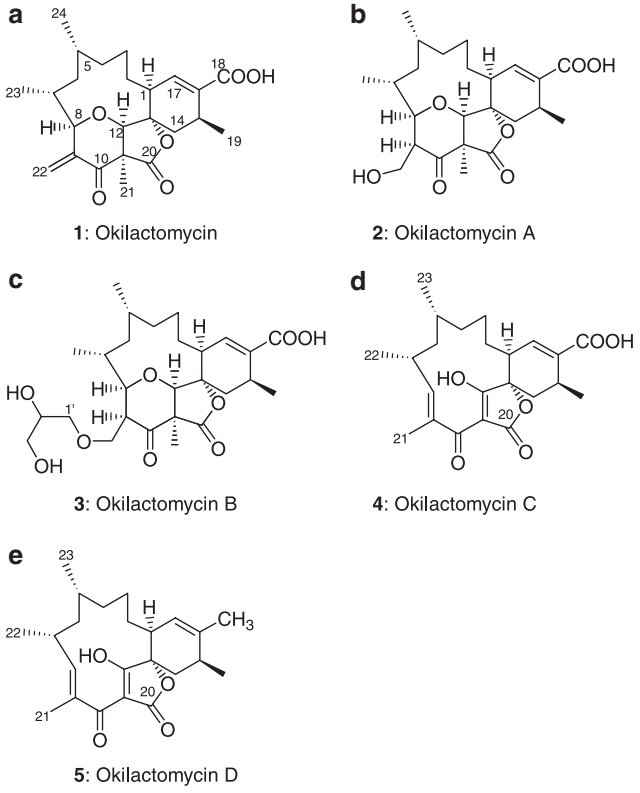

Figure 1 Chemical structures of okilactomycins. (**a**) Structure of okilactomycin, (**b**) structure of okilactomycin A, (**c**) structure of okilactomycin B, (**d**) structure of okilactomycin C and (**e**) structure of okilactomycin D.

RESULTS AND DISCUSSION

Fermentation and isolation

The producing organism was recovered from a soil sample collected in Costa Rica. The strain was characterized using morphological, chemotaxonomic and molecular identification (16S rDNA sequencing) methods, and was identified taxonomically as a new strain of *S. scabrisporus*. The strain was grown in millet, pharmamedia, glucose (MPG) liquid medium in a shake flask for 13 days.

The fermentation broth was extracted with equal volume of acetone, and the extract was concentrated to remove most of the acetone and chromatographed on Amberchrome polystyrene resin. The pooled biologically active fractions were chromatographed by reversed-phase HPLC to yield the known okilactomycin (**1**) (9.3 mg, 37.2 mg l^{-1}), and novel okilactomycins A (**2**) (5.7 mg, 15.2 mg l^{-1}), B (**3**) (0.8 mg, 2.1 mg l^{-1}), C (**4**) (4.2 mg, 11.2 mg l^{-1}) and D (**5**) (0.6 mg, 0.6 mg l^{-1}).

Structure elucidation

Compound **1** exhibited a molecular weight of 416 atomic mass units (amu), with the molecular formula $C_{24}H_{32}O_6$ (high resolution electrospray ionization fourier transform mass spectrometry (HRESIFTMS)), and was identified as okilactomycin by comparing with spectroscopic data (^{1}H, ^{13}C NMR and HRMS) and chiroptical properties ($[\alpha]^{23}_D$=+30.0 *c* 0.5, MeOH; Lit $[\alpha]_D$=+34). This was confirmed by full NMR shift assignment by 2D NMR.[19] This structure was originally determined by X-ray crystallographic studies and was recently confirmed by asymmetric total synthesis of the unnatural opposite enantiomer.[20] Okilactomycin exhibits modest antitumor activity and Gram-positive antibacterial activity.[21]

HRESIFTMS (*m/z* 435.2384 $[M+H]^+$) of okilactomycin A (**2**) suggested a molecular formula of $C_{24}H_{34}O_7$, indicating 8 degrees of unsaturation. The molecular weight comparison of compound **2** with **1** suggested that **2** contained 18 additional atomic mass units. The UV spectrum showed absorption maxima at λ_{max} 212 nm. The IR spectrum displayed absorption bands for three carbonyls, including a five-membered lactone (1778, 1695 and 1643 cm^{-1}) and an OH group (3405 cm^{-1}). The ^{13}C NMR spectra (Table 1) showed 24 carbon resonances, which confirmed the molecular formula. DEPT experiments displayed 18 signals, including four methyl groups, six methylenes and eight methines, indicating the presence of two exchangeable protons. The presence of five sp^2 carbons, including one proton-bearing carbon, two acid/ester/lactone-type carbonyls (δ_C 168.2 and δ_C 172.0) and a ketone at δ 206.0 further corroborated the okilactomycin skeleton. The key heteronuclear multiple bond correlations (HMBC) of H-8 (δ_H 3.99) to C-12 (δ_C 84.7); H-12 (δ_H 4.68) to C-1 (δ_C 42.8), C-10 (δ_C 206.0), C-13 (δ_C 85.4) and C-14 (δ_C 34.6); H-17 (δ_H 6.76) to C-13; and H-21 (δ_H 1.72) to C-10, C-11 (δ_C 54.5), C-12 and C-20 (δ_C 172.0) confirmed the okilactomycin skeleton. The only difference between okilactomycin (**1**) and compound **2** is at C-9 and C-22. Compound **2** showed the presence of a hydroxy methylene, which replaced the exocyclic olefin of **1**. The assignment was confirmed by the presence of a pair of doublet of doublets at δ_H 4.02 and δ_H 4.10 (H_2-22) in the ^{1}H NMR spectrum of (**2**), which correlated to δ_C 59.8 and the absence of olefinic methylene resonances (δ_H 5.75 and 6.37) of **1** and ^{13}C resonance at δ_C 121.9. COSY and TOCSY (TOtal Correlation SpectroscopY) correlations confirmed the presence of a methine at C-9 and its correlation to the hydroxy methylene group at C-22. This was further confirmed by HMBC correlation of H-22 to C-10. The relative configuration was determined by measuring the vicinal coupling constants and NOESY correlations. The NOESY correlations of H-8 to H-9, H-12, H-21 and H-23; H-12 to H-1, H-2 (δ_H 1.63) and H-21; and H-9 to H-21 indicated that they were present on the same α-face of the molecule. The NOESY correlations of H-7 to H-5 and H-22 indicated that they were present on the opposite face of the molecule. The NOESY correlations of pseudo-axial H-14α (δ_H 1.82) to H-3β (δ_H 1.62) confirmed the configuration at the spiro center, C-13. H-14α also showed a large coupling (*J*=10.6 Hz) with H-15, indicating a diaxial coupling and thus placing the C-19 methyl group at the pseudo-equatorial orientation in the pseudo-chair conformation of the spiro-fused cyclohexene ring. On the basis of these data, structure **2** was assigned for okilactomycin A (**2**).

Okilactomycin B (**3**) was assigned a molecular formula of $C_{27}H_{40}O_9$ by HRESIFTMS (*m/z* 509.2750, $[M+H]^+$). The ^{1}H and ^{13}C NMR spectral data of compounds **2** and **3** were nearly identical. The molecular formula of **3** suggested the presence of an additional $C_3H_6O_2$ unit. The ^{13}C NMR spectrum of **3** showed three extra oxygenated carbon signals, including two methylenes at δ_C 64.7 and δ_C 73.5, and one methine at δ_C 71.3, indicative of a glycerol unit, which was confirmed by an HMBC correlation of H-1′ to C-22. The negative ion ESIMS showed a major ion at *m/z* 415 (M-glycerol). Thus, the glycerol ether structure **3** was assigned for okilactomycin B (**3**).

The molecular formula $C_{23}H_{30}O_6$ was assigned for okilactomycin C (**4**) by HRESIFTMS (*m/z* 403.2126, $[M+H]^+$) analysis, indicating 9 degrees of unsaturation. Comparisons of ^{1}H and ^{13}C NMR spectra of compound **4** with those of **1–3** indicated that all of them belong to the same family. The UV spectrum showed absorption maxima at λ_{max} 210, 235 and 274 nm, indicating a different conjugation pattern compared with the others in the series. The IR spectrum showed

absorption bands characteristic of conjugated ketones (ν_{max}=1700 and 1631 cm^{-1}). The ^{13}C NMR spectrum (Table 2) displayed 23 carbon signals, including four methyl groups, five methylenes and six methines, indicating the presence of two exchangeable protons. The presence of nine sp^2 carbons, including two proton-bearing carbons, two downfield conjugated carbonyls (δ_C 194.2 and 196.1) and two carboxy-type carbonyls (δ_C 170.6, 173.9), and the lack of the signals for oxygenated methines indicated that the pyranone ring was no longer present and was opened in **4**. This supposition was supported by the presence of an olefinic methine δ_H 6.21 (H-8) and an olefinic methyl group at δ_H 1.84 (H_3-21). These were assigned to C-8 and C-21, respectively, by HMBC correlations of H-8 to C-6 (δ_C 47.2), C-10 (δ_C 196.1) and C-21 (δ_C 12.2), and H_3-21 to C-8, C-9 and C-10. The open pyranone α,α-diketo-lactone ring was confirmed by the key HMBC correlations of H-14α (δ_C1.89) to C-1 (δ_C 46.8), C-12 (δ_C 194.2), C-13 (δ_C 85.8) and C-16 (δ_C 134.8). The relative configuration of **4** was identical to that of **1**–**3** as determined by NOESY and vicinal *J*-values. As for compound **2**, H-14α (δ_H 1.76) showed a large coupling (*J*=10.5 Hz) with H-15, whereas H-14β (δ_H 1.89) showed a small coupling (*J*=2.0 Hz) with H-1 (δ_H 2.24) through W-type coupling, suggesting that H-15 was axially oriented in a pseudo-chair conformation. These data helped to establish structure **4** for okilactomycin C (**4**).

Okilactomycin D was assigned a molecular formula of (**5**) $C_{23}H_{32}O_4$ by HRESIFTMS (*m/z* 373.2377 $[M+H]^+$). The ^1H and ^{13}C NMR spectral data of compounds **4** and **5** were nearly identical. The absence of a carbonyl carbon at δ_C 170.6 and the presence of a methyl group at δ_H 1.72 (δ_C 21.2) indicated differences between the two compounds. The proton and carbon chemical shifts of C-17 shifted significantly upfield due to the absence of conjugation. The key HMBC correlations of H-17 to C-18; and H_3-18 to C-15, C-16 and C-17 confirmed structure **5** for okilactomycin D.

Biological activities

All five compounds were first evaluated in the *S. aureus* antisense *rpsD*-sensitized two-plate differential sensitivity assay. Okilactomycin showed the most potent activity in this assay and displayed a 20-mm zone of clearance at 62 μg ml^{-1} on the antisense plate and 13 mm on the control plate. The zone of clearance was concentration dependent and was measured by twofold dilution. At 12.5, 6.25 and 3.13 μg ml^{-1}, compound **1** showed 15, 13 and 11 mm zones of clearance on the antisense plate but no activity on the control plate. This indicated

Table 1 ^1H (500 MHz) and ^{13}C (125 MHz) NMR assignment of okilactomycins A (2) and B (3) in acetone-d_6

	2			**3**		
No.	δ_H *(mult., J in Hz)*	δ_C	*HMBC (H→C)*	δ_H *(mult., J in Hz)*	δ_C	*HMBC (H→C)*
1	2.40, brdd, 6.1, 10	42.8	C-2, 3, 13, 16, 17	2.37, brdd, 6.5, 10	42.9	
2	1.39, dd, 4.2, 10	33.0		1.37, brdd, 3.6, 10	33.1	
	1.63, m			1.60, m		
3	1.62, m	24.4		1.62, m	24.4	
	1.79, brd, 13.9			1.76, m		
4	1.08, brd, 13.5	38.4		1.04, brd, 13.5	38.4	
	1.21, dddd, 2.0, 4.7, 11.8, 13.7			1.19, brdd, 10.8, 13.5		
5	1.95, m	31.1		1.96, m	30.9	
6	0.96, dd, 7.1, 14.2	45.8		0.94, m	45.9	
	1.55, dd, 9.2, 14.2			1.53, dd, 9.6, 14.4		
7	2.10, ddq, 9.0, 10, 6.6	34.7		2.02, m	34.5	
8	3.99, dd, 4.1, 10	85.1	C-6, 7, 12, 22, 23	3.97, dd, 5.1, 10.3	84.9	C-6, 7, 12, 22
9	2.95, ddd, 3.7, 4.1, 5.5	52.7	C-10, 22	3.03, dt, 2.8, 4.4	50.7	
10		206.0			205.8	
11		54.5			54.4	
12	4.68, s	84.7	C-1, 10, 11, 13, 14, 21	4.64, s	84.9	C-1, 10, 13, 14, 21
13		85.4			85.6	
14	1.44, ddd, 2.0, 6.4, 14.9	34.6		1.42, ddd, 2.2, 6.7, 15	34.7	
	1.82, dd, 10.6, 14.9			1.77, dd, 10.6, 15		
15	2.58, ddq, 1.6, 10.5, 6.8	28.2		2.58, ddq, 1.8, 10.7, 6.9	28.3	
16		134.5			134.6	
17	6.76, dd, 2.0, 6.0	140.1	C-1, 2, 13, 15, 16, 18	6.72, dd, 2.1, 6.0	140.1	C-1, 13, 15, 16, 18
18		168.2			168.2	
19	1.09, d, 7.1	20.4	C-14, 15, 16	1.11, d, 6.6	20.5	C-14, 15, 16
20		172.0			172.1	
21	1.72, s	24.9	C-10, 11, 12, 20	1.70, s	24.8	C-10, 11, 12, 20
22	4.02, dd, 3.7, 11.2	59.8	C-8, 9, 10	3.79, dd, 2.7, 9.6	68.5	
	4.10, dd, 5.5, 11.1			4.06, dd, 5.1, 10.0		
23	0.97, d, 7.1	19.0	C-6, 7, 8	0.95, d, 6.6	19.2	C-6, 7, 8
24	0.88, d, 7.1	24.0	C-4, 5, 6	0.89, d, 6.6	23.9	C-4, 5, 6
1′				3.46, d, 5.7	73.5	C-22, 2′, 3′
2′				3.77, m	71.3	
3′				3.53, m	64.7	
				3.64, dd, 4.5, 10.9		

Table 2 ^{1}H (500 MHz) and ^{13}C (125 MHz) NMR assignment of okilactomycins C (4) and D (5) in CD_3OD

	4			5		
No.	δ_H *(mult., J in Hz)*	δ_C	*HMBC (H→C)*	δ_H *(mult., J in Hz)*	δ_C	*HMBC (H→C)*
1	2.24, brdd, 5.6, 7.9	46.8		2.02, m	47.3	C-2
2	1.14, m	28.9	C-1, 3, 4, 13, 17	1.12, m	30.0	C-1, 3, 4, 13, 17
	2.39, m			2.21, m		
3	1.39, m	26.1		1.37, m	25.6	
	1.75, m			1.73, m		
4	1.14, m	37.0		1.18, m	36.8	
	1.37, m			1.36, m		
5	1.51, m	29.4	C-3, 4, 6, 7, 23	1.45, m	29.8	C-3, 4, 6, 7, 23
6	1.20, m	47.2		1.22, m	46.4	C-4, 5, 7, 8, 23
	1.34, m			1.38, m		
7	2.59, m	33.2		2.64, m	33.1	
8	6.21, d, 7.3	151.0	C-6, 7, 10, 21	6.38, dd, 1.2, 7.5	154.3	C-6, 7, 9, 10, 21, 22
9		140.0			140.1	
10		196.1			194.3	
11		101.3			101.2	
12		194.2			187.3	
13		85.8			87.3	
14	1.76, dd, 10.5, 14.5	35.1	C-1, 12, 13, 15, 16, 22	1.73, dd, 10.4, 14.2	35.3	C-1, 12, 13, 15, 16, 19
	1.89, ddd, 2.0, 6.0, 14.5			1.80, ddd, 1.6, 5.9, 13.8		
15	2.77, ddh, 1.8, 10.5, 6.7	28.7		2.38, dq, 10.7, 6.7	32.1	
16		134.8			136.9	
17	6.94, dd, 1.8, 5.5	140.6	C-1, 13, 15, 16, 18	5.57, td, 1.5, 5.0	125.0	C-1, 13, 15, 18
18		170.6		1.72, d, 1.2	21.2	C-15, 16, 17
19	1.18, d, 6.8	20.5	C-14, 15, 16	1.10, d, 7.0	19.4	C-14, 15, 16
20		173.9			172.1	
21	1.84, s	12.2	C-8, 9, 10	1.86, d, 1.1	11.8	C-8, 9, 10
22	0.98, d, 6.8	20.5	C-6, 7, 8	1.01, d, 7.0	20.2	C-6, 7, 8
23	0.88, d, 6.8	21.0	C-4, 5, 6	0.89, d, 6.8	20.9	C-4, 5, 6

a minimum detection concentration (MDC) of 3–12.5 $\mu g\,ml^{-1}$. Okilactomycins A–D were less active than okilactomycin. Of these four, okilactomycin A (**2**) showed the best activity with an MDC of 31–62 $\mu g\,ml^{-1}$. Okilactomycins B (**3**), C (**4**) and D (**5**) showed MDC values of 250, 250 and 500 $\mu g\,ml^{-1}$, respectively.

The most potent compound okilactomycin (**1**) exhibited an MIC of 8–16 $\mu g\,ml^{-1}$ against *S. aureus* (Table 3). Compound **1** inhibited growth of *Streptococcus pneumoniae* (MIC of 8–16 $\mu g\,ml^{-1}$), *Enterococcus faecalis* (MIC of 16 $\mu g\,ml^{-1}$) and *Bacillus subtilis* (MIC of 4–16 $\mu g\,ml^{-1}$). MIC data observed in this study are consistent with that reported earlier.[21] Compound **1** did not show activity against Gram-negative bacteria, but did inhibit growth of the *Escherichia coli* (envA/tolC) strain, which harbors mutated membrane and efflux pump, and showed an MIC of 64 $\mu g\,ml^{-1}$. The other four compounds were significantly less active in this assay with only **5** showing a weak activity against *S. pneumoniae* and also *E. coli*. No clear conclusion about SAR could be drawn due to weak activity.

Mechanistically, compounds **1**, **2** and **4** showed preferential inhibition of RNA synthesis compared with DNA and protein synthesis (Figure 2a). These data are similar to the data observed for two other RPSD active compounds, pleosporone and phaeosphenone, identified by this assay. The other two compounds (**3** and **5**) showed $<50\%$ inhibition at 100 $\mu g\,ml^{-1}$ (data not shown). This phenomenon requires further study to determine why RPSD-selective compounds in the antisense assay tend to selectively inhibit RNA synthesis rather than protein synthesis.

In conclusion, antisense screening method continue to aid the discovery of novel antibiotics, even though with weak activity, as illustrated by the discovery of okilactomycin and its new congeners, okilactomycins A–D (**2**–**5**). The most abundant compound **1** remains the most active compounds in this family.

EXPERIMENTAL PROCEDURE

General experimental procedures

An Agilent HP1100 was used for analytical HPLC. Optical rotations were measured on a Perkin-Elmer 241 (Waltham, MA, USA) Polarimeter. UV spectra were recorded in MeOH on a Beckman (Fullerton, CA, USA) DU-70 Spectrophotometer. IR spectra were recorded on a Perkin-Elmer Spectrum One spectrometer. High resolution electrospray inonization mass spectrum (HRESIMS) were obtained on a Thermo Quest (Boston, MA, USA) FTMS spectrometer using electrospray ionization. The NMR spectra were recorded on a Varian (Palo Alto, CA, USA) INOVA 500 FT-NMR spectrometer at 500 MHz for ^{1}H and 125 MHz for ^{13}C in acetone-d_6 (δ_H 2.05, δ_C 29.92) and CD_3OD (δ_H 3.31, δ_C 49.15).

Microbial isolation conditions

The strain F-117,187 was isolated from soil collected in Costa Rica, at the INBio Biodiversity Garden, from a coffee tree plantation area. This soil was air dried and suspended in sterile water. The soil suspension was serially diluted, plated on selective isolation media and incubated at 28 °C for at least 6 weeks. The strain was isolated from an NZ-amine-based agar medium containing nalidixic acid (20 $\mu g\,ml^{-1}$). The colony was purified on Yeast Extract Malt Extract Glucose medium (ISP2) and preserved as frozen agar plugs in 10% glycerol.

Table 3 Antibacterial activities (MIC, μg ml^{-1})[a] of okilactomycins (1–5)

Strains[b]	*Phenotype*	*Strain no.*	***1***[c]	***2***[c]	***3***[c]	***4a***[c]	***4b***[c]
Staphylococcus aureus	meth^S	ATCC 29213	8	>64	>64	>64	>64
S. aureus	meth^S	MB2865	16 (8)	>64	>64	>64	>64
S. aureus (+50% human serum)	meth^S	MB2865	>64	>64	>64	>64	>64
Streptococcus pneumoniae[d]	pen^S, quin^S, mac^S	CL2883	16 (8)	>64	>64	>64	>64 (64)
S. pneumoniae[e]	pen^S, quin^S, mac^S	CL2883	NT	>64	>64	>64	>64 (32)
Enterococcus faecalis	van^S, mac^R	CL8516	16	>64	>64	>64	>64
Bacillus subtilis	Wt	MB964	16 (4)	>64	>64	>64	>64
Haemophilus influenzae	Amp^S, quin^S, mac^S	MB4572	>64	>64	>64	>64	>64
Escherichia coli	Wt	MB2884	>64	>64	>64	>64	>64 (32)
E. coli envA/tolC	Wt	MB5746	64	>64	>64	>64	>64
Candida albicans	Wt	MY1055	>64	>64	>64	>64	>64

Abbreviations: CAMHB, cation-adjusted Mueller–Hinton broth; MIC_{80}, MIC that inhibits 80% growth; NCCLS, National Committee for Clinical laboratory Standards.
[a]MIC, the numbers in parentheses show the concentration of compound that inhibit 80% of cell growth.
[b]All strains were tested in CAMHB medium, unless mentioned otherwise, under the NCCLS guidelines.
[c]The data in parentheses are MIC_{80}.
[d]CAMHB +2.5% lysed horse blood medium.
[e]Isosensitest medium.

Characterization of the *S. scabrisporus* strain

Sporulating characters were observed upon growth of the strain on different selective media after 21 days incubation at 28 °C. The strain grows abundantly with extensive development of a gray to grayish brown aerial mycelium on media ISP2, ISP3, ISP5 and ISP7. It exhibited sparse growth and poor aerial development on medium ISP4. Microscopically, the strain produced long chains of spores as open coils or as loops formed at the end of the aerial hyphae. Good sporulation was observed on media ISP2, ISP3, ISP4 and ISP7 but no spore chains were formed on ISP5. This macro- and micromorphology are characteristic of members of the family *Streptomycetaceae*. Whole-cell major fatty acids were branched components iso-$C_{16:0}$ (29%), iso-$C_{16:1}$H (10%), unsaturated components $C_{16:1}$ ω7c (15%) and anteiso-$C_{15:0}$ (3.9%). The strain is characterized by good growth on glucose and rhamnose as the sole carbon source and exhibits limited growth on fructose, xylose, raffinose and inositol. No growth was observed on arabinose, cellulose, saccharose or mannitol.

16S rDNA sequencing and phylogenetic analysis

Total genomic DNA from the producing strain was isolated and purified using the MasterPure Gram-Positive DNA Purification Kit (Epicentre Biotechnologies, Madison, WI, USA). PCR primers fD1 and rP2[22] were used for amplifying the 16S rRNA genes of the strain. The 1500 bp PCR products were purified and used as a template in sequencing reactions using the primers fD1 and rP2,[22] and 1100R and 926F.[23] Amplified DNA fragments were sequenced using the ABI PRISM$_{DYE}$ Terminator Cycle sequencing Kit and fragments were resolved using the ABI3130 genetic analyzer (Applied Biosystems, Foster City, CA, USA). Partial sequences were assembled using the contig editor component of GeneStudio Professional sequence analysis software (GeneStudio Inc., Suwanee, GA, USA). Almost complete 16S rDNA sequence was aligned with representative sequences of *Streptomyces* and related species as identified with BLAST searches. The phylogenetic analysis, based on the Neighbor-Joining method using matrix pairwise comparisons of sequences corrected with Jukes and Cantor algorithm,[24,25] shows that the strain is closely related to the strain type *S. scabrisporus* NBRC 100760^T. The strains share 100% sequence identity and this relatedness is well supported in the analysis by the bootstrap value (100%). All data suggest that strain F-117,187 can be identified as a new member of the species *S. scabrisporus*.

Production conditions

A seed culture of the strain was prepared by inoculation from a frozen vial containing agar plugs in a 50-ml Environmental Protection Agency (EPA) tube containing 10 ml of seed medium (in g l^{-1}: soluble starch 20.0, dextrose 10.0, NZ amine type E 5.0, Difco Beef extract 3.0, Difco Bacto Peptone 5.0, Difco yeast extract 5.0 and $CaCO_3$ 1.0). After 3 days of incubation at 28 °C, 0.5 ml of the inoculum was transferred to 50 ml EPA tubes containing 10 ml of production medium MPG (in g l^{-1}: glucose 10.0, ground millet 20.0, Pharmamedia 20.0 and MOPS 20.0), and the cultures were incubated at 28 °C with 220 r.p.m. agitation and 70% humidity for 13 days. Production in flasks was obtained transferring 2.5 ml of the inoculum from EPA tube to a 250-ml flask containing 50 ml of the same production medium, and the culture was incubated at 28 °C for 13 days in a rotary shaker at 220 r.p.m. and 70% humidity.

Extraction and isolation

A total of 40 flasks were harvested, pooled (~1 l) and extracted with 1 l acetone by shaking on a platform shaker for 60 min. The acetone extract was concentrated under reduced pressure to remove most of the acetone leaving behind mostly aqueous solution (~1 l), which was fractionated on an Amberchrome column, and eluted with a 100-min linear gradient of aqueous MeOH at a flow rate of 10 ml min^{-1}. These fractions were tested for their biological activity in the antisense *rpsD* two-plate assay. The fractions eluted with 52, 64, 78 and 90% aqueous MeOH possessed all of the biological activities.

A 25% aliquot of the Amberchrome fractions eluted with 78% aqueous MeOH was chromatographed by reversed-phase HPLC using an Atlantis C_{18} (10×250 mm) column that was eluted with a 40-min gradient of 20–95% aqueous CH_3CN containing 0.1% TFA at a flow rate of 5 ml min^{-1}. The fraction eluting at 28 min showed activity and was lyophilized to yield 9.3 mg (37.2 mg l^{-1}) of okilactomycin (**1**) as an amorphous powder.

A similar 25% aliquot of the Amberchrome fraction eluted with 64% aqueous MeOH was fractionated by reversed-phase HPLC using a Zorbax C_8 (21.2×250 mm) column that was eluted with a 40-min gradient of 40–50% aqueous CH_3CN containing 0.1% TFA at a flow rate of 10 ml min^{-1}. Lyophilization of the active fractions eluting at 20 and 33 min yielded 0.8 mg (2.1 mg l^{-1}) and 5.7 mg (15.2 mg l^{-1}) of okilactomycins B (**3**) and A (**2**), respectively, as colorless gums.

Similarly, 25% aliquot of the Amberchrome fraction eluted at 52% aqueous MeOH was further chromatographed on Zorbax C_8 (21.2×250 mm) column that was eluted with a 40-min gradient of 10–55% aqueous CH_3CN containing 0.1% TFA at a flow rate of 10 ml min^{-1}. Fractions eluting at 38 min showed activity and was lyophilized to furnish 4.2 mg (11.2 mg l^{-1}) of okilactomycin C (**4**) as a colorless gum.

Reversed-phase HPLC of the Amberchrome fraction eluted with 90% aqueous MeOH using Zorbax C_8 (21.2×250 mm) column and eluted for 40 min with 45% aqueous CH_3CN containing 0.1% TFA followed by a 10-min gradient of 45–95% aqueous CH_3CN at a flow rate of 10 ml min^{-1}, and lyophilization of the active fraction eluting at 69 min yielded 0.6 mg (0.6 mg l^{-1}) of okilactomycin D (**5**) as a colorless gum.

Okilactomycin A (**2**): $[\alpha]^{23}_D$ −20 (ca. 0.1, CH_3OH), UV (CH_3OH) λ_{max} 212(ε 10 234) nm; IR (ZnSe) ν_{max} 3405, 2952, 1778, 1694, 1643, 1457, 1385,

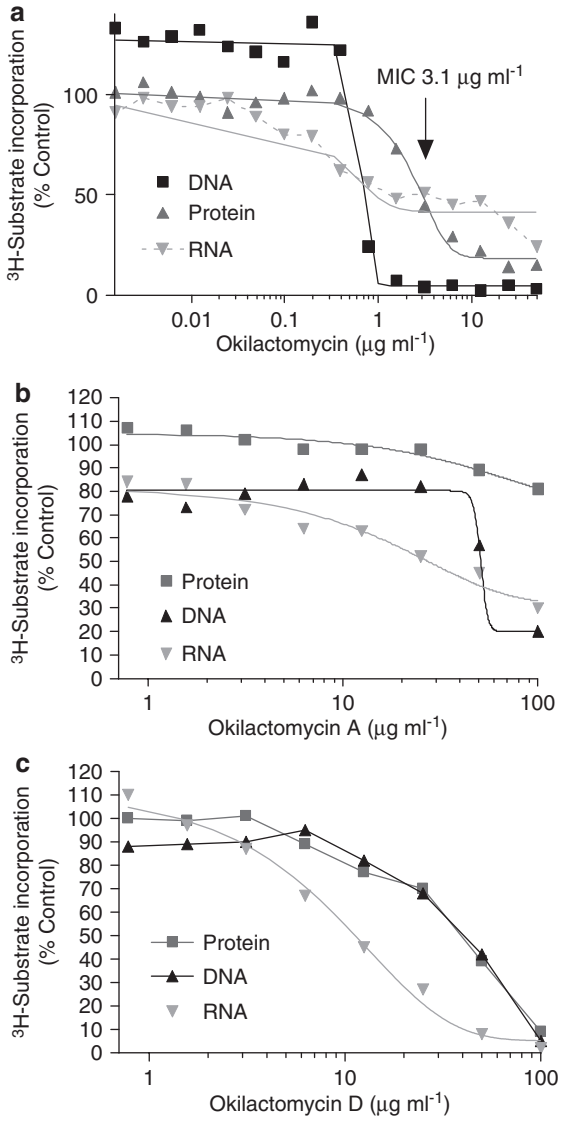

Figure 2 Macromolecular synthesis inhibition by okilactomycins (**1**, **2**, **4**). (**a**) Inhibition by okilactomycin (**1**), (**b**) inhibition by okilactomycin A (**2**) and (**c**) inhibition by okilactomycin D (**4**). Okilactomycins B and C showed <50% inhibition of DNA, protein and RNA at 100 μg ml^{-1}, therefore the data are not shown.

1261, 1233, 1189, 1138, 1113, 1068, 1024, 982, 965, 801, 776 and 723 cm^{-1}; ^{1}H and ^{13}C NMR data, see Table 1; HRESI-FTMS *m/z* 435.23839 (calcd for $C_{24}H_{34}O_7$+H: 435.23826).

Okilactomycin B (**3**): $[\alpha]^{23}_{D}$ −20 (ca. 0.1, CH_3OH); UV (CH_3OH) λ_{max} 212(ε 6147) nm; IR (ZnSe) ν_{max} 3419, 2952, 1779, 1700, 1642, 1456, 1261, 1187, 1138, 1112, 1079, 1039, 1004, 962 and 687 cm^{-1}; ^{1}H and ^{13}C NMR data, see Table 1; HRESI-FTMS *m/z* 509.27497 (calcd for $C_{27}H_{40}O_9$+H: 509.27503).

Okilactomycin C (**4**): $[\alpha]^{23}_{D}$ −30 (ca. 0.1, CH_3OH); UV (CH_3OH) λ_{max} 210(ε 11 328) 235(ε 8281) 274(ε 5797) nm; IR (ZnSe) ν_{max} 2952, 2927, 1700, 1631, 1454, 1258, 1134, 1025 and 988 cm^{-1}; ^{1}H and ^{13}C NMR data, see Table 2; HRESI-FTMS *m/z* 403.2126 (calcd for $C_{23}H_{30}O_6$+H: 403.2120).

Okilactomycin D (**5**): $[\alpha]^{23}_{D}$ −50 (ca. 0.1, CH_3OH); UV (CH_3OH) λ_{max} 204(ε 9940) 236(ε 8824) 270(ε 8295) nm; IR (ZnSe) ν_{max} 3421, 2928, 2868, 1688, 1621, 1594, 1456, 1377, 1205, 1136, 1003 and 968 cm^{-1}; ^{1}H and ^{13}C NMR data, see Table 2; HRESI-FTMS *m/z* 373.2377 (calcd for $C_{23}H_{32}O_4$+H: 373.2378).

Two-plate differential sensitivity RPSD assay

S. aureus cells (RN450) carrying either plasmid S1-782B bearing antisense to RPSD (*rpsD* AS-RNA strain) or empty vector (control strain) were inoculated from a frozen vial source into a 13-mm disposable tissue culture tube containing 3 ml of Miller's LB Broth (Invitrogen, Carlsbad, CA, USA) and 34 μg ml^{-1} of chloramphenicol. Tubes were incubated at 37 °C with shaking at 220 r.p.m. for 18–20 h and kept at room temperature until use. Each culture was diluted (1:1000) to a final optical density at 600 nm (OD_{600}) of 0.003 absorption unit (AU) into a flask containing Miller's LB broth medium supplemented with 1.2% Select agar (Invitrogen, autoclaved and cooled to 48 °C), 0.2% glucose, 15 μg ml^{-1} chloramphenicol and 12 mM of xylose (added for the antisense strain only). Two-assay plates, one seeded with the *rps*D AS-RNA strain and the second with the control strain, were prepared by pouring 100 ml of each of the above mixtures into a 20×20 cm (NUNC) assay plate. Well-caster templates were placed into the agar, which was allowed to solidify at room temperature for 30 min. Then, 20 μl of test samples were added to the wells and the plates incubated at 37 °C for 18 h and zones of inhibition measured. MDC values were determined by two-fold serial dilution.

Antibiotic assay (MIC)

MIC against each of the strains was determined using National Committee for Clinical Laboratory Standards (NCCLS)—now called National Laboratory Standard Institute (NLSI)—guidelines as described earlier.[26] Cells were inoculated at 10^5 colony-forming units per milliliter followed by incubation at 37 °C with a twofold serial dilution of compounds in the growth medium for 20 h. MIC is defined as the lowest concentration of an antibiotic inhibiting visible growth.

Macromolecular synthesis inhibition

The assay was performed as described earlier.[11,27] Briefly, mid-log (OD_{600}=0.5–0.6, AU) *S. aureus* growth was incubated at an increasing concentration of each inhibitor at 37 °C for 20 min with 1 μCi ml^{-1} 6-[^{3}H]-thymidine, 1 μCi ml^{-1} 5,6-[^{3}H]uracil or 5 μCi ml^{-1} 4,5-[^{3}H]leucine to measure DNA, RNA and protein synthesis, respectively. The reaction was stopped by the addition of 10% trichloroacetic acid and the cells were harvested using a glass fiber filter (Perkin-Elmer Life Sciences, 1205-401). The filter was dried and counted with scintillation fluid.

1 Klevens, R. M. *et al.* Invasive methicillin-resistant *Staphylococcus aureus* infections in the United States. *J. Am. Med. Assoc.* **298,** 1763–1771 (2007).
2 Poehlsgaard, J. & Douthwaite, S. The bacterial ribosome as a target for antibiotics. *Nat. Rev. Microbiol.* **3,** 870–881 (2005).
3 Singh, S. B. & Barrett, J. F. Empirical antibacterial drug discovery—foundation in natural products. *Biochem. Pharmacol.* **71,** 1006–1015 (2006).
4 Ramakrishnan, V. Ribosome structure and the mechanism of translation. *Cell* **108,** 557–572 (2002).
5 Culver, G. M. Assembly of the 30S ribosomal subunit. *Biopolymers* **68,** 234–249 (2003).
6 Ogle, J. M., Carter, A. P. & Ramakrishnan, V. Insights into the decoding mechanism from recent ribosome structures. *Trends Biochem. Sci.* **28,** 259–266 (2003).
7 Grundy, F. J. & Henkin, T. M The rpsD gene, encoding ribosomal protein S4, is autogenously regulated in *Bacillus subtilis*. *J. Bacteriol.* **173,** 4595–4602 (1991).
8 Forsyth, R. A. *et al.* A genome-wide strategy for the identification of essential genes in *Staphylococcus aureus*. *Mol. Microbiol.* **43,** 1387–1400 (2002).
9 Young, K. *et al.* Discovery of FabH/FabF inhibitors from natural products. *Antimicrob. Agents Chemother.* **50,** 519–526 (2006).
10 Singh, S. B., Phillips, J. W. & Wang, J. Highly sensitive target based whole cell antibacterial discovery strategy by antisense RNA silencing. *Curr. Opin. Drug Discov. Devel.* **10,** 160–166 (2007).
11 Wang, J. *et al.* Platensimycin is a selective FabF inhibitor with potent antibiotic properties. *Nature* **441,** 358–361 (2006).
12 Wang, J. *et al.* Platencin is a dual fabf and fabh inhibitor with potent *in vivo* antibiotic properties. *Proc. Natl Acad. Sci. USA* **104,** 7612–7616 (2007).
13 Singh, S. B. *et al.* Isolation, structure, and absolute stereochemistry of platensimycin, a broad spectrum antibiotic discovered using an antisense differential sensitivity strategy. *J. Am. Chem. Soc.* **128,** 11916–11920 and 15547 (2006).
14 Jayasuriya, H. *et al.* Isolation and structure of platencin: a novel FabH and FabF dual inhibitor with potent broad spectrum antibiotic activity produced by *Streptomyces platensis* MA7339. *Angew. Chem. Int. Ed.* **46,** 4684–4688 (2007).

15 Singh, S. B. *et al*. Discovery of lucensimycins A and B from *Streptomyces lucensis* MA7349 using an antisense strategy. *Org. Lett.* **8,** 5449–5452 (2006).
16 Ondeyka, J. G. *et al*. Coniothyrione, a chlorocyclopentandienylbenzopyrone as a bacterial protein synthesis inhibitor discovered by antisense technology. *J. Nat. Prod.* **70,** 668–670 (2007).
17 Zhang, C. *et al*. Isolation, structure and antibacterial activity of pleosporone from a pleosporalean ascomycete discovered by using antisense strategy. *Bioorg. Med. Chem.* (2008); e-pub ahead of print 12 April 2008; doi:10:1016/j.bmc.2008.04.18.
18 Zhang, C. *et al*. Isolation, structure and antibacterial activity of phaeosphenone from a *Phaeosphaeria* sp. discovered by antisense strategy. *J. Nat. Prod.* **71,** 1304–1307 (2008).
19 Imai, H. *et al*. Okilactomycin, a novel antibiotic produced by a *Streptomyces* species. II. Structure determination. *J. Antibiot. (Tokyo)* **40,** 1483–1489 (1987).
20 Smith, A. B. III, Basu, K. & Bosanac, T. Total synthesis of (−)-okilactomycin. *J. Am. Chem. Soc.* **129,** 14872–14874 (2007).
21 Imai, H. *et al*. Okilactomycin, a novel antibiotic produced by a *Streptomyces* species. I. Taxonomy, fermentation, isolation and characterization. *J. Antibiot. (Tokyo)* **40,** 1475–1482 (1987).
22 Weisburg, W. G., Barns, S. M., Pelletier, D. A. & Lane, D. J. 16S ribosomal DNA amplification for phylogenetic study. *J. Bacteriol.* **173,** 697–703 (1991).
23 Lane, D. J. *16S/23S rRNA Sequencing, in Nucleic Acid Techniques in Bacterial Systematics* (eds Stackebrandt, E. & Goodfellow, M.) 115–175 (Wiley, New York, 1991).
24 Saitou, N. & Nei, M. The neighbor-joining method: a new method for reconstructing phylogenetic trees. *Mol. Biol. Evol.* **4,** 406–425 (1987).
25 Jukes, T. H. & Cantor, C. *Evolution of Protein Molecules, in Mammalian Protein Metabolism* 21–132 (Academic Press, New York, 1969).
26 Kodali, S. *et al*. Determination of selectivity and efficacy of fatty acid synthesis inhibitors. *J. Biol. Chem.* **280,** 1669–1677 (2005).
27 Onishi, H. R. *et al*. Antibacterial agents that inhibit lipid A biosynthesis. *Science* **274,** 980–982 (1996).

The Journal of Antibiotics (2009) 62, 63–67

www.nature.com/ja

ORIGINAL ARTICLE

Ceramidastin, a novel bacterial ceramidase inhibitor, produced by *Penicillium* sp. Mer-f17067

Hiroyuki Inoue[1], Tetsuya Someno[1], Taira Kato[2], Hiroyuki Kumagai[3], Manabu Kawada[1] and Daishiro Ikeda[1]

Decrease of ceramide in the skin is one of the aggravating factors of atopic dermatitis. The skin is often infected by ceramidase-producing bacteria, such as *Pseudomonas aeruginosa*. The bacterial ceramidase then degrades ceramide in the skin. To develop anti-atopic dermatitis drugs, we searched for ceramidase inhibitors, which led to the discovery of ceramidastin, a novel inhibitor of bacterial ceramidase, from the culture broth of *Penicillium* sp. Mer-f17067. Ceramidastin inhibited the bacterial ceramidase with an IC_{50} value of 6.25 μg ml^{-1}. Here we describe the isolation, physicochemical properties, structure determination and biological activity of ceramidastin.
The Journal of Antibiotics (2009) **62,** 63–67; doi:10.1038/ja.2008.10; published online 9 January 2009

Keywords: atopic dermatitis; ceramidase; ceramidastin; *Penicillium*; *Pseudomonas*

INTRODUCTION

In the skin, ceramide forms a multilamelle structure in the stratum corneum and functions as a permeability barrier as well as a water retainer.[1] However, the content of ceramide is found to be decreased in lesions of atopic skin.[2] The decrease of ceramide induces dryness in the skin of patients with atopic dermatitis and compromises the permeability barrier, permitting the invasion of allergens or irritants.[3] Interestingly, such atopic skin is frequently colonized by ceramidase-producing bacteria.[4] Ceramidase is an enzyme that catalyzes the hydrolysis of the *N*-acyl linkage of ceramide to produce a free fatty acid and a sphingosine base. Ito and colleagues[5] have isolated a ceramidase-producing bacterium, *Pseudomonas aeruginosa* AN17, from the skin of patients with atopic dermatitis and cloned the gene encoding its ceramidase.[6] The hypothesis driving this study is that the ceramidase from colonizing bacteria contribute to the decrease of ceramide in atopic skin lesions, and that inhibiting bacterial ceramidase will prevent the decrease of ceramide in atopic skin and improve the disease. In the course of our screening for ceramidase inhibitors, we discovered ceramidastin, a novel inhibitor of bacterial ceramidase, from the culture broth of *Penicillium* sp. Mer-f17067. Here we describe the isolation, physicochemical properties, structure determination and biological activity of ceramidastin.

MATERIALS AND METHODS

Microorganism

Fungal strain *Penicillium* sp. Mer-f17067 was isolated from a soil sample collected from Iriomote Island, Okinawa prefecture, Japan. The fungal strain was cultured and kept on potato dextrose agar (Difco, Detroit, MI, USA). This strain has been deposited as NITE P-580 at the NITE Patent Microorganisms Depositary, Japan.

Taxonomic studies

The following media were used to identify the producing fungus: potato dextrose agar, 2% malt agar, oatmeal agar and Miura's medium (LcA). The formed colonies were observed after 1-week incubation at 25 °C. The colors used in this study were taken from Kornerup and Wanscher.[7]

Fermentation

Fungal strain *Penicillium* sp. Mer-f17067 grown on an agar slant was inoculated into 100 ml of a seed medium containing 2% potato starch, 1% glucose, 2% Soypro (J-Oil Mills Inc., Tokyo, Japan), 0.1% KH_2PO_4, 0.05% $MgSO_4 \cdot 7H_2O$ and three glass beads, and cultured at 25 °C for 3 days on a rotary shaker at 220 r.p.m. In all, 1 ml of the seed culture was inoculated into a 500-ml flask containing 100 ml of a culture medium consisting of 5% maltose hydrate, 1.5% Pharmamedia (Traders Protein, Memphis, TN, USA), 1% malt extract, 0.5% ammonium sulfate, 1% mineral solution (solution of 2% $CoCl_2 \cdot 6H_2O$, 2% $CaCl_2$ and 2% $MgCl_2$; adjusted at pH 7 before sterilization) and cultured at 25 °C for 4 days on a rotary shaker at 220 r.p.m.

Analytical measurement

Melting points were obtained on a Yanagimoto micro melting point apparatus (Yanagimoto, Kyoto, Japan). Optical rotations were measured on a JASCO P-1030 polarimeter (JASCO, Tokyo, Japan). UV spectra were recorded on a Hitachi 228 A spectrometer (Hitachi, Tokyo, Japan). ^1H and ^{13}C NMR spectra were measured on a JEOL JNM A400 spectrometer (JEOL, Tokyo, Japan) using tetramethylsilane (TMS) as an internal standard. HRESI-MS spectra were measured with a JEOL JMS-T100LC spectrometer (JEOL).

[1]Microbial Chemistry Research Center, Numazu Bio-Medical Research Institute, Miyamoto, Numazu-shi, Shizuoka, Japan; [2]Mercian Corporation Bioresource Laboratories, Nakaizumi, Iwata-shi, Shizuoka, Japan and [3]Mercian Cleantec Co., Ltd, Fujisawa-shi, Kanagawa, Japan
Correspondence: Dr M Kawada, Microbial Chemistry Research Center, Numazu Bio-Medical Research Institute, 18–24 Miyamoto, Numazu-shi, Shizuoka 410-0301, Japan.
E-mail: kawadam@bikaken.or.jp
Received 11 September 2008; accepted 11 November 2008; published online 9 January 2009

Ceramidase activity

Ceramidase activity was assessed according to the method used by Okino *et al.*,[5] with minor modifications. *P. aeruginosa* no. 12 was cultured in 3% Trypto-Soya Broth (Nissui Seiyaku, Tokyo, Japan) at 37 °C for 3 h on a rotary shaker at 100 r.p.m. In all, 15 µl of the seed culture was inoculated into 3 ml of a synthetic medium consisting of 0.05% NH_4Cl, 0.05% K_2HPO_4, 0.5% NaCl (adjusted at pH 7.2 before sterilization) with 0.05% taurodeoxycholate and 0.05% sphingomyelin, and cultured at 30 °C for 24 h on a rotary shaker at 100 r.p.m. After filtration, the cultured supernatant was used as a source for bacterial ceramidase.

The activity of ceramidase was measured using 7-nitrobenz-2-oxa-1, 3-diazole-labeled *N*-dodecanoylsphingosine (C12-NBD-ceramide; Avanti Polar Lipids, Alabaster, AL, USA) as a substrate. Here, 10 µl of 10 µM C12-NBD-ceramide in 50 mM Tris-HCl (pH 8.5) was mixed with 10 µl of the bacterial ceramidase solution and incubated with ceramidastin at 37 °C for 2.5 h. The reaction was terminated by the addition of 100 µl of chloroform/methanol (2/1, v/v). The resulting solution was evaporated and resolved in 100 µl of chloroform/methanol (2/1, v/v). A sample of 20 µl was applied on a thin layer chromatography (TLC) plate, which was developed with chloroform:methanol:25% ammonia (90:20:0.5). The spot of C12-NBD-fatty acid released by the reaction of the enzyme on the TLC plate was quantified by an FLA5000 Image Reader (Fujifilm, Tokyo, Japan).

Atopic dermatitis model

We used NC/Nga female mice (6-week old; Charles River, Yokohama, Japan) as an atopic dermatitis model.[8,9] Hair was removed from the backside of the mice anesthetized with Nembutal. The hairless area was defatted by acetone:ether (1:1) and washed with distilled water. Then, 200 µl of 1/4 diluted ceramidase solution was applied on the defatted back. After 30 min, 200 µl of 1 mg ml^{-1} ceramidastin dissolved in distilled water was applied on the defatted back. The procedure of defatting and applications of ceramidase and ceramidastin were repeated twice a day for 5 days a week and continued until the end of the experiment. Forty days after the first treatment, the mouse was killed and the skin on the backside was excised. The skin was fixed in formalin solution and embedded in paraffin, cut into 4-µm sections and stained with toluidine blue.

Cytotoxicity

Cells were inoculated in 96-well plates at 5000 cells per well with ceramidastin and cultured for 2 days. The growth was determined using 3-(4,5-dimethylthiazol- 2-yl)-2,5-diphenyltetrazolium bromide (MTT; Sigma, St Louis, MO, USA).

RESULTS

Taxonomy of the producing strain Mer-f17607

Colonies on potato dextrose agar plates were 32–34 mm in diameter, floccose to velvet and grayish blue (23C-4) to orange (5A6-7). Colonies on MA were 30–32 mm in diameter, velvet, and olive (1F-8) to pale orange (5A-3). Colonies on oatmeal agar plates were 35–37 mm in diameter, floccose to velvet, and dark green (25F-7) to light orange (5A4-5). Colonies on LcA plates were 25–28 mm in diameter, velvet, and olive (1F-8) to pale orange (5A-3). Soluble pigment was not found in the culture on any media. Vegetative hyphae were formed in or on agar plates, colorless and smooth in surface with septate hyphae. Conidiophores were orthotropous in vegetative hyphae, colorless and smooth in surface with metulae at the apex. Metulae were cylindrical and phialides were needle-like. Conidia were phialoconidia, one-celled, subrounded to rounded, smooth in surface and connected to each other like a chain from a phialide. Sexual reproductive organs were not found when the culture was observed for 2 weeks. These cultural and morphological characteristics suggest that the strain belonged to the genus *Penicillium*. On the basis of 28S rDNA-D1/D2 gene sequence data, the strain formed a distinct phyletic line from any known species in the genus *Penicillium*. Therefore, we classified it as a strain of *Penicillium* called *Penicillium* sp.

Isolation procedure for ceramidastin

The culture broth (5 l) was filtered and the filtrate was passed through a DIAION HP20 column (500 ml) equilibrated with H_2O. After washing with H_2O (2 l) and 20% acetone (2 l), the active material was eluted with 75% acetone (2 l). The eluate was concentrated *in vacuo* to remove acetone and diluted with H_2O up to 2.2 l. After adjusting the pH to 8, the aqueous solution was extracted with BuOH. The aqueous layer was concentrated *in vacuo* to remove the residual BuOH and diluted with H_2O up to 2.6 l. After adjusting the pH to 3, the aqueous solution was extracted with EtOAc (1.3 l×2). The organic layer was concentrated *in vacuo* to give a brown material (1.5 g). A portion of the material was dissolved in a small volume of 20% acetonitrile containing 0.1% trifluoro acetic acid (TFA) and passed through an Inertsil ODS-3 column (20×250 mm) packed with the same solution. Active ingredients containing ceramidastin were eluted from the column using a linear gradient system (20–60% acetonitrile containing 0.1% TFA). The active ingredients containing ceramidastin were diluted with 10 volumes of H_2O and applied on an HP20 column. After washing the column with H_2O, elution was carried out using acetone to afford 245 mg of ceramidastin.

Physicochemical properties

The physicochemical properties of ceramidastin are summarized in Table 1. Ceramidastin was isolated as a white powder, which was soluble in water, MeOH, acetone and DMSO.

Structure determination

The molecular formula of ceramidastin was determined to be $C_{26}H_{34}O_{11}$ on the basis of HRESI-MS (Table 1) and ^{13}C NMR information. The ^{13}C NMR spectrum (DMSO-d_6) showed 26 discrete carbon signals, which were classified into one methyl, nine methylenes, eight methines, including two sp^2 and six sp^3 methines, four sp^2 quaternary carbons and four carbonyl carbons by analysis of DEPT spectra. The connectivity of proton and carbon atoms was established by the ^{13}C–^1H heteronuclear multiple quantum coherence (HMQC) spectrum. Four of five hydroxyl signals were detected in the ^1H NMR spectrum (Table 2). The connectivity of these hydroxyl moieties and relevant carbon atoms was established by the ^1H–^1H COSY and heteronuclear multiple bond connectivity (HMBC) experiments (Table 2 and Figure 2). The general features of ^1H and ^{13}C NMR spectra resembled those of rubratoxin A and B.[10,11] As shown by the bold lines in Figure 2, five partial structures, composed of I (-CH_2-CH=CH-), II (-CH_2-CH(CH_2-)-CH(OH)-), III (-CH-CH(OH)-), IV (-CH-OH) and V (-CH_2-CH_3), were deduced from the ^1H–^1H COSY spectra. The arrow lines show that the partial structure from C-6 to

Table 1 Physicochemical properties of ceramidastin

Appearance	White powder
Molecular formula	$C_{26}H_{34}O_{11}$
HRESI-MS (m/z)	
(Positive mode)	
Found	545.2047 $(M+Na)^+$
Calculated	545.1999 for $C_{26}H_{34}O_{11}Na$
(Negative mode)	
Found	521.2011 $(M-H)^-$
Calculated	521.2023 for $C_{26}H_{33}O_{11}$
Melting point	121–124 °C
UVλ_{max} nm (H_2O)	End
UVλ_{max} nm (0.01 N HCl)	275 (sh)
$[\alpha]_D^{24}$ (ca. 0.5, H_2O)	+29°

Table 2 The ^{13}C and ^{1}H NMR assignments of ceramidastin in DMSO-d_6

Position	*^{13}C (mult.)*	*p.p.m.*	*^{1}H p.p.m. (mult., J(Hz))*
1	61.7	(t)	3.90 (d, 5.0)
2	132.5	(d)	5.55 (dt, 15.3, 5.0)
3	126.5	(d)	5.65 (dt, 15.3, 7.0)
4	35.8	(t)	2.05 (m), 2.25 (m)
5	71.5	(d)	3.50 (ddd, 10.4, 7.2, 4.0)
5-OH			3.90 (br s)
6	78.0	(d)	3.20 (m)
6-OH			4.90 (br s)
7	36.0	(d)	1.85 (m)
8	24.1	(t)	2.35 (m), 2.62 (m)
9	143.8	(s)	
10	142.5	(s)	
11	63.0	(d)	5.28 (d, 10.5)
11-OH			5.95 (br s)
12	47.0	(d)	3.10 (m)
13	138.4	(s)	
14	148.0	(s)	
15	31.8	(t)	2.45 (m), 2.80 (m)
16	68.8	(d)	4.12 (m)
16-OH			4.84 (br s)
17	35.5	(t)	1.20 (m)
18	25.7	(t)	1.35 (m)
19	28.0	(t)	1.20 (m)
20	31.0	(t)	1.20 (m)
21	22.0	(t)	1.23 (m)
22	13.5	(q)	0.85 (t, 7.0)
23	165.8	(s)	
24	163.0	(s)	
25	167.0	(s)	
26	166.4	(s)	

Chemical shifts in p.p.m. from trimethylsilane (TMS) as an internal standard.
The ^{13}C and ^{1}H NMR were measured at 100 and 400 MHz, respectively.

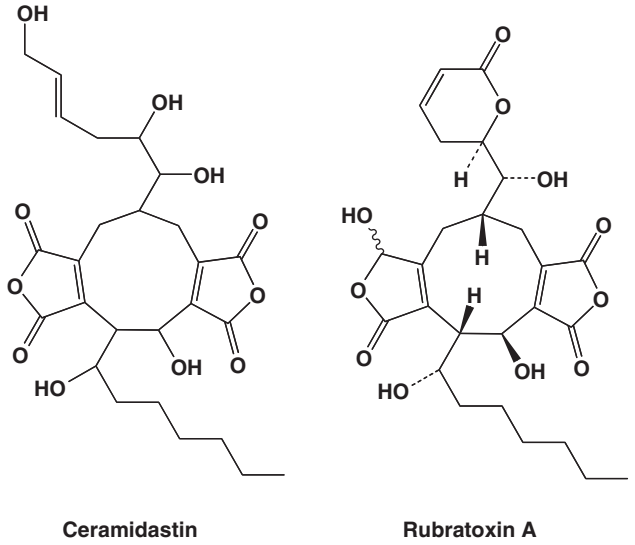

Figure 1 Structures of ceramidastin and rubratoxin A.

C-26 in ceramidastin, which is completely preserved in rubratoxin B, was deduced from the HMBC spectra. Furthermore, ^{1}H and ^{13}C chemical shifts and coupling constants of ceramidastin were very similar to

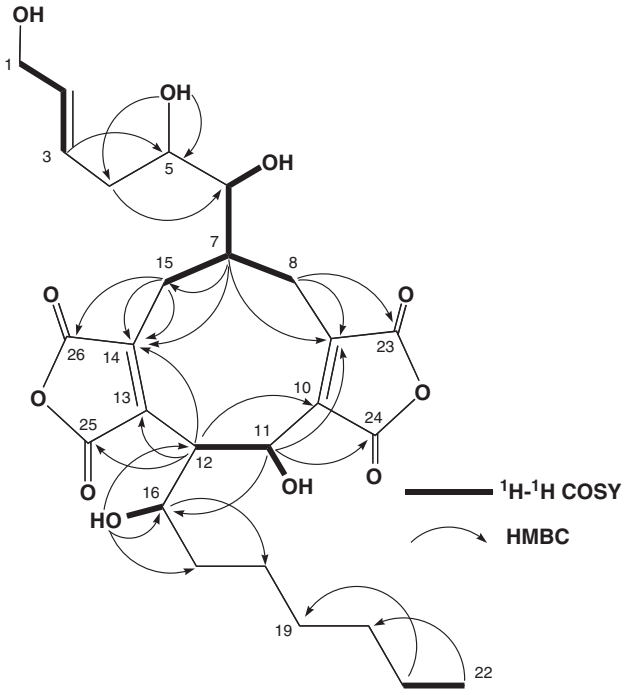

Figure 2 1H-1H COSY and HMBC correlations in ceramidastin.

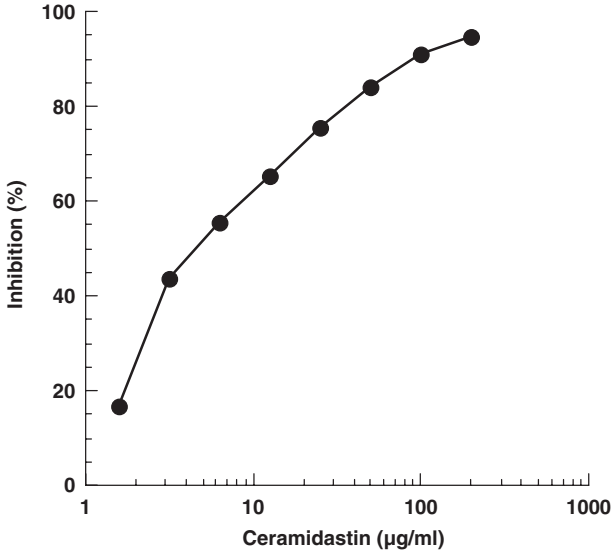

Figure 3 Effect of ceramidastin on *Pseudomonas* ceramidase. Values are means of duplicate determinations. Each SE is less than 10%.

those of reported rubratoxin B, suggesting the same stereochemistry between the two compounds. The remaining part (HO-CH_2-CH=CH-CH_2-CH(OH)-), including the partial structure of ceramidastin, was elucidated to connect C-6 by the HMBC correlation from H-4 as shown in Figure 2. The coupling constant between 2-H and 3-H (J=15.3 Hz) indicated that the configuration at C-2/C-3 is *E*. Consequently, the total structure of ceramidastin was elucidated as shown in Figures 1 and 2.

Inhibition of *Pseudomonas* ceramidase

The effect of ceramidastin on bacterial ceramidase was assessed according to the method used by Okino *et al.*,[5] with minor modifica-

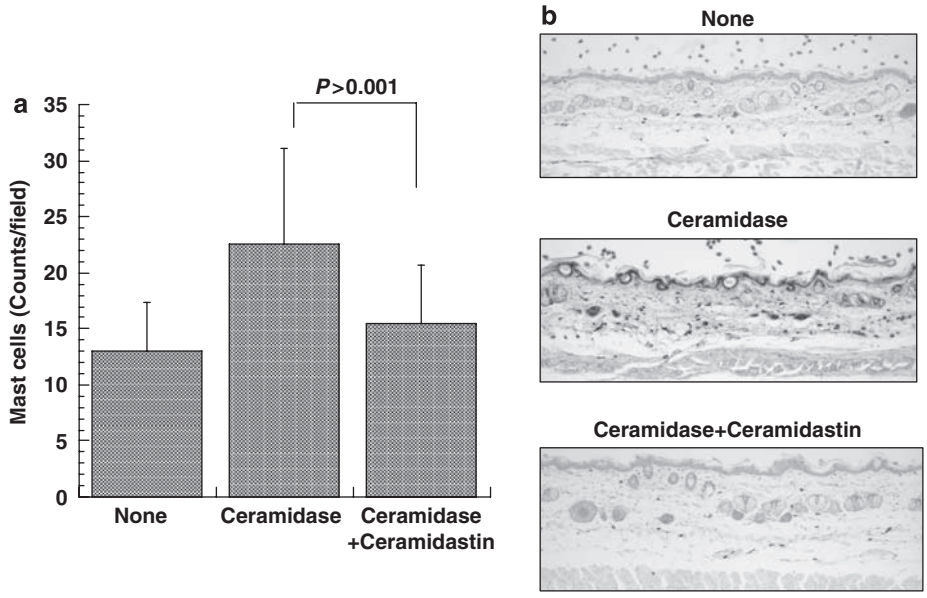

Figure 4 Effects of ceramidastin on NC/Nga mice skin. NC/Nga mice (6 mice per group) were treated with *Pseudomonas* ceramidase on the back skin with or without ceramidastin. Mast cells in the dermis were stained by toluidine blue and counted. (**a**) Mast cell counts in the dermis. The values were means ± s.d. of 6 mice. (**b**) Representative photos of the dermis sections stained by toluidine blue.

tions. We used the supernatant of a culture of *P. aeruginosa* no. 12 as a source for bacterial ceramidase. As shown in Figure 3, ceramidastin inhibited *Pseudomonas* ceramidase with an IC_{50} value of 6.25 μg ml^{-1}. On the contrary, ceramidastin did not inhibit human ceramidase even at 200 μg ml^{-1}. Ceramidastin did not show anti-microbial and anti-fungal activities, including against *P. aeruginosa,* at 100 μg ml^{-1}.

We next examined the effect of ceramidastin on atopic dermatitis model NC/Nga mice.[8,9] Mast cells are increased in the dermis with dermatitis.[8] As shown in Figure 4, mast cells were increased in the dermis by *Pseudomonas* ceramidase application. However, ceramidastin treatment significantly inhibited the increase of mast cells in the dermis.

Cytotoxicity *in vitro* and toxicity in mice

Ceramidastin did not show any cytotoxicity against human lung cancer cell lines, HCI-H23 and NCI-H522 cells, human colon cancer HT-29 cells, mouse melanoma B16BL6 cells, mouse colon cancer colon 26 cells, mouse lymphoma cell lines, EL-4 and L-1210 cells up to 100 μg ml^{-1}.

Acute toxicity of ceramidastin in mice was examined using ICR female mice. When ceramidastin was administered intravenously, no fatality was observed up to 6.25 mg kg^{-1}.

DISCUSSION

It is reported that D-MAPP, a ceramide analog, inhibits human ceramidase.[12] However, ceramidastin did not show inhibitory activity against human ceramidase. It is also reported that GCAS-4 and GCAS-7, other ceramide analogs, as well as D-MAPP inhibit the ceramidase activity of *Pseudomonas* culture with an IC_{50} value of 500 μM.[13] We tested the effect of D-MAPP on *Pseudomonas* ceramidase in our assay system, and found that D-MAPP inhibited it with an IC_{50} value of 500 μg ml^{-1}. Thus, ceramidastin is considered to be a more selective and stronger inhibitor of bacterial ceramidase.

Ceramidastin is structurally related to rubratoxins.[10] We also examined the effect of rubratoxin A on *Pseudomonas* ceramidase, which showed that rubratoxin A did not inhibit it even at 100 μg ml^{-1}. Thus, the structural difference of ceramidastin must be significant for its inhibitory action against bacterial ceramidase.

To evaluate the efficacy of ceramidastin on atopic dermatitis, we used NC/Nga mice. It is reported that tacrolimus hydrate improves spontaneous dermatitis in NC/Nga mice.[8] Mast cells are increased in the dermis by allergic responses. Our result showed that ceramidastin inhibited the increase of mast cells in the dermis induced by *Pseudomonas* ceramidase. Ceramidastin showed neither anti-microbial nor anti-fungal activities, which is an advantage because there is a low possibility of inducing drug-resistant bacteria. Thus, it is suggested that ceramidastin would improve atopic dermatitis exacerbated by bacterial infection.

ACKNOWLEDGEMENTS

We are grateful to Dr K Isshiki and Dr N Sakata (Mercian Corporation Bioresource Laboratories) for their valuable discussions. We also thank Dr R Sawa and Mrs Y Kubota (Microbial Chemistry Research Center) for HRESI-MS and NMR measurements.

1 Elias, P. M. & Menon, G. K. Structural and lipid biochemical correlates of the epidermal permeability barrier. *Adv. Lipid Res.* **24,** 1–26 (1991).
2 Imokawa, G. *et al.* Decreased level of ceramides in stratum corneum of atopic dermatitis: an etiologic factor in atopic dry skin? *J. Invest. Dermatol.* **96,** 523–526 (1991).
3 Bos, J. D., Kapsenberg, M. L. & Smitt, J. H. Pathogenesis of atopic eczema. *Lancet.* **343,** 1338–1341 (1994).
4 Ohnishi, Y., Okino, N., Ito, M. & Imayama, S. Ceramidase activity in bacterial skin flora as a possible cause of ceramide deficiency in atopic dermatitis. *Clin. Diagn. Lab. Immunol.* **6,** 101–104 (1999).
5 Okino, N., Tani, M., Imayama, S. & Ito, M. Purification and characterization of a novel ceramidase from *Pseudomonas aeruginosa. J. Biol. Chem.* **273,** 14368–14373 (1998).
6 Okino, N., Ichinose, S., Omori, A., Imayama, S., Nakamura, T. & Ito, M. Molecular cloning, sequencing, and expression of the gene encoding alkaline ceramidase from *Pseudomonas aeruginosa*: cloning of a ceramidase homologue from Mycobacterium tuberculosis. *J. Biol. Chem.* **274,** 36616–36622 (1999).
7 Kornerup, A. & Wanscher, J. H. *Methen Handbook of Colour,* 3rd edn (Eyre Methen, London, UK, 1978).

8 Hiroi, J. *et al*. Effect of tacrolimus hydrate (FK506) ointment on spontaneous dermatitis in NC/Nga mice. *Jpn. J. Pharmacol*. **76,** 175–183 (1998).
9 Aioi, A. *et al*. Impairment of skin barrier function in NC/Nga Tnd mice as a possible model for atopic dermatitis. *Br. J. Dermatol*. **144,** 12–18 (2001).
10 Buchi, G., Snider, K. M., White, J. D., Gougoutas, J. Z. & Singh, S. Structure of rubratoxin A and B. *J. Am. Chem. Soc*. **92,** 6638–6641 (1970).
11 Nieminen, S. & Tamm, C. 1H- and 13C-NMR spektroskopie der nonadride. *Helv. Chim. Acta*. **64,** 2791–2801 (1981).
12 Bielawska, A. *et al*. (1*S*,2*R*)-D-*erythro*-2-(*N*-myristoylamino)-1-phenyl-1-propanol as an inhibitor of ceramidase. *J. Biol. Chem*. **271,** 12646–12654 (1996).
13 Kita, K. *et al*. Activation of bacterial ceramidase by anionic glycerophospholipids: possible involvement in ceramidase hydrolysis on atopic skin by *Pseudomonas* ceramidase. *Biochem. J*. **362,** 619–626 (2002).

The Journal of Antibiotics (2009) 62, 69–74

www.nature.com/ja

ORIGINAL ARTICLE

Total synthesis of amidepsine B and revision of its absolute configuration

Tohru Nagamitsu[1], Kaori Marumoto[1], Asami Nagayasu[1], Takeo Fukuda[1], Shiho Arima[1], Ryuji Uchida[1], Taichi Ohshiro[1], Yoshihiro Harigaya[1], Hiroshi Tomoda[1] and Satoshi Ōmura[2]

The total synthesis of (−)-amidepsine B, a potent diacylglycerol acyltransferase inhibitor, has been achieved. This synthetic study resulted in the revision of the previously assigned stereostructure of the natural amidepsine B and determined the absolute configuration.
The Journal of Antibiotics (2009) **62,** 69–74; doi:10.1038/ja.2008.12; published online 23 January 2009

Keywords: absolute configuration; (−)-amidepsine B; total synthesis

INTRODUCTION

Amidepsines A–E were isolated from the culture broth of fungal strains FO-2942 and FO-5969 and found to be inhibitors of diacylglycerol acyltransferase (DGAT),[1–3] which is exclusively involved in triacylglycerol formation. Excessive accumulation of triacylglycerol can cause fatty liver, obesity and hypertriglyceridemia, which leads to serious diseases, such as atherosclerosis, diabetes and metabolic disorders. Therefore, DGAT inhibitors have the potential to become drugs. Spectroscopic analyses of the amidepsines elucidated depsipeptide structures consisting of three 4,6-dihydroxy-2-methylbenzoic acid derivatives and an amino acid (except for amidepsine D), as shown in Figure 1. The DGAT inhibitory activity of the amidepsines was tested by a cellular assay using Raji cells, and the results showed that amidepsine B (**1**) was the most potent inhibitor. Amidepsine B (**1**) was previously determined to be a mixture of stereoisomers at its single chiral center, the alanine alpha carbon. A 3:2 mixture of L- and D-alanines was revealed by acid hydrolysis followed by HPLC analyses using a chiral column (Amidepsines A and C were also reported as a 3:2 mixture of L- and D-amino acids[2]). Herein, the total synthesis of amidepsine B and a revision of its absolute configuration will be described.

RESULTS AND DISCUSSION

The synthesis used a known aldehyde **2**, which is a common starting material for the preparation of key substrates **5** and **10** (scheme 1).[4] Regioselective *p*-*O*-methylation (In this reaction, reactivity of the hydroxy group adjacent to the formyl group in **3** would be precluded by the formation of an intramolecular hydrogen bond. Similar reactivity was observed.[5]) followed by benzylation gave **4** quantitatively, which was treated with $NaClO_2$ to afford carboxylic acid **5** quantitatively. Furthermore, similar conversion of **2** to **8**, including the formation of a *p*-*O*-methoxymethyl ether instead of methylation, was also accomplished quantitatively. Esterification of **8** with allyl bromide followed by deprotection of the methoxymethyl ether afforded **10** quantitatively.

Next, the key substrates **5** and **10** were coupled by treatment with trifluoroacetic anhydride (TFAA) to give rise to **11** quantitatively. Deprotection of the allyl ester in the presence of a palladium catalyst gave carboxylic acid **12** in 98% yield.

Subsequent esterification of **12** with **10** was troublesome. Esterification conditions, such as TFAA, 1-[(3-dimethylamino)propyl]-3-ethylcarbodiimide/dimethylaminopyridine (DMAP) and benzotriazol-1-yloxytris(dimethylamino)phosphonium hexafluorophosphate (BOP)/Et_3N/DMAP led to a low yield of the desired product **14** with side products, such as the anhydride of **12**. Therefore, we next focused on esterification through the acid fluoride.[6] Reaction of **12** with (diethylamino)sulfur trifluoride (DAST) proceeded in 89% yield to furnish the stable acid fluoride **13**. Treatment of **13** with sodium alkoxide, derived from **10** and sodium hydride, was effected to give the desired allyl ester **14** quantitatively. The allyl ester was then deprotected under palladium-catalyzed conditions to afford **15** quantitatively.

Having constructed the depside **15**, we next turned to condensation with L-alanine before preparing the 3:2 mixture of L- and D-alanines toward the total synthesis (scheme 2). Treatment of **15** with L-alanine benzyl ester in the presence of BOP and Et_3N produced benzyl ester (+)-**16** in 79% yield. Finally, global deprotection by hydrogenolysis completed the total synthesis of (−)-amidepsine B [(−)-**1**] in 83% yield.

The physical properties (^1H and ^{13}C NMR, m.p., IR and MS) of synthetic (−)-amidepsine B (**1**) were completely identical to those of a

[1]School of Pharmacy, Kitasato University, Tokyo, Japan and [2]Kitasato Institute for Life Sciences and Graduate School of Infection Control Sciences, Kitasato University, Tokyo, Japan
Correspondence: Professor S Ōmura, Kitasato Institute for Life Sciences and Graduate School of Infection Control Sciences, Kitasato University, 5-9-1 Shirokane, Minato-ku, Tokyo 108-8641, Japan.
E-mail: omura-s@kitasato.or.jp
Received 18 November 2008; accepted 18 November 2008; published online 23 January 2009

natural sample, and the optical rotation of synthetic (−)-**1** ($[\alpha]_D^{23}$ −17.3°; *c* 0.10, MeOH) also corresponded with that of the authentic sample of (**1**) ($[\alpha]_D^{25}$ −16°; *c* 0.1, MeOH). This result triggered the need for the re-assignment of the absolute configuration of natural amidepsine B (**1**). According to the procedure shown above, (+)-amidepsine B [(+)-**1**] by condensation of **15** with D-alanine was also synthesized.

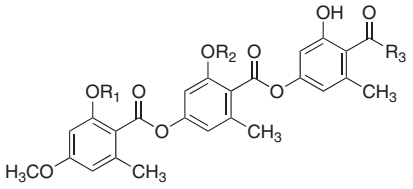

Amidepsine	A	B	C	D	E
R_1	Me	H	H	Me	Me
R_2	H	H	H	H	Me
R_3	alanine**	L-alanine*	valine**	OH	alanine

Figure 1 Structure of amidepsines A–E. *The original isomeric mixture reported for amidepsine B has been corrected by this work. **The actual configurations of amidepsines A and C are now in question.[2]

We next analyzed the synthetic amidepsines (+)-**1** and (−)-**1** and the natural amidepsine B (**1**) with a chiral HPLC column. When the 1:1 mixture of the synthetic amidepsines (+)-**1** and (−)-**1** was injected onto the chiral HPLC system, each enantiomer was separated completely as shown in Figure 2a. Figures 2b and c show the HPLC analytical data of (+)-**1** and (−)-**1**, respectively. Next, the natural amidepsine B (**1**) was also subjected to HPLC analysis and it was determined that the retention time was identical to that of (−)-amidepsine B [(−)-**1**] as shown in Figure 2d.

This result shows that the absolute configuration of amidepsine B is *S*, derived from L-alanine, and that the previous determination of the absolute configuration of amidepsine B was inaccurate. It is likely that the acid hydrolysis of amidepsine B must have led to the epimerization of the resulting alanine. It is highly likely that amidepsines A and C are also L-amino acids, which will be reported in due course.

In conclusion, we have achieved the total synthesis of amidepsine B. Moreover, we have revised the absolute configuration of natural amidepsine B. Extension of this chemistry to the synthesis of structural analogs of amidepsine B so that the structure–activity

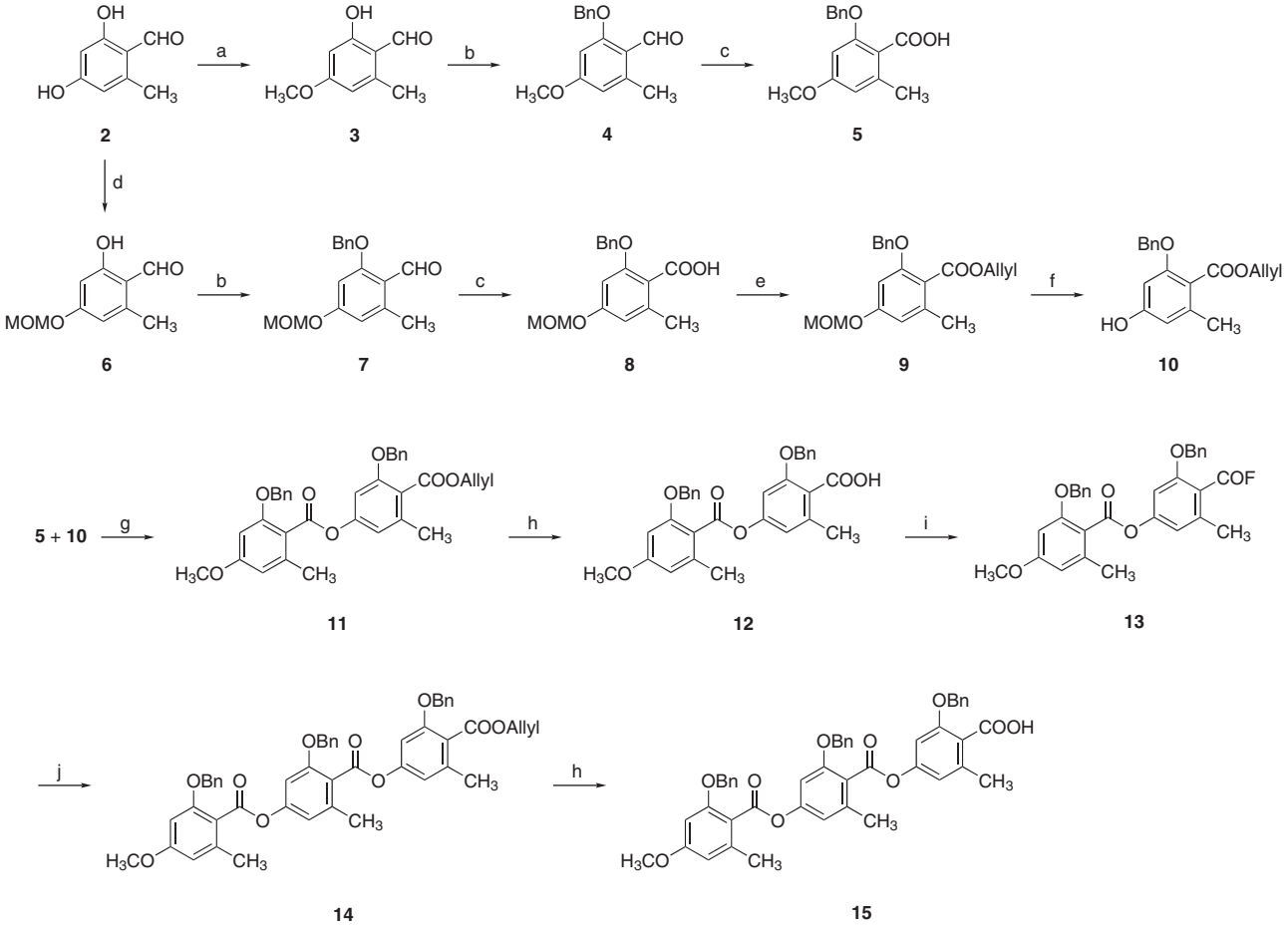

Scheme 1 Synthesis of depside **15**. Reagents and conditions: (a) CH_3I, K_2CO_3, acetone, rt, quant.; (b) Benzyl chloride, K_2CO_3, DMF, rt, quant. for **4** and **7**; (c) $NaClO_2$, 2-methyl-2-butene, $NaH_2PO_4{\cdot}2H_2O$, *t*-BuOH/H_2O, 0°C to rt, quant. for **5** and **8**; (d) Methoxymethyl chloride, *i*-Pr_2NEt, CH_2Cl_2, 0°C to rt, quant.; (e) Allyl Br, NaH, DMF, 0°C to rt, quant.; (f) 6N HCl, MeOH, 60°C, quant.; (g) Trifluoroacetic anhydride, toluene, rt, quant.; (h) HCOOH, $Pd(PPh_3)_4$, Et_3N, THF, 0°C to rt, 98% for **12**, quant. for **15**; (i) (Diethylamino)sulfur trifluoride, Et_2O/CH_2Cl_2, rt, 89%; (j) **10**, NaH, THF, 0°C, then **13**, rt, quant.

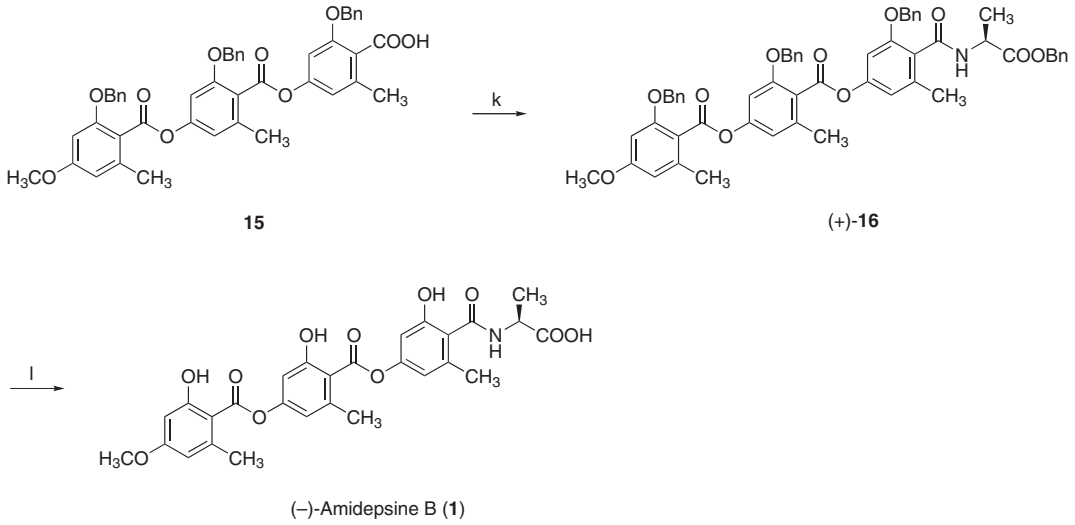

Scheme 2 Completion of the total synthesis of (–)-amidepsine B [(–)-**1**]. Reagents and conditions: (k) L-alanine benzyl ester, BOP, Et_3N, DMF, rt, 79%. For (–)-**16**: D-alanine benzyl ester, BOP, Et_3N, DMF, rt, 89%; (l) H_2, $Pd(OH)_2$, THF/EtOH, rt, 83%. For (+)-**1**: 94%.

relationships can be explored is currently under way and will be reported in due course.

EXPERIMENTAL PROCEDURE

Commercially available solvents were dried and distilled before use. Reactions were monitored by TLC using Merck $F60_{254}$ silica gel plates (0.25 mm). Spots were visualized with ultraviolet (UV) light (254 nm) and stained with phosphomolybdic acid. Flash column chromatography was performed on silica gel 60N (spherical, neutral, particle size 40–50 μm). Preparative TLC was performed on Merck $F60_{254}$ silica gel plates (0.50 mm). The chiral HPLC system was comprised of a Daicel-CHIRALPAK IA column (0.46 cm ϕ×25 cm), and a mobile phase of hexane/THF (tetrahydrofuran)/TFAA (80:20:0.1) (Senshu HPLC system; 10 μl injection; UV, 254 nm; flow rate, 1.0 ml min^{-1}).

Melting points were determined on a Yanagimoto micro melting apparatus and uncorrected. Optical rotations were obtained with a JASCO DIP-1000 polarimeter. Mass spectra were recorded on a JEOL JMS-700 mass spectrometer. FT-IR spectra were recorded on a Horiba FT-710 spectrometer. ^{1}H-NMR spectra were recorded on a JEOL JNM-EX270 (270 MHz), MERCURY-300 (300 MHz) and UNITY-400 (400 MHz) spectrometers in $CDCl_3$ or DMSO-d_6. ^{1}H-NMR spectral data are reported according to the following conventions: chemical shifts relative to $CDCl_3$ (7.26 p.p.m.) or DMSO-d_6 (2.48 p.p.m.), multiplicity (s=singlet, d=doublet, t=triplet, q=quartet, m=multiplet, br s=broad singlet, br d=broad doublet and dd=double doublet), coupling constant and integration. ^{13}C-NMR spectral data are reported in p.p.m. relative to $CDCl_3$ (77.0 p.p.m.) or DMSO-d_6 (39.5 p.p.m.).

2-Hydroxy-4-methoxy-6-methylbenzaldehyde (3)

To a solution of 2,4-dihydroxy-6-methylbenzaldehyde (**2**) (0.56 g, 3.68 mmol) in acetone (36.8 ml), K_2CO_3 (0.51 g, 3.68 mmol) and CH_3I (3.44 ml, 55.2 mmol) were added. The reaction mixture was stirred for 2.5 h at room temperature, quenched with H_2O and extracted with EtOAc. The combined organic extracts were dried over anhydrous Na_2SO_4 and concentrated *in vacuo*. The residue was purified by flash column chromatography on silica gel with an eluent (20:1 hexanes/EtOAc) to give **3** (0.61 g, quant.) as a white powder; m.p. 65–67 °C; IR (KBr): 3084, 2966, 2906, 2846, 1635, 1576, 1473 and 1429 cm^{-1}; ^{1}H-NMR (300 MHz, $CDCl_3$) δ 12.45 (s, 1H), 10.05 (s, 1H), 6.23 (s, 2H), 3.80 (s, 3H), 2.49 (s, 3H); ^{13}C-NMR (75 MHz, $CDCl_3$) δ 192.8, 166.6, 166.4, 143.7, 113.2, 110.4, 98.5, 55.4 and 18.2; HRMS (FAB, *m*–NBA): calcd. for $C_9H_{11}O_3$: 167.0708 $[M+H]^+$, found: *m/z* 167.0703.

2-Benzyloxy-4-methoxy-6-methylbenzaldehyde (4)

To a solution of **3** (0.60 g, 3.64 mmol) in *N*,*N*-dimethylformamide (DMF) (18.2 ml), K_2CO_3 (5.03 g, 36.4 mmol) and BnCl (6.29 ml, 56.4 mmol) were added at 0 °C. After stirring for 2.5 h at room temperature, the reaction was quenched with H_2O and extracted with CH_2Cl_2. The combined organic extracts were dried over anhydrous Na_2SO_4 and concentrated *in vacuo*. The residue was purified by flash column chromatography on silica gel with an eluent (20:1 to 10:1 hexanes/EtOAc) to give **4** (0.93 g, quant.) as a white powder; m.p. 78–80 °C; IR (KBr): 3321, 3091, 3049, 2966, 2925, 2871, 2789, 1666, 1603 and 1448 cm^{-1}; ^{1}H-NMR (270 MHz, $CDCl_3$) δ 10.59 (s, 1H), 7.38 (m, 5H), 6.40 (d, *J*=1.8 Hz, 1H), 6.34 (d, *J*=1.8 Hz, 1H), 5.14 (s, 2H), 3.84 (s, 3H), 2.60 (s, 3H); ^{13}C-NMR (75 MHz, $CDCl_3$) δ 190.4, 164.2, 164.2, 144.6, 136.0, 128.6, 128.1, 127.2, 117.5, 109.1, 97.0, 70.5, 55.3 and 22.3; HRMS (FAB, *m*–NBA): calcd. for $C_{16}H_{17}O_3$: 257.1178 $[M+H]^+$, found: *m/z* 257.1176.

2-Benzyloxy-4-methoxy-6-methylbenzoic acid (5)

To a solution of **4** (0.16 g, 0.61 mmol) in *t*-BuOH/H_2O (1:1) (6.2 ml) 2-methyl-2-butene (0.26 ml, 2.45 mmol), $NaH_2PO_4{\cdot}2H_2O$ (0.29 g, 1.84 mmol) and $NaClO_2$ (0.17 ml, 1.84 mmol) were added at 0 °C. The reaction mixture was stirred for 24 h at room temperature, diluted with H_2O and extracted with CH_2Cl_2. The combined organic extracts were dried over anhydrous Na_2SO_4 and concentrated *in vacuo*. The residue was purified by flash column chromatography on silica gel with an eluent (5:1 to 3:1 hexanes/EtOAc) to give **5** (0.18 g, quant.) as a white powder; m.p. 98–100 °C; IR (KBr): 3298, 3022, 2935, 2877, 2837, 1705, 1604 and 1448 cm^{-1}; ^{1}H-NMR (270 MHz, $CDCl_3$) δ 10.22 (br s, 1H), 7.40 (m, 5H), 6.48 (s, 2H), 5.20 (s, 2H), 3.83 (s, 3H), 2.61 (s, 3H); ^{13}C-NMR (75 MHz, $CDCl_3$) δ 169.9, 162.0, 158.4, 142.7, 135.6, 128.7, 128.3, 127.3, 113.5, 108.9, 97.9, 71.3, 55.3 and 22.0; HRMS (FAB, *m*–NBA): calcd. for $C_{16}H_{16}O_4$: 272.1049 $[M]^+$, found: *m/z* 272.1049.

2-Hydroxy-4-methyoxymethoxy-6-methylbenzaldehyde (6)

To a solution of **5** (0.56 g, 3.70 mmol) in CH_2Cl_2 (37.0 ml) *i*-Pr_2NEt (0.71 ml, 4.07 mmol) and chloromethyl methyl ether (MOMCl) (0.56 ml, 7.39 mmol) were added at 0 °C. After stirring for 45 min at room temperature, the reaction was quenched with H_2O and extracted with CH_2Cl_2. The combined organic extracts were dried over anhydrous Na_2SO_4 and concentrated *in vacuo*. The residue was purified by flash column chromatography on silica gel with an eluent (30:1 hexanes/EtOAc) to give **6** (0.72 g, quant.) as a white powder; m.p. 46–48 °C; IR (KBr): 3089, 2964, 1631, 1493 and 1431 cm^{-1}; ^{1}H-NMR (270 MHz, $CDCl_3$) δ 12.31 (s, 1H), 10.11 (s, 1H), 6.42 (d, *J*=2.2 Hz, 1H), 6.36 (d, *J*=2.2 Hz, 1H), 5.19 (s, 2H), 3.46 (s, 3H), 2.53 (s, 3H); ^{13}C-NMR

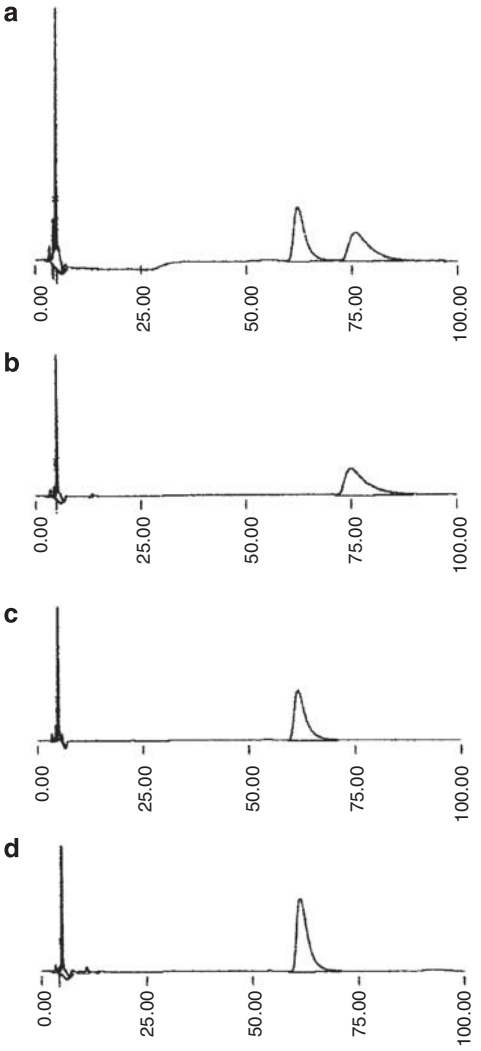

Figure 2 HPLC analysis of natural and synthetic amidepsines B. The abscissa axis indicates retention time. (**a**) a 1:1 mixture of synthetic amidepsines B (+)-**1** and (−)-**1**; (**b**) synthetic amidepsine B [(+)-**1**] (derived from D-alanine); (**c**) synthetic amidepsine B [(−)-**1**] (derived from L-alanine); (**d**) natural amidepsine B.

(75 MHz, $CDCl_3$) δ 193.1, 165.9, 164.1, 144.0, 113.9, 110.9, 101.3, 93.8, 56.3 and 183.3; HRMS (FAB, *m*–NBA): calcd. for $C_{10}H_{13}O_4$: 197.0814 $[M+H]^+$, found: *m/z* 197.0808.

2-Benzyloxy-4-methoxymethoxy-6-methylbenzaldehyde (7)

To a solution of **6** (0.76 g, 3.86 mmol) in DMF (19.3 ml) K_2CO_3 (5.33 g, 38.6 mmol) and BnCl (4.44 ml, 38.6 mmol) were added at 0 °C. After stirring for 45 min at room temperature, the mixture was warmed to 50 °C and stirred for 30 min. The mixture was quenched with H_2O and extracted with CH_2Cl_2. The combined organic extracts were dried over anhydrous Na_2SO_4 and concentrated *in vacuo*. The residue was purified by flash column chromatography on silica gel with an eluent (20:1 hexanes/EtOAc) to give **7** (1.09 g, 99%) as a white powder; m.p. 43–46°C; IR (KBr): 2927, 1674, 1601, 1450 and 1415 cm^{-1}; ^{1}H-NMR (270 MHz, $CDCl_3$) δ 10.59 (s, 1H), 7.39 (m, 5H), 6.57 (d, *J*=2.0 Hz, 1H), 6.48 (d, *J*=2.0 Hz, 1H), 5.19 (s, 2H), 5.13 (s, 2H), 3.48 (s, 3H), 2.58 (s, 3H); ^{13}C-NMR (75 MHz, $CDCl_3$) δ 190.6, 164.1, 161.9, 144.5, 135.9, 128.6, 128.1, 127.3, 118.2, 111.3, 98.5, 93.9, 70.5, 56.2 and 22.1; HRMS (FAB, *m*–NBA): calcd. for $C_{17}H_{17}O_4$: 285.1132 $[M-H]^-$, found: *m/z* 285.1119.

2-Benzyloxy-4-methoxymethoxy-6-methylbenzoic acid (8)

To a solution of **7** (0.70 g, 2.45 mmol) in *t*-BuOH/H_2O (1:1) (24.4 ml), 2-methyl-2-butene (1.04 ml, 9.79 mmol), $NaH_2PO_4{\cdot}2H_2O$ (1.10 g, 7.34 mmol) and $NaClO_2$ (0.66 ml, 7.34 mmol) were added at 0 °C. The reaction mixture was stirred for 24 h at room temperature, diluted with H_2O and extracted with CH_2Cl_2. The combined organic extracts were dried over anhydrous Na_2SO_4 and concentrated *in vacuo*. The residue was purified by flash column chromatography on silica gel with an eluent (5:1 hexanes/EtOAc) to give **8** (0.74 g, quant.) as a yellow oil. IR (KBr): 3168, 2927, 1697, 1601 and 1448 cm^{-1}; ^{1}H-NMR (300 MHz, $CDCl_3$) δ 9.75 (br s, 1H), 7.41 (m, 5H), 6.59 (d, *J*=2.2 Hz, 1H), 6.58 (d, *J*=2.2 Hz, 1H), 5.17 (s, 2H), 5.16 (s, 2H), 3.47 (s, 3H), 2.51 (s, 3H); ^{13}C-NMR (75 MHz, $CDCl_3$) δ 169.3, 159.6, 158.3, 142.7, 135.5, 128.7, 128.3, 127.4, 114.4, 111.5, 99.4, 94.1,71.4, 56.1 and 21.9; HRMS (FAB, *m*–NBA): calcd. for $C_{17}H_{19}O_5$: 303.1232 $[M+H]^+$, found: *m/z* 303.1244.

2-Benzyloxy-4-methoxymethoxy-6-methylbenzoic acid allyl ester (9)

To a solution of **8** (1.06 g, 3.51 mmol) in DMF (35.1 ml), NaH (0.21 g, 5.27 mmol) and allyl bromide (0.91 ml, 10.5 mmol) were added at 0 °C under N_2. After stirring for 30 min, the reaction mixture was warmed to room temperature and stirred for 1.5 h. The mixture was quenched with H_2O and extracted with EtOAc. The combined organic extracts were dried over anhydrous Na_2SO_4 and concentrated *in vacuo*. The residue was purified by flash column chromatography on silica gel with an eluent (15:1 hexanes/EtOAc) to give **9** (1.14 g, quant.) as a colorless oil. IR (KBr): 2945, 1726, 1599 and 1446 cm^{-1}; ^{1}H-NMR (270 MHz, $CDCl_3$) δ 7.33 (m, 5H), 6.50 (d, *J*=2.3 Hz, 2H), 5.95 (m, 1 H), 5.35 (dd, *J*=17.2, 1.5 Hz, 1H), 5.19 (dd, *J*=10.2, 1.5 Hz, 1H), 5.13 (s, 2H), 5.06 (s, 2H), 4.78 (br d, *J*=5.6 Hz, 2H), 3.44 (s, 3H), 2.30 (s, 3H); ^{13}C-NMR (75 MHz, $CDCl_3$) δ 167.7, 158.8, 157.0, 138.2, 136.5, 132.1, 128.3, 127.7, 127.1, 118.4, 117.8, 109.6, 99.1, 94.2, 70.3, 65.6, 55.9 and 19.7; HRMS (FAB, *m*–NBA): calcd. for $C_{20}H_{23}O_5$: 343.1545 $[M+H]^+$, found: *m/z* 343.1556.

2-Benzyloxy-4-hydroxy-6-methylbenzoic acid allyl ester (10)

To a solution of **9** (2.10 g, 6.13 mmol) in CH_3OH (30.5 ml), 6 N HCl (30.5 ml) was added. After stirring for 30 min at 60 °C, the reaction mixture was neutralized with a saturated aqueous $NaHCO_3$ solution and extracted with CH_2Cl_2. The combined organic extracts were dried over anhydrous Na_2SO_4 and concentrated *in vacuo*. The residue was purified by flash column chromatography on silica gel with an eluent (10:1 hexanes/EtOAc) to give **10** (1.83 g, quant.) as a yellow oil. IR (KBr): 3381, 3080, 3033, 2937, 2875, 1697, 1603 and 1458 cm^{-1}; ^{1}H-NMR (270 MHz, $CDCl_3$) δ 7.31 (m, 5H), 6.26 (d, *J*=2.0 Hz, 1H), 6.20 (d, *J*=2.0 Hz, 1H), 5.93 (m, 1H), 5.35 (dd, *J*=17.2, 1.3 Hz, 1H), 5.19 (dd, *J*=10.6, 1.3 Hz, 1H), 4.92 (s, 2H), 4.77 (br d, *J*=5.6 Hz, 2H), 2.21 (s, 3H); ^{13}C-NMR (75 MHz, $CDCl_3$) δ 169.0, 158.1, 157.5, 138.6, 136.4, 131.8, 128.3, 127.8, 127.1, 118.7, 115.7, 109.6, 98.2, 70.2, 66.0 and 19.6; HRMS (FAB, *m*–NBA): calcd. for $C_{18}H_{19}O_4$: 299.1283 $[M+H]^+$, found: *m/z* 299.1296.

2-Benzyloxy-4-(2-benzyloxy-4-methoxy-6-methyl) benzoyloxy-6-methylbenzoic acid allyl ester (11)

To a solution of **5** (0.19 g, 0.69 mmol) and **10** (0.17 g, 0.57 mmol) in toluene (2.3 ml), TFAA (0.57 ml) was added. The reaction mixture was stirred for 1 h at room temperature, quenched with H_2O and extracted with EtOAc. The combined organic extracts were dried over anhydrous Na_2SO_4 and concentrated *in vacuo*. The residue was purified by flash column chromatography on silica gel with an eluent (40:1 to 20:1 hexanes/EtOAc) to give **11** (0.32 g, quant.) as a white powder; m.p. 122–125 °C; IR (KBr): 2927, 2856, 1738, 1597 and 1437 cm^{-1}; ^{1}H-NMR (270 MHz, $CDCl_3$) δ 7.33 (m, 10H), 6.54 (d, *J*=1.7 Hz, 1H), 6.52 (d, *J*=1.7 Hz, 1H), 6.45 (d, *J*=1.7 Hz, 1H), 6.40 (d, *J*=2.0 Hz, 1H), 5.91 (m, 1H), 5.34 (dd, *J*=17.2, 1.2 Hz, 1H), 5.19 (dd, *J*=10.2, 1.2 Hz, 1H), 5.09 (s, 2H), 4.86 (s, 2H), 4.77 (br d, *J*=5.6 Hz, 2H), 3.82 (s, 3H), 2.43 (s, 3H), 2.26 (s, 3H); ^{13}C-NMR (75 MHz, $CDCl_3$) δ 167.3, 166.4, 161.8, 157.8, 156.6, 152.2, 139.0, 137.9, 136.3, 136.2, 131.9, 128.5, 128.3, 128.1, 127.8, 127.7, 127.3, 121.6, 118.5, 115.8, 115.5, 107.2, 104.2, 97.4, 70.7, 70.5, 65.8, 55.4, 20.0 and 19.4; HRMS (FAB, *m*–NBA+NaI): calcd. for $C_{34}H_{32}O_7Na$: 575.2046 $[M+Na]^+$, found: *m/z* 575.2072.

2-Benzyloxy-4-(2-benzyloxy-4-methoxy-6-methyl) benzoyloxy-6-methylbenzoic acid (12)

To a solution of **11** (0.32 g, 0.58 mmol) in THF (5.8 ml), HCOOH (0.10 ml, 2.90 mmol), Et_3N (0.40 ml, 2.90 mmol) and $Pd(PPh_3)_4$ (34.0 mg, 29.0 μmol) were added at 0 °C. The reaction mixture was stirred for 24 h at room temperature, quenched with H_2O and extracted with EtOAc. The combined organic extracts were dried over anhydrous Na_2SO_4 and concentrated *in vacuo*. The residue was purified by flash column chromatography on silica gel with an eluent (1:1 hexanes/EtOAc) to give **12** (0.29 g, 98%) as a white powder; m.p. 155–158 °C; IR (KBr): 3475, 2991, 2958, 2931, 2873, 2659, 2561, 1741, 1691, 1597 and 1442 cm^{-1}; ^{1}H-NMR (300 MHz, $CDCl_3$) δ 7.36 (m, 10H), 6.62 (d, *J*=1.8 Hz, 1H), 6.61 (d, 1H, *J*=1.8 Hz), 6.47 (d, 1H, *J*=1.9 Hz), 6.43 (d, *J*=2.1 Hz, 1H), 5.10 (s, 2H), 4.93 (s, 2H), 3.83 (s, 3H), 2.45 (s, 3H), 2.43 (s, 3H); ^{13}C-NMR (75 MHz, $CDCl_3$) δ 170.1, 166.3, 161.9, 157.9, 157.3, 152.9, 140.7, 139.2, 136.3, 135.5, 128.6, 128.5, 128.2, 128.2, 127.7, 127.4, 119.2, 117.0, 115.3, 107.3, 104.7, 97.4, 71.2, 70.7, 55.4, 20.8 and 20.1; HRMS (FAB, *m*–NBA+NaI): calcd. for $C_{31}H_{28}O_7Na$: 535.1733 $[M+Na]^+$, found: *m/z* 535.1758.

2-Benzyloxy-4-(2-benzyloxy-4-methoxy-6-methyl) benzoyloxy-6-methylbenzoyl fluoride (13)

To a solution of **12** (0.03 g, 0.06 mmol) in Et_2O/CH_2Cl_2 (2:1) (0.9 ml) DAST (18.6 μl, 0.14 mmol) was added. The reaction mixture was stirred for 1.5 h at room temperature, quenched with H_2O and extracted with CH_2Cl_2. The combined organic extracts were dried over anhydrous Na_2SO_4 and concentrated *in vacuo*. The residue was purified by flash column chromatography on silica gel with an eluent (25:1 hexanes/EtOAc) to give **13** (27.0 mg, 89%) as a white powder; m.p. 111–114 °C; IR (KBr): 3624, 3458, 3035, 2924, 2852, 1817, 1732, 1593 and 1442 cm^{-1}; ^{1}H-NMR (300 MHz, $CDCl_3$) δ 7.38 (m, 10H), 6.62 (s, 1H), 6.48 (d, *J*=2.0 Hz, 1H), 6.44 (d, *J*=1.9 Hz, 1H), 5.10 (s, 2H), 4.92 (s, 2H), 3.84 (s, 3H), 2.46 (s, 3H), 2.41 (s, 3H); ^{13}C-NMR (75 MHz, $CDCl_3$) δ 166.0, 162.0, 158.9 ($^3J_{CF}$=2.2 Hz), 158.0, 156.6 ($^1J_{CF}$=351.7 Hz), 154.5, 141.8 ($^3J_{CF}$=2.4 Hz), 139.2, 136.2, 135.6, 128.5, 128.2, 128.0, 127.7, 127.1, 116.6 ($^4J_{CF}$=2.4 Hz), 115.0, 114.5 ($^2J_{CF}$=56.2 Hz), 107.3, 104.7, 97.4, 70.7, 70.6, 55.3, 20.5 ($^4J_{CF}$=1.2 Hz), 20.0; HR-MS (FAB, *m*–NBA+NaI): calcd. for $C_{31}H_{27}FO_6Na$: 537.1684 $[M+Na]^+$, found: *m/z* 537.1687.

2-Benzyloxy-4-[2-benzyloxy-4-(2-benzyloxy-4-methoxy-6-methyl) benzoyloxy-6-methyl]benzoyloxy-6-methylbenzoic acid allyl ester (14)

To a solution of **10** (22.0 mg, 0.07 mmol) in THF (0.5 ml), NaH (6.0 mg, 0.15 mmol) was added at 0 °C under N_2. After stirring for 5 min at room temperature, a solution of **13** (26.0 mg, 0.05 mmol) in THF (0.5 ml) was added dropwise. After 30 min, the mixture was treated with MOMCl (3.8 μl, 0.05 mmol) for the conversion of an excess amount of **10** into **9** and then stirred for 30 min. The resulting mixture was quenched with H_2O and extracted with EtOAc. The combined organic extracts were dried over anhydrous Na_2SO_4 and concentrated *in vacuo*. The residue was purified by flash column chromatography on silica gel with an eluent (10:1 to 1:1 hexanes/EtOAc) to give **14** (40.0 mg, quant.) as a white powder; m.p. 183–187 °C; IR (KBr): 2925, 2858, 1741, 1597 and 1439 cm^{-1}; ^{1}H-NMR (270 MHz, $CDCl_3$) δ 7.33 (m, 15H), 6.59 (d, *J*=2.0 Hz, 1H), 6.58 (d, *J*=2.0 Hz, 1H), 6.49 (d, *J*=2.1 Hz, 1H), 6.47 (d, *J*=2.0 Hz, 1H), 6.46 (d, *J*=2.1 Hz, 1H), 6.41 (d, *J*=2.0 Hz, 1H), 5.91 (m, 1H), 5.33 (dd, *J*=17.2, 1.5 Hz, 1H), 5.18 (dd, *J*=10.5, 1.5 Hz, 1H), 5.10 (s, 2H), 4.85 (s, 2H), 4.82 (s, 2H), 4.76 (br d, *J*=5.9 Hz, 2H), 3.83 (s, 3H), 2.45 (s, 3H), 2.37 (s, 3H), 2.24 (s, 3H); ^{13}C-NMR (75 MHz, $CDCl_3$) δ 167.3, 166.4, 166.0, 161.9, 157.9, 157.0, 156.6, 152.8, 152.0, 139.1, 138.2, 137.9, 136.3, 136.2, 136.0, 132.0, 128.5, 128.5, 128.4, 128.2, 128.2, 127.9, 127.9, 127.8, 127.3, 121.8, 120.5, 118.6, 116.0, 115.7, 115.4, 107.2, 104.1, 97.4, 70.8, 70.7, 70.5, 65.8, 55.4, 20.1, 19.4 and 19.3; HRMS (FAB, *m*–NBA+NaI): calcd. for $C_{49}H_{44}O_{10}Na$: 815.2832 $[M+Na]^+$, found: *m/z* 815.2806.

2-Benzyloxy-4-[2-benzyloxy-4-(2-benzyloxy-4-methoxy-6-methyl)benzoyloxy-6-methyl]benzoyloxy-6-methylbenzoic acid (15)

To a solution of **14** (40.0 mg, 0.05 mmol) in THF (0.5 ml), HCOOH (9.4 μl, 0.25 mmol), Et_3N (34.8 μl, 0.25 mmol) and $Pd(PPh_3)_4$ (29.0 mg, 3.00 μmol) were added at 0 °C. The reaction mixture was stirred for 24 h at room temperature, quenched with H_2O and extracted with EtOAc. The combined organic extracts were dried over anhydrous Na_2SO_4 and concentrated *in vacuo*. The residue was purified by flash column chromatography on silica gel with an eluent (2:1 hexanes/EtOAc) to give **15** (38.0 mg, quant.) as a white powder; m.p. 215–216 °C; IR (KBr): 3446, 2924, 2858, 1745, 1691, 1597 and 1441 cm^{-1}; ^{1}H-NMR (270 MHz, $CDCl_3$) δ 7.40 (m, 15H), 6.60 (br s, 2H), 6.58 (d, *J*=2.0 Hz, 1H), 6.56 (d, *J*=2.1 Hz, 1H), 6.47 (d, *J*=2.2 Hz, 1H), 6.42 (d, *J*=2.3 Hz, 1H), 5.10 (s, 2H), 4.88 (s, 2H), 4.85 (s, 2H), 3.83 (s, 3H), 2.47 (s, 3H), 2.44 (s, 3H), 2.38 (s, 3H); ^{13}C-NMR (75 MHz, $CDCl_3$) δ 167.2, 166.4, 165.9, 161.9, 158.0, 157.5, 157.2, 153.0, 152.9, 142.4, 139.2, 138.4, 136.3, 136.0, 135.1, 128.8, 128.6, 128.6, 128.5, 128.3, 128.2, 128.0, 127.9, 127.7, 120.2, 118.4, 117.6, 116.1, 115.4, 107.3, 104.6, 104.2, 97.5, 71.6, 70.9, 70.8, 55.5, 21.5, 20.1 and 19.5; HRMS (FAB, *m*–NBA+NaI): calcd. for $C_{46}H_{40}O_{10}Na$: 775.2519 $[M+Na]^+$, found: *m/z* 775.2510.

(2*S*)-2{2-Benzyloxy-4-[2-benzyloxy-4-(2-benzyloxy-4-methoxy-6-methyl)benzoyloxy-6-methyl]benzoyloxy-6-methylbenzoy}aminopropionic acid benzyl ester [(+)-(16)]

To a solution of **15** (92.0 mg, 0.12 mmol) in DMF (1.2 ml), L-Ala-OBn · HCl (58.0 mg, 0.27 mmol), Et_3N (68.0 μl, 0.49 mmol) and BOP (135.0 mg, 0.30 mmol) were added. The reaction mixture was stirred for 3.5 h at room temperature, quenched with H_2O and extracted with EtOAc. The combined organic extracts were dried over anhydrous Na_2SO_4 and concentrated *in vacuo*. The residue was purified by flash column chromatography on silica gel with an eluent (3:1 to 2:1 hexanes/EtOAc) to give (+)-(**16**) (88.0 mg, 79%) as a white powder; m.p. 179–181 °C; $[\alpha]^{27}_D$ +21.5 (*c* 0.1, $CHCl_3$); IR (KBr): 2925, 1741, 1595 and 1446 cm^{-1}; ^{1}H-NMR (270 MHz, $CDCl_3$) δ 7.38 (m, 20H), 6.61 (br s, 2H), 6.51 (d, *J*=1.3 Hz, 1H), 6.48 (br s, 2H), 6.43 (d, *J*=1.6 Hz, 1H), 6.41 (d, *J*=7.6 Hz, 1H), 5.18 (d, *J*=12.3 Hz, 1H), 5.13 (d, *J*=12.3 Hz, 1H), 5.11 (s, 2H), 4.87 (s, 2H), 4.79 (m, 1H), 4.78 (s, 2H), 3.84 (s, 3H), 2.47 (s, 3H), 2.39 (s, 3H), 2.28 (s, 3H), 1.35 (d, *J*=7.0 Hz, 3H); ^{13}C-NMR (75 MHz, $CDCl_3$) δ 172.5, 166.4, 166.4, 166.2, 161.9, 157.9, 157.1, 156.2, 152.8, 151.8, 139.1, 139.1, 138.3, 136.3, 136.0, 136.0, 135.3, 128.6, 128.6, 128.6, 128.4, 128.4, 128.3, 128.2, 128.2, 128.0, 128.0, 127.8, 127.6, 123.8, 120.5, 116.2, 116.0, 115.4, 107.3, 104.2, 104.0, 97.4, 70.8, 70.8, 70.5, 67.0, 55.4, 48.1, 20.1, 19.5 and 18.3; HRMS (FAB, *m*–NBA): calcd. for $C_{56}H_{52}NO_{11}$: 914.3540 $[M+H]^+$, found: *m/z* 914.3497.

(2*S*)-2{2-Benzyloxy-4-[2-benzyloxy-4-(2-benzyloxy-4-methoxy-6-methyl)benzoyloxy-6-methyl]benzoyloxy-6-methylbenzoy}aminopropionic acid{(−)-Amidepsine B [(−)-1]}

A mixture of (+)-(**16**) (25.1 mg, 0.03 mmol) and $Pd(OH)_2$ (12.2 mg) in THF/EtOH (1:1) (2.8 ml) was stirred under H_2 atmosphere for 16 h. The mixture was filtered through a pad of Celite and the filtrate was concentrated. The residue was purified by preparative TLC on silica gel (5:1 $CHCl_3/CH_3OH$) with an eluent (3:1 $CHCl_3/CH_3OH$) to give (−)-(**1**) as a white powder (13.0 mg, 87%). Moreover, this sample was dissolved in $CHCl_3/CH_3OH$ (25:1) (5 ml) and washed with 1% aqueous H_3PO_4 (1 ml). The organic phase was dried over anhydrous Na_2SO_4 and concentrated *in vacuo* to give (−)-(**1**) (12.4 mg, 83%) as a white powder; m.p. 153–156 °C; $[\alpha]^{29}_D$ –17.3 (*c* 0.1, CH_3OH); IR (KBr): 3087, 2937, 2858, 1668, 1610 and 1454 cm^{-1}; ^{1}H-NMR (270 MHz, $CDCl_3$) δ 10.4 (br s, 1H), 8.44 (d, *J*=6.8 Hz, 1 H), 6.68 (br s, 1H), 6.66 (br s, 1H), 6.56 (br s, 1H), 6.53 (br s, 1H), 6.39 (br s, 1H), 6.36 (br s, 1H), 4.35 (m, 1H), 3.74 (s, 3H), 2.45 (s, 3H), 2.38 (s, 3H), 2.35 (s, 3H), 1.31 (d, *J*=7.1 Hz, 3H); ^{13}C-NMR (75 MHz, $CDCl_3$) δ 174.1, 166.7, 166.4, 165.8, 162.1, 159.1, 156.1, 155.0, 152.0, 150.5, 139.6, 137.8, 137.6, 123.5, 118.4, 114.1, 113.3, 110.7, 108.1, 107.1, 106.4, 99.0, 55.2, 47.6, 20.8, 19.2, 18.8 and 16.9; HRMS (FAB, *m*–NBA): calcd. for $C_{28}H_{26}NO_{11}$: 552.1506 $[M-H]^-$, found: *m/z* 552.1510.

(2*R*)-2{2-Benzyloxy-4-[2-benzyloxy-4-(2-benzyloxy-4-methoxy-6-methyl)benzoyloxy-6-methyl]benzoyloxy-6-methylbenzoy}aminopropionic acid benzyl ester [(−)-(16)]

According to the conversion of **15** into (+)-**16**, **15** (30.0 mg, 0.04 mmol) was subjected to a condensation reaction with D-Ala-OBn·*p*-TsOH (21.8 mg, 0.060 mmol) to afford (−)-(**16**) (32.6 mg, 89 %) as a white powder; m.p. 181–183 °C; $[\alpha]^{23}_D$ –8.7 (*c* 0.1, $CHCl_3$); IR (KBr): 2925, 1741, 1595 and

1446 cm^{-1}; ^{1}H-NMR (270 MHz, $CDCl_3$) δ 7.38 (m, 20H), 6.61 (br s, 2H), 6.51 (d, *J*=1.3 Hz, 1H), 6.48 (br s, 2H), 6.43 (d, *J*=1.6 Hz, 1H), 6.41 (d, *J*=7.6 Hz, 1H), 5.18 (d, *J*=12.3 Hz, 1H), 5.13 (d, *J*=12.3 Hz, 1H), 5.11 (s, 2H), 4.87 (s, 2H), 4.79 (m, 1H), 4.78 (s, 2H), 3.84 (s, 3H), 2.47 (s, 3H), 2.39 (s, 3H), 2.28 (s, 3H), 1.35 (d, *J*=7.0 Hz, 3H); ^{13}C-NMR (75 MHz, $CDCl_3$) δ 172.5, 166.4, 166.4, 166.2, 161.9, 157.9, 157.1, 156.2, 152.8, 151.8, 139.1, 139.1, 138.3, 136.3, 136.0, 136.0, 135.3, 128.6, 128.6, 128.6, 128.4, 128.4, 128.3, 128.2, 128.2, 128.0, 128.0, 127.8, 127.6, 123.8, 120.5, 116.2, 116.0, 115.4, 107.3, 104.2, 104.0, 97.4, 70.8, 70.8, 70.5, 67.0, 55.4, 48.1, 20.1, 19.5 and 18.3; HRMS (FAB, *m*–NBA+NaI): calcd. for $C_{56}H_{51}NO_{11}Na$: 936.3360 $[M+Na]^+$, found: *m*/*z* 936.3383.

(2*R*)-2{2-Benzyloxy-4-[2-benzyloxy-4-(2-benzyloxy-4-methoxy-6-methyl)benzoyloxy-6-methyl]benzoyloxy-6-methylbenzoy}aminopropionic acid{(+)-Amidepsine B [(+)-1]}

According to the conversion of (+)-**16** into (−)-**1**, (−)-(**16**) (30.8 mg, 0.03 mmol) gave (+)-(**1**) (17.7 mg, 94%) as a white powder; m.p. 156–159°C; $[\alpha]^{25}_D$ +10.4 (*c* 0.1, CH_3OH); IR (KBr): 3087, 2937, 2858, 1668, 1610 and 1454 cm^{-1}; ^{1}H-NMR (270 MHz, $CDCl_3$) δ 10.4 (br s, 1H), 8.44 (d, *J*=6.8 Hz, 1H), 6.68 (br s, 1H), 6.66 (br s, 1H), 6.56 (br s, 1H), 6.53 (br s, 1H), 6.39 (br s, 1H), 6.36 (br s, 1H), 4.35 (m, 1H), 3.74 (s, 3H), 2.45 (s, 3H), 2.38 (s, 3H), 2.35 (s, 3H), 1.31 (d, *J*=7.1 Hz, 3H); ^{13}C-NMR (75 MHz, $CDCl_3$) δ 174.1, 166.7, 166.4, 165.8, 162.1, 159.1, 156.1, 155.0, 152.0, 150.5, 139.6, 137.8, 137.6, 123.5, 118.4, 114.1, 113.3, 110.7, 108.1, 107.1, 106.4, 99.0, 55.2, 47.6, 20.8, 19.2, 18.8 and 16.9; HRMS (FAB, *m*–NBA): calcd. for $C_{28}H_{28}NO_{11}$: 554.1662 $[M+H]^+$, found: *m*/*z* 554.1663.

1 Tomoda, H., Ito, M., Tabata, N., Masuma, R., Yamaguchi, Y. & Ōmura, S. Amidepsines, inhibitors of diacylglycerol acyltransferase produced by *Humicola* sp. FO-2942. I. Production, isolation and biological properties. *J. Antibiot.* **48,** 937–941 (1995).
2 Tomoda, H., Tabata, N., Ito, M. & Ōmura, S. Amidepsines, inhibitors of diacylglycerol acyltransferase produced by *Humicola* sp. FO-2942. II. Structure elucidation of amidepsines A, B and C. *J. Antibiot.* **48,** 942–947 (1995).
3 Tomoda, H., Yamaguchi, Y., Tabata, N., Kobayashi, T., Masuma, R., Tanaka, H. & Ōmura, S. Amidepsine E, an inhibitor of diacylglycerol acyltransferase produced by *Humicola* sp. FO-5969. *J. Antibiot.* **49,** 929–931 (1996).
4 Koch, K., Podlech, J., Pfeiffer, E. & Metzler, M. Total synthesis of alternariol. *J. Org. Chem.* **70,** 3275–3276 (2005).
5 Katoh, T., Ohmori, O., Iwasaki, K. & Inoue, M. Synthetic studies on Sch 202596, an antagonist of the galanin receptor subtype GalR1: an efficient synthesis of (±)-geodin, the spirocoumaranone part of Sch 202596. *Tetrahedron* **58,** 1289–1299 (2002).
6 Nicolaou, K. C., Mitchell, H. J., Suzuki, H., Rodríguez, R. M., Baudoin, O. & Fylaktakidou, K. C. Total synthesis of everninomicin 13,384-1 Part 1: Synthesis of the A_1B(A)C fragment. *Angew Chem. Int. Ed.* **38,** 3334–3339 (1999).

The Journal of Antibiotics (2009) 62, 75–79

www.nature.com/ja

ORIGINAL ARTICLE

Albidopyrone, a new α-pyrone-containing metabolite from marine-derived *Streptomyces* sp. NTK 227 ☆

Claudia Hohmann[1,6], Kathrin Schneider[2,6], Christina Bruntner[1], Roselyn Brown[3], Amanda L Jones[3], Michael Goodfellow[3], Marco Krämer[4], Johannes F Imhoff[4], Graeme Nicholson[5], Hans-Peter Fiedler[1] and Roderich D Süssmuth[2]

Albidopyrone, a new α-pyrone-containing secondary metabolite, was produced by *Streptomyces* sp. NTK 227, a strain isolated from Atlantic Ocean sediment and found to be a member of the *Streptomyces albidoflavus* 16S rRNA gene clade. The structure of the compound was determined by MS and NMR spectroscopy, and found to have a moderate inhibitory activity against protein-tyrosin phosphatase B.
The Journal of Antibiotics (2009) **62,** 75–79; doi:10.1038/ja.2008.15; published online 9 January 2009

Keywords: fermentation; isolation; marine *Streptomyces*; α-pyrone; protein-phosphatase inhibitor; structure elucidation

INTRODUCTION

In our HPLC–diode array screening program to detect novel secondary metabolites from actinomycetes isolated from marine sediments,[1,2] extracts of culture filtrates of the strain NTK 227 were found to be of special interest. This organism, which was isolated from a marine sediment, produced a main metabolite in HPLC that runs at a retention time of 6.4 min in a standardized gradient elution profile (Figure 1). The characteristic UV–visible (Vis) spectrum of the metabolite differed from those of 867 reference compounds stored in our HPLC–UV–Vis database.[3] The metabolite was characterized as a new member of the α-pyrone family by MS and NMR spectroscopy and was named albidopyrone (**1**); its structure is shown in Figure 2. Furthermore, metabolites in the culture filtrate extract of strain NTK 227 were identified by an HPLC–diode array analysis as ferulic acid (retention time 5.9 min) and fredericamycin A (retention time 11.4 min). In the mycelium extract, several members of the antimycin A complex and two representatives of yet non-characterized heptane macrolides were monitored. This study describes the taxonomy of the producing strain, and the fermentation, isolation and structural elucidation of albidopyrone, as well as on its biological activity.

RESULTS

Taxonomy of the producing strain

Strain NTK 227 contained LL-diaminopimelic acid, hydrogenated menaquinones with nine isoprene units, produced a yellow white aerial spore mass and a brown diffusible pigment on oatmeal agar, and formed straight chains of smooth surfaced spores, properties typical of members classified in the genus *Streptomyces*.[4] The organism formed a distinct phyletic line in the *Streptomyces albidoflavus* 16S rRNA gene clade,[5] which was most closely related to the type strains of *S. albidoflavus*, *S. canescens*, *S. coelicolor*, *S. felleus*, *S. limosus* and *S. odiferus* sharing a 16S rRNA similarity with them of 99.9%, a value corresponding to eight nucleotide differences at 1429 locations; these values are consistent with the strain being seen as a new species.

Fermentation and isolation

When grown in a 10-l stirred tank fermentor, strain NTK 227 reached a maximal biomass of 8.5 mg dry weight/ml after incubation for 10 days. Production of **1** started at 72 h, reaching a maximal yield of 56 mg l^{-1} after an incubation period of 14 days.

Structure **1** was isolated from the mycelium by extraction with MeOH–Me_2CO. The extracts were concentrated to an aqueous residue, combined with the culture filtrate and separated by Amberlite XAD-16 chromatography. After extraction with *n*-BuOH, the crude product was purified by preparative reversed-phase HPLC. Structure **1** was obtained as a white powder after concentration to dryness.

Structural elucidation

The mass spectrum derived from HPLC-ESI-MS chromatograms revealed the molecular mass for **1** [$(M+H)^+$=260.2]. The exact

[1]Mikrobiologisches Institut, Universität Tübingen, Auf der Morgenstelle 28, Tübingen, Germany; [2]Institut für Chemie, Technische Universität Berlin, Berlin, Germany; [3]School of Biology, University of Newcastle, Newcastle upon Tyne, UK; [4]Institut für Meereswissenschaften IFM-GEOMAR, Kiel, Germany and [5]Institut für Organische Chemie, Universität Tübingen, Tübingen, Germany
Correspondence: Professor H-P Fiedler, Mikrobiologisches Institut, Universität Tübingen, Auf der Morgenstelle 28, Tübingen 72076, Germany.
E-mail: hans-peter.fiedler@uni-tuebingen.de or Professor RD Süssmuth, Institut für Chemie, Technische Universität Berlin, Berlin, Straß des. Juni 124, Berlin 10623, Germany.
E-mail: suessmuth@chem.tu-berlin.de
[6]These authors contributed equally to this work.
☆Art. no. 49 in 'Biosynthetic Capacities of Actinomycetes'. Art. no. 48: see ref. 1.
Received 18 November 2008; accepted 18 November 2008; published online 9 January 2009

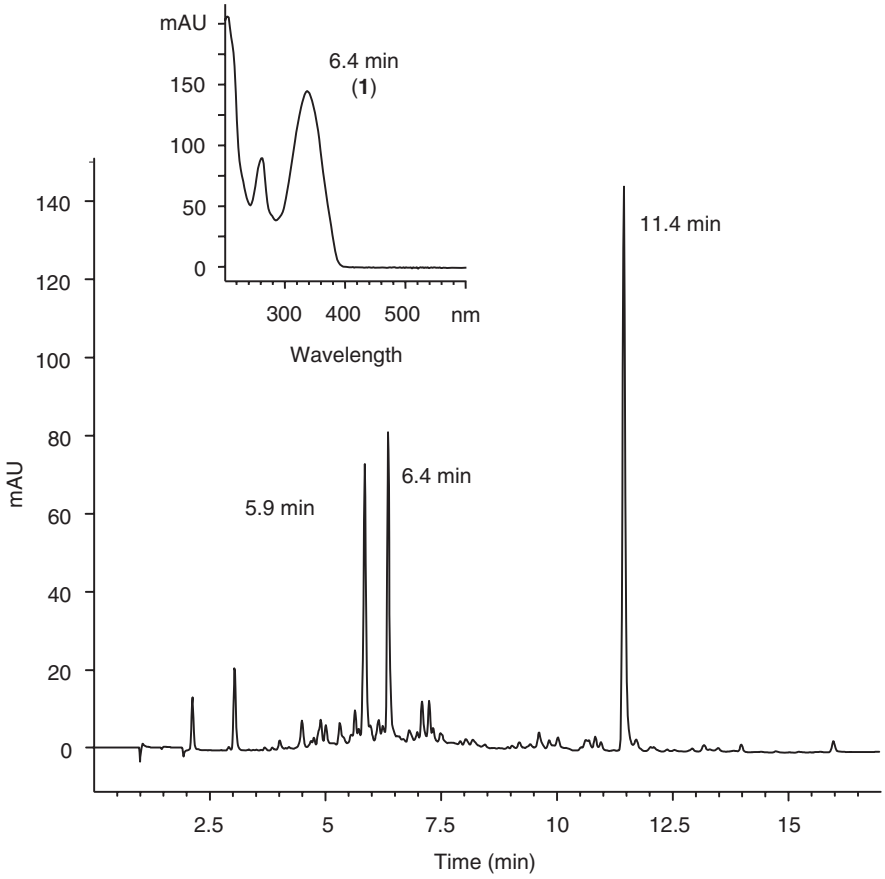

Figure 1 HPLC analysis of a culture filtrate extract from *Streptomyces albidoflavus* NTK 937 at a fermentation time of 14 days, monitored at 310 nm. 5.9 min=ferulic acid; 6.4 min=albidopyrone (**1**); 11.4 min=fredericamycin A; inset: UV–visible spectrum of **1**.

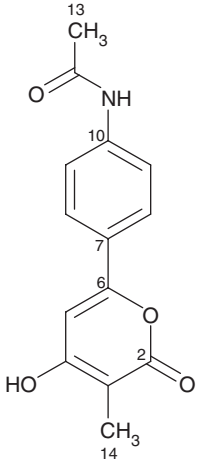

1

Figure 2 Structure of albidopyrone (**1**).

molecular mass was determined by high-resolution ESI-FT-ICR-MS as 260.09161 Da [$(M+H)^+$] (**1**), this corresponds to the molecular formula $C_{14}H_{13}NO_4$ (**1**) [$(M+H)^+_{theor}$=260.09173; Δm=0.46 p.p.m.].

The ^{1}H-NMR-spectrum of **1** showed two signals in the aromatic region, one signal at 10.2 p.p.m., one broad signal at 11.28 p.p.m. and two signals in the aliphatic region. The integration of the signals revealed that one of the two signals in the aromatic region corresponded to four protons. The other signal in the aromatic region, as well as the two signals at 10.2 p.p.m. and at 11.28 p.p.m., correspond each to one proton, and each of the two signals in the aliphatic region to three protons suggesting that two methyl groups are present in the compound (Table 1). Remarkably, the ^{13}C-NMR spectrum showed 12 signals instead of the expected 14 signals (Table 1). Comparing the ^{13}C-spectrum with the DEPT spectrum confirmed the assumption that two methyl groups are present in the compound. Furthermore, the DEPT spectrum showed three signals between 95 and 130 p.p.m.

The correlation of ^{1}H-NMR signals to the corresponding C-atoms was carried out by means of interpretation of the Heteronuclear Multiple Quantum Coherence (HMQC) NMR experiment. In accordance with the DEPT spectrum, five signals were found. The signal in the aromatic region, which corresponds to four protons, showed correlations to only two carbons. This led to the conclusion that the two of them are chemically equivalent, suggesting symmetry for this part of the molecule, and thus explains the absence of two signals in the ^{13}C-spectrum. The signals at 10.2 p.p.m. and at 11.28 p.p.m. in the ^{1}H-spectrum could not be assigned to any C-atom, suggesting the presence of two heteroatom-bound protons (OH or NH). Interestingly, no correlation was seen in the ^{1}H-^{1}H-COSY experiment. Nevertheless, the structure could be fully elucidated using the HMBC spectrum. The chemical shifts in combination with the correlations from H-5 to C-3, C-4, C-6 and C-7; from H-8 to C-6, C-8 and C-10; from H-9 to C-7 and C-9; from H-11 to C-9 and C-12; from H-13 to

Table 1 ^{1}H and ^{13}C NMR spectral data of albidopyrone (1) in DMSO-d_6

	Structure ***1*** *in DMSO*-d_6	
No.	*δ (^{1}H) (p.p.m.) J in Hz*	*δ (^{13}C) (p.p.m.)*
2	—	164.3
3	—	97.7
4	—	165.1
5	6.60 s	96.6
6	—	156.5
7	—	125.5
8	7.69 m	125.8
9	7.70 m	119.0
10	—	141.4
11	10.20 s	—
12	—	168.7
13	2.06 s	24.1
14	1.81 s	8.7
OH	11.28 bs	—

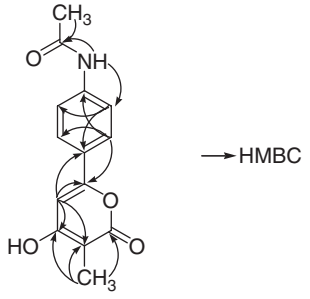

1

Figure 3 Selected 2D NMR correlations for albidopyrone (**1**).

C-12; and from H-14 to C-2, C-3 and C-4, shown in Figure 3, provided proof for the structure of **1**, particularly for the position of the methyl groups, of the amide and hydroxy function, respectively.

The physico-chemical properties of albidopyrone (**1**) are summarized in Table 2.

Biological activity

Albidopyrone (**1**) did not show any growth inhibitory activity either against the Gram-negative bacteria (*Escherichia coli* and *Pseudomonas fluorescens*) and Gram-positive bacteria (*Bacillus subtilis* and *S. lentus*) or against the yeast (*Candida glabrata*). Structure **1** inhibited the PTP1B with an IC_{50} of 128 μg ml^{-1}.

DISCUSSION

Herein we report on the fermentation, isolation, structural elucidation and the evaluation of the biological activity of albidopyrone (**1**), a metabolite that contains a 4-hydroxy-2-pyrone unit as its characteristic structural feature. α-Pyrones represent a class of six-membered lactones that are sub-structures of various natural products and which are highly abundant in animals, bacteria, insects and plants.[6] They exhibit a wide range of biological activities, such as antifungal, cytotoxic, neurotoxic and phytotoxic properties.[6,7] The structural highly related benzo-α-pyrones **2**, **3**, **4** and **5** (Figure 4) have been

Table 2 Physico-chemical properties of albidopyrone (1)

	Structure ***1***
Appearance	White powder
Molecular weight	259
Molecular formula	$C_{14}H_{13}NO_4$
ESI-FT-ICR MS (*m/z*)	
Found	260.09161 $(M+H)^+$
Calcd	260.09173 $(M+H)^+$
UV λ_{max}^{MeOH} (nm) (ε (cm^2 mmol^{-1}))	203 (8.3), 262 (4.2), 338 (6.63)
IR ν_{max} (cm^{-1})	3421, 3239, 3185, 3103, 3077, 3062, 2956, 2922, 2853, 2747, 2706, 1672, 1654, 1636, 1597, 1580, 1533, 1426, 1400, 1370, 1155

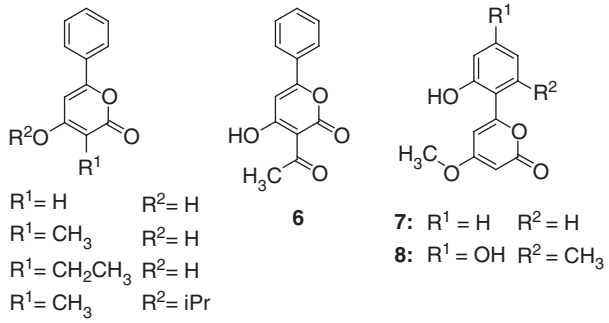

2: R^1= H R^2= H
3: R^1= CH_3 R^2= H
4: R^1= CH_2CH_3 R^2= H
5: R^1= CH_3 R^2= iPr

7: R^1 = H R^2 = H
8: R^1 = OH R^2 = CH_3

Figure 4 Structures of natural and synthetic α-pyrones.

synthesized, and their biological activities evaluated to some extent.[6–10] The competitive inhibition of HIV-1 protease by **2**, **4** and some other derivatives has been explored, revealing that the pyran-2-one group, the 4-hydroxyl group, and the substitution at position 3 were necessary for inhibitory activity.[9] Moreover, 4-hydroxy-2-pyrones have become one of the most important classes of anti-HIV agents in recent years.[6] These non-peptide compounds seem to be promising candidates for treatment of AIDS. In comparison with peptides, the small α-pyrones are interesting lead candidates for synthetic strategies because of their lack of chiral centers.[6,9] Recently, Lin *et al.*[11] isolated two new 5-hydroxy-2-pyrone derivatives from a marine *Aspergillus flavus* strain, which might prove to be ligands for G-protein-coupled receptors.

Some structurally related benzo- and phenyl-α-pyrones have been isolated from plants, such as **6**, **7** and **8**; the structures of these compounds are shown in Figure 4. Pogopyrone B (**6**) was isolated from *Pogostemon heynianus*,[12,13] whereas 6-(2-hydroxyphenyl)-4-methoxy-2-pyrone (**7**) was isolated in a bioassay-guided purification of ether extracts from *Alpinia officinarum*,[14] this metabolite exhibited a potent platelet-activating factor receptor-binding inhibitory activity. The aloenin aglycon (**8**) was isolated from the leaf exudate of *Aloe nyeriensis* var. *kedongensis* along with the *O*-glycosylated aloenin.[15] The hitherto unknown albidopyrone (**1**) extends the structural diversity of this group of natural products. In particular, the amide function at C-10 has never been reported in related compounds neither in synthetic nor in natural products.

Albidopyrone (**1**) inhibited specifically the PTP1B, other biological activities have yet to be found. Protein tyrosine phosphatases and their counterpart protein tyrosine kinases leading to reversible protein

tyrosine phosphorylation are of importance in the regulation of various cellular signal transduction systems. PTP1B is the major negative regulator of insulin signaling because it regulates the phosphorylation state of the insulin receptor or insulin receptor substrate.[16] Type II diabetes and obesity are characterized by resistance to insulin because of attenuated or diminished signaling from the receptors. Therefore, pharmacological agents capable of inhibiting PTP1B can increase the action of insulin, and thus serve as a very attractive target for treatment of both type II diabetes and obesity and various inhibitors were identified.[16,17]

MATERIALS AND METHODS

Producing organism and taxonomy

Strain NTK 227 was isolated from Atlantic Ocean sediment. The organism was examined for chemotaxonomic and morphological properties known to be of value in streptomycete systematics.[18,19] 16S rRNA gene amplification and sequencing were carried out using an established method,[20] and the resultant almost complete sequence compared with corresponding sequences of *Streptomyces* type strains using the neighbor-joining algorithm.[21]

Fermentation and isolation

Batch fermentations of strain NTK 227 were carried out in a 10-liter stirred tank fermentor (Biostat E; B Braun, Melsungen, Germany) in a complex medium that consisted of (per liter tap water) oatmeal (Holo Hafergold, Neuform, Germany) 20 g and trace element solution 5 ml, which was composed of (per liter deionized water) $CaCl_2 \times 2H_2O$ 3 g, iron(III) citrate 1 g, $MnSO_4 \times 1H_2O$ 200 mg, $ZnCl_2$ 100 mg, $CuSO_4 \times 5H_2O$ 25 mg, $Na_2B_4O_7 \times 10H_2O$ 20 mg, $CoCl_2 \times 6H_2O$ 4 mg and $Na_2MoO_4 \times 2H_2O$ 10 mg; the pH was adjusted to 7.3 (5 M HCl) before sterilization. The fermentor was inoculated with 5% by volume of a shake flask culture grown in a seed medium at 27 °C in 500-ml Erlenmeyer flasks with a single baffle for 72 h on a rotary shaker at 120 r.p.m. The seed medium consisted of glucose 10 g, glycerol 10 g, oatmeal 5 g, soybean meal (Schoenenberger, Magstadt, Germany) 10 g, yeast extract (Ohly Kat, Deutsche Hefewerke, Hamburg, Germany) 5 g, Bacto casamino acids 5 g and $CaCO_3$ 1 g in 1 l tap water. The fermentation was carried out for 14 days at an aeration rate of 0.5 volume air/volume/min and with agitation at 250 r.p.m. The pH was kept constant at 7.0 during the whole fermentation period.

Hyphlo Super-cel (2%) was added to the fermentation broth, and the resultant preparation was separated by multiple sheet filtration into culture filtrate and mycelium. The mycelium was extracted three times with 1 l MeOH–Me_2CO (1:1). The mycelium extracts were concentrated *in vacuo* to an aqueous residue (500 ml), combined with the culture filtrate (6 l) and applied to an Amberlite XAD-16 column (resin volume 800 ml). The resin was washed with each of 3.2 l H_2O and H_2O–MeOH (8:2); albidopyrone (**1**) was eluted with 2.4 l H_2O–MeOH (2:8) and concentrated *in vacuo* to an aqueous residue. After defatting with 250 ml petroleum benzene (40–60 °C), the concentrate was extracted six times with *n*-BuOH (1 l in total), and the organic extracts combined and concentrated *in vacuo* to dryness (3.4 g). The crude product was dissolved in DMSO; 1 ml of this preparation was diluted with the same volume H_2O directly before separation and subject to preparative HPLC (LaPrep P110; VWR, Darmstadt, Germany) using a C18 column (Nucleosil 100 C-18, 10 µm, 250×16 mm; Maisch, Ammerbuch, Germany) with 0.5% HCOOH–MeOH (a linear gradient from 30 to 50% MeOH over 15 min) at a flow rate of 24 ml min^{-1}. The eluate was monitored at 240 and 360 nm. Structure **1**-containing fractions were combined and concentrated *in vacuo* to dryness and a white powder (130 mg) was obtained.

HPLC–diode array detection analyses

The chromatographic system consisted of an HP 1090M liquid chromatograph equipped with a diode-array detector and an HP Kayak XM 600 ChemStation (Agilent, Waldbronn, Germany). Multiple wavelength monitoring was performed at 210, 230, 260, 280, 310, 360, 435 and 500 nm, and UV–Vis spectra measured from 200 to 600 nm. A 10-ml aliquot of the fermentation broth was centrifuged, and the supernatant adjusted to pH 4.0 and extracted with the same volume of EtOAc. After centrifugation, the organic layer was concentrated to dryness *in vacuo* and resuspended in 1 ml MeOH. Aliquots of the samples, in volumes of 10 µl, were injected into an HPLC column (125×4.6 mm) fitted with a guard-column (20×4.6 mm) filled with 5-µm Nucleosil-100 C-18 (Maisch). The samples were analyzed by linear gradient elution using 0.1% *ortho*-phosphoric acid as solvent A and MeCN as solvent B at a flow rate of 2 ml min^{-1}. The gradient was from 0 to 100% for solvent B in 15 min with a 2-min hold at 100% for solvent B.

Structural elucidation

LC-MS experiments were performed on an Applied Biosystems QTrap 2000 (Applied Biosystems, Darmstadt, Germany) coupled to an Agilent 1100 HPLC system (Agilent). High-resolution ESI-FT-ICR mass spectra were recorded on an APEX II FTICR mass spectrometer (4.7 T; Bruker-Daltronics, Bremen, Germany) and NMR experiments on a DRX 500 NMR spectrometer (Bruker, Karlsruhe, Germany) equipped with a BBI probe head with *z* gradients. DMSO-d_6 was used as a solvent for NMR experiments and chemical shifts are referenced to tetramethylsilane.

Biological activity

An agar plate diffusion assay was used to determine the antibacterial and antifungal properties of albidopyrone (**1**) using *Escherichia coli* K12 (DSM 498), *Pseudomonas fluorescens* (NCIMB 10586), *Bacillus subtilis* (DSM 347), *Staphylococcus lentus* (DSM 6672) and *Candida glabrata* (DSM 6425).

Analysis of the effect of **1** on human recombinant protein tyrosine phosphatase 1B (PTP1B) was carried out with final concentrations of the substance of 20 µg ml^{-1} in PTP1B assay buffer containing 100 mM Hepes buffer (pH 7.2), 2 mM EDTA, 2 mM dithiothreitol and 0.1% nonylphenylpolyethylene glycol (NP-40) (Cat. no. KI-131; Biomol, Hamburg, Germany), 5 ng bovine serum albumin and 3 ng (150 U (150 pmol min^{-1})) recombinant human PTP1B (Cat. no. SE332-0050; Biomol) in a volume of 45 µl per well. The reaction was started with 5 µl of the 1.5 mM PTP1B phosphopeptide substrate EGFR (988-998) (Cat. no. P323-0001; Biomol) dissolved in PTP1B assay buffer. After an incubation period of 15 min at 30 °C, the reaction was stopped by adding 100 µl of Biomol Green (Cat. no. AK111-9090; Biomol); the *ortho*-phosphate concentration was quantified after incubating for 20 min at room temperature. Optimal density was measured at 620 nm using the microtiter plate reader Infinite M200 (Tecan). As a positive control for inhibition of PTP1B, 200 µM of RK-682 (Cat. no. 557322-200UG; Calbiochem) was added instead of the test substance.

ACKNOWLEDGEMENTS

This work was supported by Boehringer-Ingelheim Pharma GmbH (Biberach, Germany), the European Commission (project ACTINOGEN, 6th framework, Grant LSHM-CT-2004-005224). We thank Mr G Grewe, Universität Tübingen, for technical assistance in the fermentations, and Agilent Technologies (Waldbronn, Germany) for HPLC software support.

1 Hohmann, C. *et al*. Caboxamycin, a new antibiotic of the benzoxazole family, produced by the deep-sea strain *Streptomyces* sp. NTK 937. *J. Antibiot.*, in press.
2 Fiedler, H.-P. *et al*. Marine actinomycetes as a source of novel secondary metabolites. *Antonie van Leeuwenhoek* **87,** 37–42 (2005).
3 Fiedler, H.-P. Biosynthetic capacities of actinomycetes. 1. Screening for novel secondary metabolites by HPLC and UV–visible absorbance libraries. *Nat. Prod. Lett.* **2,** 119–128 (1993).
4 Manfio, G. P., Zakrezewska-Czerwinska, J., Atalan, E. & Goodfellow, M. Towards minimal standards for the description of *Streptomyces* species. *Bioteckhnologia* **7–8,** 242–253 (1995).
5 Lanoot, B. *et al*. Grouping of streptomycetes using 16S-ITS RFLP fingerprinting. *Res. Microbiol*. **156,** 755–762 (2005).
6 McGlacken, G. & Fairlamb, I. J. S. 2-Pyrone natural products and mimetics: isolation, characterisation and biological activity. *Nat. Prod. Rep.* **22,** 369–385 (2005).
7 Katritzky, A. R., Wang, Z., Wang, M., Hall, C. D. & Suzuki, K. Facile syntheses of 2,2-dimethyl-6-(2-oxoalkyl)-1,3-dioxin-4-ones and the corresponding 6-substituted 4-hydroxy-2-pyrones. *J. Org. Chem.* **70,** 4854–4856 (2005).

8 Morris, J., Luke, G. P. & Wishka, D. G. Reaction of phosgeniminium salts with enolates derived from Lewis acid complexes of 2′-hydroxypropiophenones and related β-diketones. *J. Org. Chem.* **61,** 3218–3220 (1996).
9 Tummino, P. J., Ferguson, D., Huper, L. & Hupe, D. Competitive inhibition of HIV-1 protease by 4-hydroxy-benzopyran-2-ones and by 4-hydroxy-6-phenylpyran-2-ones. *Biochem. Biophys. Res. Commun.* **200,** 1658–1664 (1994).
10 Liebeskind, L. S. & Wang, J. A synthesis of substituted 2-pyrones by carbonylative cross-coupling-thermolysis of 4-halocyclobutenones with alkenyl-, aryl-, and heteroarylstannanes. *Tetrahedron* **49,** 5461–5470 (1993).
11 Lin, A. *et al.* Two new 5-hydroxy-2-pyrone derivatives isolated from a marine-derived fungus *Aspergillus flavus*. *J. Antibiot.* **61,** 245–249 (2008).
12 Thailambal, V. G. & Pattabhi, V. Structure of 3-acetyl-4-hydroxy-6-phenyl-2-pyrone, $C_{13}H_{10}O_4$. *Acta Crystallogr. C* **41,** 802–804 (1985).
13 Purushothaman, K. K., Sarada, A. & Connolly, J. D. Structures of pogopyrones A and B. *Indian J. Chem., Sect B, Org. Chem. Med. Chem.* **23B,** 611–614 (1984).
14 Fan, G., Kang, Y.-H., Han, Y. N. & Han, B. H. Platelet-activating factor (PAF) receptor binding antagonists from *Alpinia officinarum*. *Bioorg. Med. Chem. Lett.* **17,** 6720–6722 (2007).
15 Conner, J. M., Gray, A. I., Reynolds, T. & Waterman, P. G. Anthraquinone, anthrone and phenylpyrone components of *Aloe nyeriensis* var. *kedongensis* leaf exudate. *Phytochemistry* **26,** 2995–2997 (1987).
16 Zhang, S. & Zhang, Z.-Y. PTP1B as a drug target: recent developments in PTP1B inhibitor discovery. *Drug Discov. Today* **12,** 373–381 (2007).
17 Taylor, S. D. Inhibitors of protein tyrosine phosphatase 1B (PTP1B). *Curr. Top. Med. Chem.* **3,** 759–782 (2003).
18 Williams, S. T., Goodfellow, M. & Alderson, G. Genus *Streptomyces* Waksman and Henrici 1943, 339^{AL}. in: Williams S.T., *et al. Bergey's Manual of Systematic Bacteriology*, Vol. 4. (eds Williams, S. T. *et al.*) (Williams & Wilkins, Baltimore, 1989).
19 Xu, C. *et al.* Neutrotolerant acidophilic *Streptomyces* species isolated from acidic soils in China: *Streptomyces guanduensis* sp.nov., *Streptomyces paucisporus* sp. nov., *Streptomyces rubidus* sp. nov. and *Streptomyces yanglinensis* sp. nov. *Int. J. Syst. Evol. Microbiol.* **56,** 1109–1115 (2006).
20 Kim, S. B., Falconer, C., Williams, S. T. & Goodfellow, M. *Streptomyces thermocarboxydovorans* sp. nov. and *Streptomyces thermocarboxydus* sp. nov., two moderately thermophilic carboxydotrophic species from soil. *J. Syst. Bacteriol.* **48,** 59–88 (1998).
21 Saitou, N. & Nei, M. The neighbour-joining method: a new method for reconstructing phylogenetic trees. *Mol. Biol. Evol.* **4,** 406–425 (1987).

The Journal of Antibiotics (2009) 62, 81–87

www.nature.com/ja

ORIGINAL ARTICLE

Synergistic fungicidal activities of polymyxin B and ionophores, and their dependence on direct disruptive action of polymyxin B on fungal vacuole

Akira Ogita[1], Yukiko Konishi[2], Baiyinlang Borjihan[2], Ken-ichi Fujita[2] and Toshio Tanaka[2]

Polymyxin B (PMB) acts selectively on Gram-negative bacteria by electrostatic and hydrophobic interactions with anionic cell envelope components such as phospholipids and lipopolysaccharides. In this study, PMB was shown to exhibit marked fungicidal activity against yeasts and filamentous fungi in combination with ionophores such as salinomycin (SAM) and monensin (MON), which can selectively interact with monovalent cations. Ca^{2+}-selective ionophores, A23187 and ionomycin, were absolutely ineffective in enhancing the fungicidal activity of PMB. SAM and MON increased the rate of cellular uptake of PMB possibly in favor of its intracellular action on the organelle. PMB could indeed directly disrupt the spherical membrane-enclosed architecture of the isolated vacuoles equally in the absence and presence of the ionophores. The loss of energy barrier for transmembrane transport of monovalent cations is considered to be a cause of enhanced incorporation of larger cationic compounds such as PMB across fungal plasma membrane.
The Journal of Antibiotics (2009) **62,** 81–87; doi:10.1038/ja.2008.13; published online 9 January 2009

Keywords: *Aspergillus niger*; *Candida albicans*; ionophores; polymyxin B; *Saccharomyces cerevisiae*; vacuole

INTRODUCTION

Polymyxin B (PMB; Figure 1), a complex antibacterial antibiotic produced by *Bacillus polymyxa*, consists of a cyclic heptapeptide moiety, a straight tripeptide side chain, and a fatty acid attached to the N terminus of the side chain.[1] The molecule carries five positively charged residues of diaminobutyric acid. Owing to its charge and amphiphilicity, PMB may be prevented from penetration into the outer membrane of Gram-negative bacteria. However, PMB binds to lipopolysaccharide so as to form a complex and increases the permeability of the outer membrane to a variety of molecules, including also its own uptake.[2] In addition, when yeast cells are incubated with PMB at the concentration too low to affect their growth in the presence of various antibiotics, for instance tetracycline or miconazole, PMB increases the permeability of plasma membrane to each antibiotic and their combinations can induce cell death.[3–5] In our recent study, PMB was found to cause vacuolar membrane-disruptive damage in *Saccharomyces cerevisiae* cells when this bactericidal antibiotic is added alone at a high concentration and also at a non-lethal concentration in combination with allicin (Figure 1), an allyl sulfur compound from garlic.[6]

The vacuole-disruptive damage in fungi was first observed when *S. cerevisiae* cells were treated with a polyol macrolide antibiotic niphimycin (NM).[7,8] NM consists of two major structural domains such as polyol lactone ring and alkylguanidinium chain attached to the ring. These molecular domains were suggested to interact with each other for exhibition of the vacuole-targeting fungicidal activity.[9] This was later supported by a synergistic cooperation between the synthetic analog of this alkyl side chain and a polyene macrolide antibiotic amphotericin B (AmB) as a substitute for the lactone ring of NM.[7] In another experiment using *S. cerevisiae* cells, AmB was shown to exhibit a vacuole-targeting fungicidal activity at a high concentration under hypoosmotic condition, and the AmB-induced intracellular lethal event was also markedly enhanced in the presence allicin.[10] We are focusing our attention to the enhancement effect of allicin and consider its inhibitory effect on a mechanism of ergosterol trafficking from the plasma membrane to the vacuolar membrane to be a cause of enhancement of the vacuole-targeting activity of AmB (A. Ogita *et al.*, unpublished results). Allicin could alternatively facilitate the vacuole-targeting fungicidal activity of PMB because of its role as an enhancer of cellular uptake of this cationic cyclic peptide.[6] These findings highly suggest a possibility to apply PMB for antifungal chemotherapy if its vacuole-targeting activity can be enhanced with a compound that is more suitable for clinical use than allicin.

[1]Research Center for Urban Health and Sports, Osaka City University, Sumiyoshi-ku, Osaka, Japan and [2]Department of Biology and Geosciences, Graduate School of Science, Osaka City University, Sumiyoshi-ku, Osaka, Japan
Correspondence: Dr T Tanaka, Department of Biology and Geosciences, Graduate School of Science, Osaka City University, 3-3-138 Sugimoto, Sumiyoshi-ku, Osaka 558-8585, Japan.
E-mail: tanakato@sci.osaka-cu.ac.jp
Received 19 November 2008; accepted 19 November 2008; published online 9 January 2009

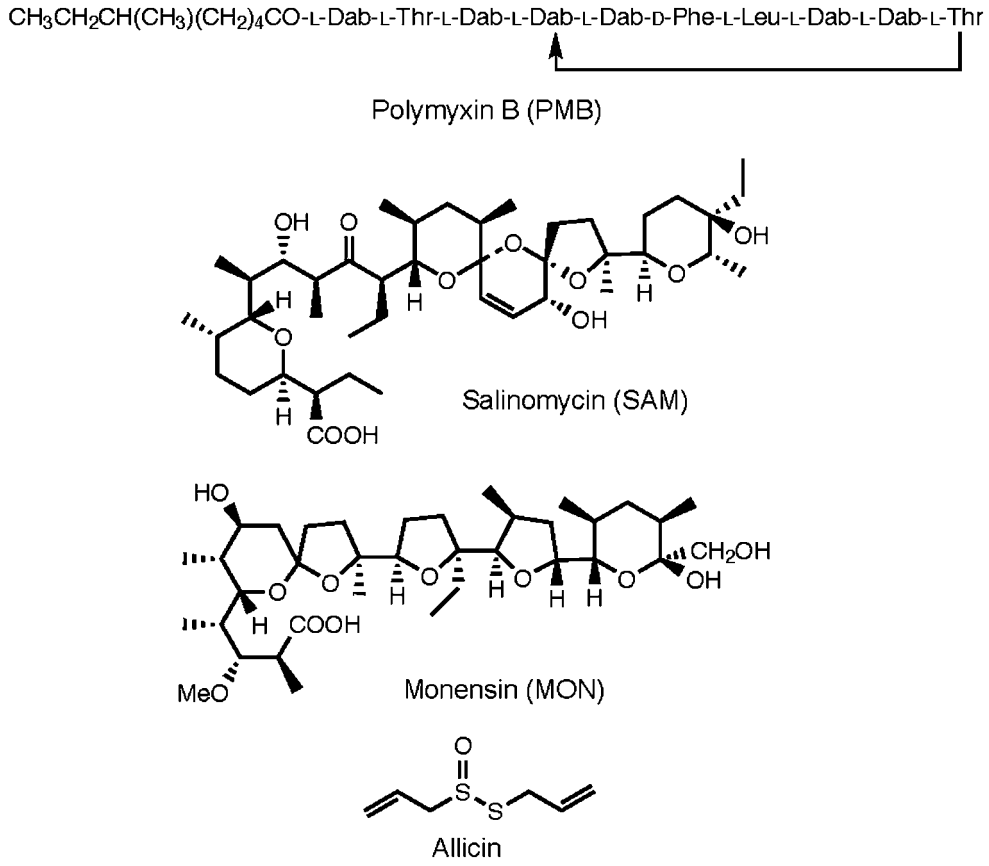

Figure 1 Structures of PMB, SAM, MON, and allicin. MON, monensin; PMB, polymyxin B; SAM, salinomycin.

Salinomycin (SAM) is a fermentation product of *Streptomyces albus*, whereas monensin (MON) is from *Streptomyces cinnamonensis*.[11] These compounds belong to monovalent carboxylic ionophorous polyether antibiotics that interfere with the plasma membrane ion transport system (Figure 1). Ionophores generally lower the energy barrier necessary for the transmembrane transport of ions and catalyze an electroneutral cation–proton exchange across the barrier. Consequently, they abolish the gradients of K^+, Na^+, Ca^{2+}, and Mg^{2+} depending on the affinity to each of these metal ions.[12] SAM transports K^+ more efficiently than Na^+, whereas MON transports Na^+ more efficiently than K^+.[13] The cell walls of most Gram-negative bacteria do not permit the penetration of hydrophobic compounds with molecular weights of $\geqslant 600$, and thus render the bacterial cells mostly resistant to the action of ionophores.[12] Instead, SAM and MON can effectively inhibit the growth of Gram-positive bacteria, and have been used as antimicrobial growth promoters in animal feed especially for bovine and swine.[14]

In this study, we found a synergistic relationship between PMB and each of these ionophores in the growth inhibition of pathogenic fungal strains such as *Candida albicans* and *Aspergillus niger* in addition to *S. cerevisiae*. PMB could indeed disintegrate the vacuolar membrane of both *S. cerevisiae* and *A. niger* cells at a non-lethal concentration in combination with either SAM or MON, and was found to cause disruptive damages directly on the vacuoles isolated from *S. cerevisiae* cells by its own action. Our study suggests that the plasma membrane barrier against monovalent cations also functions for preventing incorporation of positively charged larger compounds such as PMB into cells.

MATERIALS AND METHODS

Measurement of cell growth and viability

MICs of PMB, SAM, and MON were determined against *Escherichia coli* IFO 3545, *Bacillus subtilis* IFO 3007, *S. cerevisiae* W303-1A, *C. albicans* IFO 1061, *A. niger* ATCC 6275, and *Mucor mucedo* IFO 7684 according to our earlier described method.[6,7] The effects of PMB and these ionophores on cell viability were also examined against *S. cerevisiae* by counting viable cell numbers as colony-forming units.

Assay of plasma membrane phospholipid peroxidation

The extent of plasma membrane phospholipid peroxidation was examined using a florescence probe, diphenyl-1-pyrenylphosphine, as reported earlier.[15,16] The fluorescence intensities of the cell suspensions were measured using an FP-1520S fluorescence detector (JASCO, Tokyo, Japan), in which the wavelengths of excitation and emission were adjusted at 351 nm and at 380 nm, respectively. The arbitrary units were based directly on fluorescence intensity.

Vacuole isolation

Vacuoles were isolated from *S. cerevisiae* cells according to the earlier described methods[17–19] with the following modifications: cells were grown overnight in YPD medium, harvested by centrifugation, and suspended in the spheroplasting buffer (50 mM Tris-HCl, pH 7.5; 1.0 M sorbitol; 10 mM sodium azide; 0.5% 2-mercaptoethanol) at the density of 1×10^9 cells/ml, and the cell suspension was incubated at 30 °C for 30 min. After the addition of Yeast Lytic Enzyme at 5.0 mg ml^{-1} in the cell suspension, cells were converted to spheroplasts by incubation at 30 °C for 60 min with gentle agitation. The spheroplasts were collected by centrifugation, carefully washed with the vacuole-isolating buffer (10 mM sodium citrate, pH 6.8; 0.6 M sorbitol), and suspended in the buffer at 5×10^9 cells/ml. Further procedures were all carried out on ice. The spheroplasts were homogenized by 20 strokes in a Dounce homogenizer. The homogenate (15 ml) was transferred to an centrifugation tube, gently overlaid with 10 ml of

the vacuole-isolating buffer containing 7.0% Ficoll and 10 ml of the buffer containing 8.0% Ficoll on the top, and centrifuged (3000*g*) at 4 °C for 30 min. Vacuoles were collected from the 0 to 7.0% Ficoll interface.

Vacuole staining

Vacuoles were visualized according to the method of Vida and Emr[20] as follows: *S. cerevisiae* cells were grown overnight in YPD medium at 30 °C and harvested by centrifugation. *A. niger* cells were pre-incubated for 24 h in malt extract medium at 30 °C with shaking and harvested by filtration. These fungal cells were washed with fresh medium and suspended in each of the above media to obtain a density of 1×10^7 cells/ml (*S. cerevisiae*) or to obtain the original mycelial concentration (*A. niger*). The fluorescent probe FM4-64 was added to the cell suspensions at a final concentration of 5.0 μM. Cells were then incubated with shaking at 30 °C for 30 min, and then harvested and washed again with the fresh medium. Cells were finally suspended in the fresh medium to obtain a density of 1×10^7 cells/ml (*S. cerevisiae*) or to obtain the original mycelial concentration (*A. niger*). These cell suspensions were shaken in the absence and the presence of each compound at 30 °C for 120 min. Cells were then observed under the bright field and fluorescence microscope with excitation at 480 nm and emission at 530 nm.

HPLC analysis of PMB

S. cerevisiae cells were grown overnight in YPD medium and harvested by centrifugation. Cells were washed with YPD medium and suspended in the medium to obtain a density of 1×10^8 cells/ml. The cell suspensions were then shaken with PMB in the absence and the presence of each ionophore at 30 °C for 120 min. The supernatants obtained after cell removal by centrifugation were assayed for PMB content by HPLC using a reverse-phase column (4.7 by 250 mm, YMC-Pack ODS-AM, YMC Inc., Wilmington, NC, USA). The chromatographic solvents were 0.1% (v/v) trifluoroacetic acid in water (solvent A) and 0.075% (v/v) trifluoroacetic acid in CH_3CN (solvent B). A linear gradient was achieved from 10 to 80% of solvent B in 20 min at a flow rate of 1.0 ml min^{-1} and the absorbance was monitored at 210 nm.

Chemicals

PMB sulfate, SAM sodium salt, and ionomycin were purchased from Wako Pure Chemical Industries (Osaka, Japan). MON sodium salt and A23187 were obtained from Sigma Aldrich (St Louis, MO, USA). The fluorescent probe FM4-64 and diphenyl-1-pyrenylphosphine were products of Molecular Probe (Eugene, OR, USA) and Dojindo (Kumamoto, Japan), respectively. Ficoll 400 was from Alfa Aesar (Ward Hill, MA, USA), and Yeast Lytic Enzyme was from ICN Biomedicals (Aurora, OH, USA). The other chemicals used were of analytical reagent grade.

RESULTS AND DISCUSSION

Synergy between PMB and ionophores

PMB has been re-evaluated for its clinical use because of the lower toxicities than those reported earlier.[21] This cyclic peptide could also be valuable as an antifungal antibiotic when fungal cells are made susceptible to its vacuole-targeting activity with the aid of another agent such as allicin. In our screening experiment, SAM and MON were selected as such agents that can amplify the growth inhibitory activity of PMB on *S. cerevisiae* cells among a number of antibiotics and drugs. The combination effects of PMB and either SAM or MON were then examined against bacteria, yeasts, and filamentous fungi by using the checkerboard technique. As shown in Figure 2a, PMB exhibited a potent growth inhibitory activity on *E. coli*, a Gram-negative bacterium, at 3.13 μg ml^{-1}, and the MIC remained unchanged with increasing concentration of SAM or MON up to 400 μg ml^{-1}. On the contrary to the fact, these ionophores were equally effective in inhibiting the growth of *B. subtilis*, a Gram-positive bacterium, at 0.78 μg ml^{-1}, whereas their MICs were kept unchanged with increasing concentration of PMB (Figure 2b). Unlike the case with these bacterial strains, PMB exhibited a growth inhibitory activity on *S. cerevisiae* at a quite high concentration of 200 μg ml^{-1}, but the MIC drastically decreased to 3.13 and 12.5 μg ml^{-1} with increasing

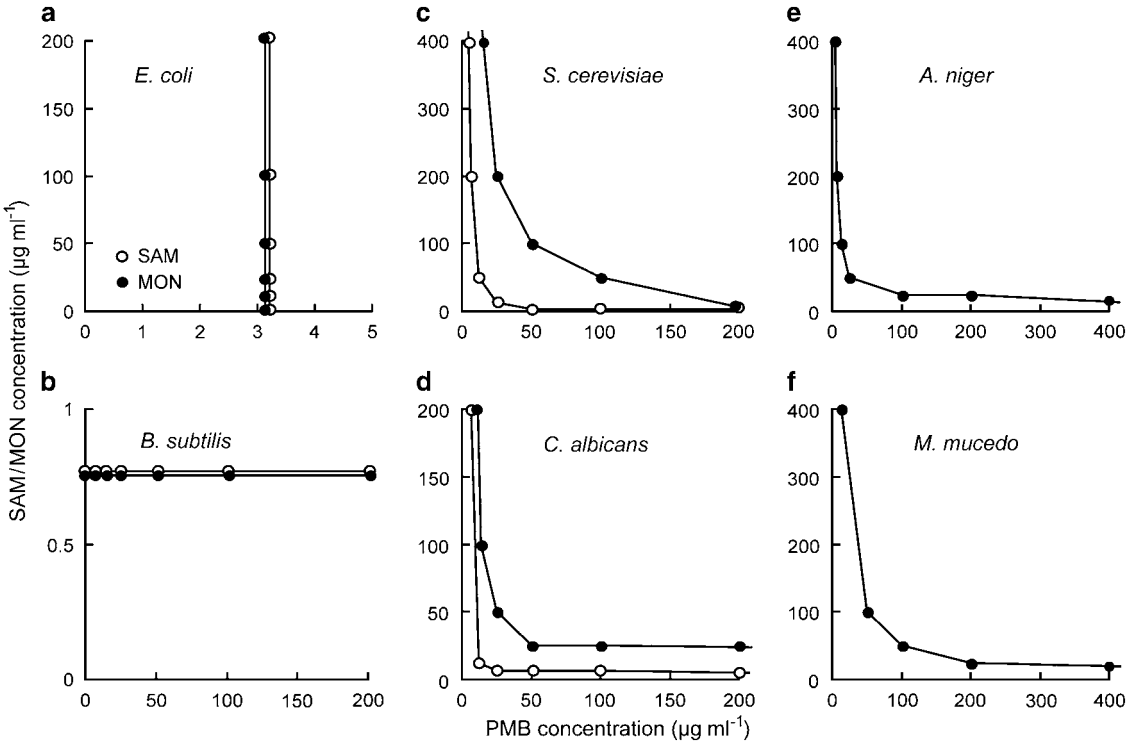

Figure 2 Isobolograms showing synergy of PMB and each of SAM and MON. Each point represents a combination of the MICs of PMB and either SAM (○) or MON (●) against *Escherichia coli*, *Bacillus subtilis*, *Saccharomyces cerevisiae*, *Candida albicans*, *Aspergillus niger*, and *Mucor mucedo*.

concentrations of SAM and MON, respectively, up to 400 μg ml^{-1} (Figure 2c).

Such synergistic relationships were more markedly observed against *C. albicans*, though this pathogenic yeast was less sensitive to PMB than *S. cerevisiae* (Figure 2d). SAM was superior to MON as a counterpart of PMB at least in inhibiting the growth of these yeast strains, but this K^+ ionophore was absolutely ineffective in inhibiting the growth of filamentous fungi such as *M. mucedo* and *A. niger* at 400 μg ml^{-1} even in combination with PMB at 400 μg ml^{-1}. On the other hand, MON could render cells of these filamentous fungi sensitive to PMB, suggesting the dependence of their elevated sensitivities to a type of ionophore, which is characterized by more increased selectivity toward Na^+ than K^+ (Figures 2e and f). It was therefore confirmed whether the fungicidal activity of PMB could be enhanced by two different types of ionophore, A23187 and ionomycin, which are selective for divalent cations such as Ca^{2+} (refs 22, 23). The MIC of PMB against *S. cerevisiae* remained at a constant level of 200 μg ml^{-1} equally in the absence and the presence of each Ca^{2+} ionophore. These results highly supported the dependence of PMB-mediated fungal growth inhibition on the plasma membrane function involved in the permeability to monovalent cations.

The mode of growth inhibition by PMB was examined using *S. cerevisiae* cells in the absence and the presence of either SAM or MON by means of the colony-counting method. These ionophores scarcely caused lethal effects on cells of eukaryotic microbial strains used in this study including *S. cerevisiae*. On the other hand, the yeast cell growth was partly repressed in the presence of SAM at 50 μg ml^{-1}, but not all affected in the presence of MON at the same concentration (data not shown). As shown in Figure 3, the yeast cells were mostly viable upon PMB treatment at 100 μg ml^{-1}, but were subjected to the lethal effect of this antibiotic alone at 200 μg ml^{-1} in a time-dependent manner. In the presence of 50 μg ml^{-1} SAM, PMB exhibited the lethal effect at 50 μg ml^{-1} and could reduce the viable cell number to 10% of the original level at ~3 h incubation at 100 μg ml^{-1}. MON could similarly render the yeast cells susceptible to the lethal effect of PMB in a dose-dependent manner. In these experiments, PMB, SAM, and MON were required at the higher concentrations than expected from their MIC values (see Figure 2), as the cell densities were adjusted to the higher levels such as 10^7 ml^{-1} essential for conducting the following physiological experiments.

Effects of SAM and MON on PMB-induced vacuole morphological change

PMB causes vacuolar membrane-disruptive damage in *S. cerevisiae* cells when this bactericidal antibiotic is added alone at a high concentration and also at a non-lethal concentration in combination with allicin.[6] We thus attempted to examine whether SAM or MON can enhance the vacuole-disruptive activity of PMB by microscopic

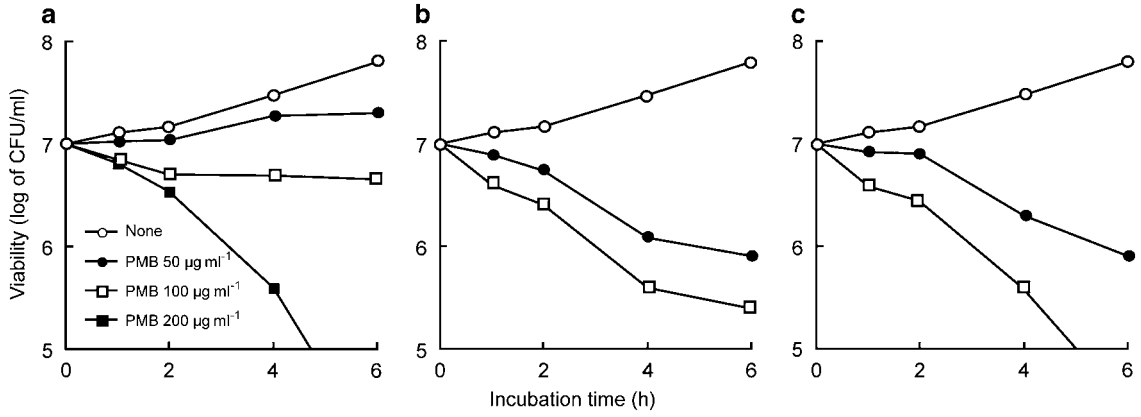

Figure 3 Growth inhibitory effects of PMB on *Saccharomyces cerevisiae* cells in the absence and the presence of either SAM or MON. (**a**) Cells (10^7 ml^{-1}) were incubated in YPD medium with PMB at 0 (○), 50 (●), 100 (□), and 200 μg ml^{-1} (■). (**b**) Cells were incubated in YPD medium containing 50 μg ml^{-1} SAM and PMB at 0 (○), 50 (●), and 100 μg ml^{-1} (□). (**c**) Cells were incubated in YPD medium with 50 μg ml^{-1} MON and PMB at 0 (○), 50 (●), and 100 μg ml^{-1} (□).

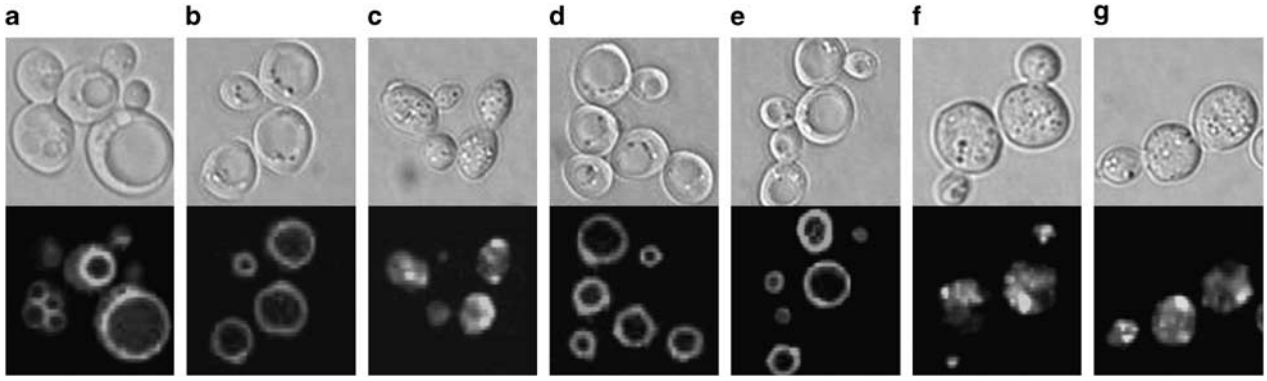

Figure 4 Effects of PMB, SAM and MON, and the combination of PMB and either SAM or MON on the vacuole morphology of *Saccharomyces cerevisiae* cells. After FM4-64 fluorescent dye treatment, cells (10^7 ml^{-1}) were incubated in YPD medium with none (**a**), 50 μg ml^{-1} PMB (**b**), 200 μg ml^{-1} PMB (**c**), 200 μg ml^{-1} SAM (**d**), 200 μg ml^{-1} MON (**e**), both 50 μg ml^{-1} PMB and 50 μg ml^{-1} SAM (**f**), and both 50 μg ml^{-1} PMB and 50 μg ml^{-1} MON (**g**) at 30 °C for 120 min. Cells were observed under the bright field microscope (top) and a fluorescence microscope (bottom).

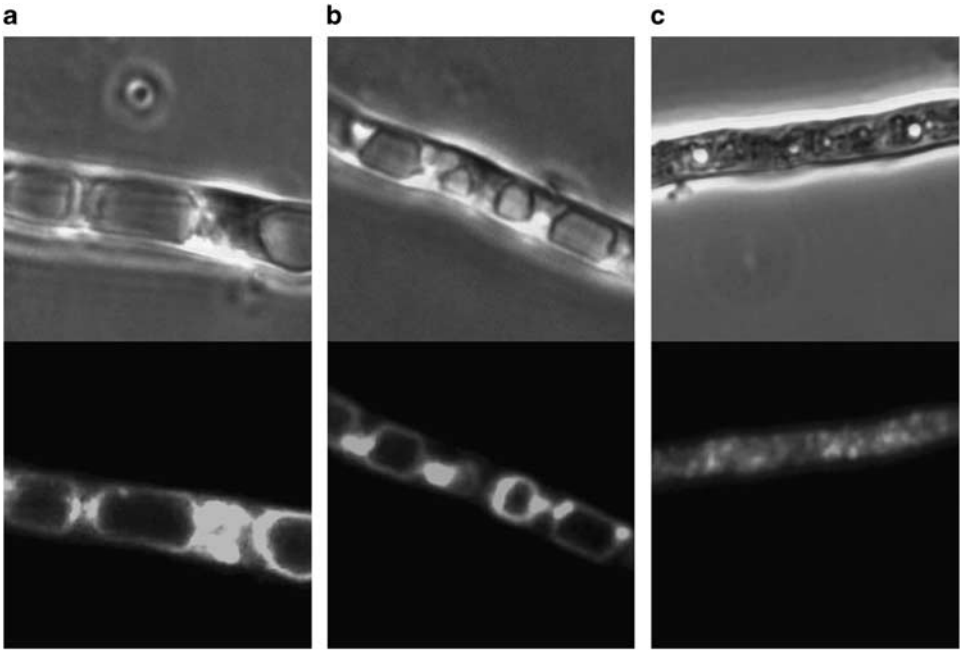

Figure 5 Effects of PMB in the absence and the presence of MON on vacuole morphology of *Aspergillus niger* cells. After FM4-64 fluorescent dye treatment, mycelia were incubated in malt extract medium with none (**a**), 200 μg ml^{-1} PMB (**b**), and both 50 μg ml^{-1} PMB and 50 μg ml^{-1} MON (**c**) at 30 °C for 120 min. Mycelia were observed under a phase-contrast microscope (top) and a fluorescence microscope (bottom).

observation of *S. cerevisiae* and *A. niger* cells. The vacuoles were observed with swollen spherical architectures in untreated cells of *S. cerevisiae* and those treated with PMB alone at 50 μg ml^{-1} (Figures 4a and b). In agreement with our earlier finding, the yeast vacuoles were observed as small discrete dots in the cytoplasm, representing fragmentation or disruption of the membranous architecture of the organelle when cells were treated with PMB at 200 μg ml^{-1} (Figure 4c). Although SAM and MON induced none of alterations in the vacuole morphology at 200 μg ml^{-1}, the presence of each ionophore at 50 μg ml^{-1} made the organelles susceptible to the disruptive action of PMB at 50 μg ml^{-1} in a similar manner (Figures 4e–g). The vacuoles of *A. niger* were observed with the oval to rectangular architectures in the filamentous chains of untreated cells as well as those treated with PMB alone at 200 μg ml^{-1}, as shown in Figure 5. The organelles lost the original morphology, being visible with faintly stained amorphous images upon PMB treatment at 50 μg ml^{-1} in combination with MON at 50 μg ml^{-1}.

Effects of SAM and MON on cellular uptake of PMB

Allicin is a sulfur-containing compound, and increases plasma membrane oxidation status in *S. cerevisiae* cells to a limited extent through its inhibitory effect on cell surface localization of alkyl hydroperoxide reductase 1 (ref. 24). The yeast plasma membrane was thus made permeable to intracellular K^+, but was prevented from further structural modifications leading to irreversible disruption, possibly with the aid of unknown activity of allicin. This is supported by the fact that the yeast cells are absolutely viable even if the cell growth can be fully repressed upon allicin treatment at a high concentration.[24] SAM stimulates alkali cation transport and thus inhibits oxidative phosphorylation in the rat liver mitochondria.[25] An impairment of mitochondrial electron transport function can be a cause of mitochondrial reactive oxygen species generation, and this intracellular oxidative stress may consequently enhance plasma membrane

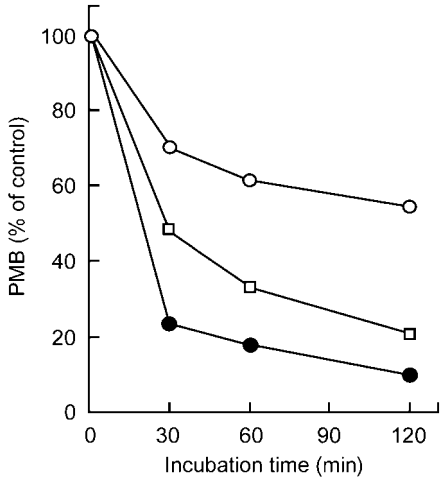

Figure 6 Effects of SAM and MON on the cellular uptake of PMB in *Saccharomyces cerevisiae* cells. Cells (10^7 cells^{-1}) were incubated in YPD medium with 100 μg ml^{-1} PMB (○), both 100 μg ml^{-1} PMB and 100 μg ml^{-1} SAM (●), and both 100 μg ml^{-1} PMB and 100 μg ml^{-1} MON (□) at 30 °C.

phospholipid peroxidation, as in the case with allicin-dependent cellular uptake of PMB.[26,27] The effects of SAM and MON on the cellular uptake of PMB were therefore examined by measuring the extracellular concentration of PMB by HPLC analysis. As shown in Figure 6, PMB indeed disappeared from the supernatant when cells were incubated with the antibiotic alone, but the rate of its disappearance was reduced along with the time of incubation. This may be due to its penetration into the plasma membrane, but not into the cytoplasm. The presence of either SAM or MON apparently contributed to elevation in the rate of PMB uptake by cells, possibly

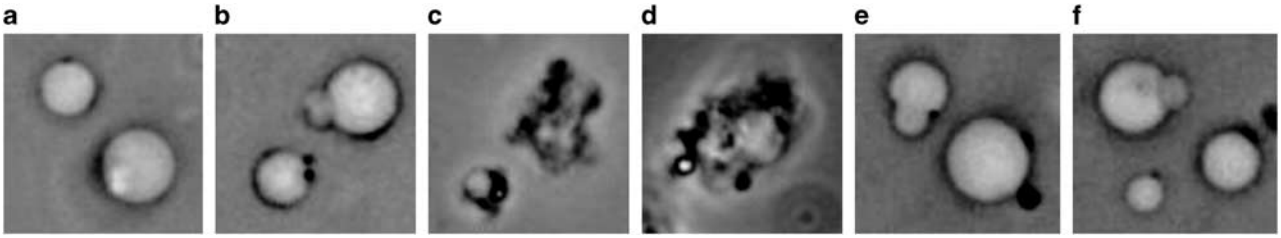

Figure 7 Disruptive effects of PMB on the isolated vacuoles in the absence and the presence of either SAM or MON. The isolated vacuoles were incubated with PMB at 6.25 (**a**), 12.5 (**b**), 25 (**c**), and 50 μg ml^{-1} (**d**) at 30 °C for 120 min. The organelles were also incubated with 12.5 μg ml^{-1} PMB in the presence of either 200 μg ml^{-1} SAM (**e**) or 200 μg ml^{-1} MON (**f**) at 30 °C for 120 min.

representing the corresponding accumulation of this antibiotic inside the cells.

We next confirmed whether SAM or MON increases the oxidation status of plasma membrane phospholipid using *t*-butyl hydroperoxide as a positive control that can also increase the rate of cellular uptake of PMB.[6] The extent of phospholipid peroxidation was kept unchanged with or without each ionophore at 200 μg ml^{-1} in comparison with its increase (1.6-fold of untreated control) in *t*-butyl hydroperoxide-treated cells. These findings highly support the idea that the loss of energy barrier for transmembrane transport of monovalent cations can be a cause of enhanced incorporation of larger cationic compounds such as PMB across the fungal plasma membrane.

Direct disruptive action of PMB on the isolated vacuoles

The results obtained above suggest the possibility that PMB can directly interact with the vacuole when this cationic cyclic peptide is incorporated into the cytoplasm of fungal cells. To confirm this possibility, the organelles were isolated from *S. cerevisiae* cells and were incubated with PMB in the absence and the presence of each ionophore. As shown in Figure 7, the isolated vacuoles were observed as spherical membrane-enclosed architectures with various sizes and were subjected to drastic disruptive damages after incubation with PMB alone. The minimum concentration of PMB effective for its complete disruption was 25 μg ml^{-1}. The isolated vacuoles were not disrupted with PMB at 12.5 μg ml^{-1} even if the assay mixture was further supplemented with each ionophore at 200 μg ml^{-1}. This agrees well with the above idea that these ionophores can facilitate cellular uptake of PMB in favor of its direct action on this organelle inside the cells.

Vacuoles perform various functions, such as pH and ion homeostasis, osmoregulation, and volume regulation, by undergoing the organized membrane fusion and fission.[28] Fusion of the isolated vacuoles is provoked by ATP supplementation for activating various peripheral membrane proteins. PMB-induced morphological change of the organelle should be attributed to unorganized disintegration of phospholipid membrane, but not to *in vitro* induction of organized or systemic fission process of the organelle. The vacuolar membrane of *S. cerevisiae* is characterized by the lowest content of ergosterol among various subcellular membranous architectures including plasma membrane with the highest ergosterol content.[29] Instead, inositolphosphorylceramide is highly enriched in the vacuolar membrane where phosphatidylcholine is detected as the major phospholipid component.[30] PMB may exhibit a disruptive effect on the fungal vacuole through its interaction with inositolphosphorylceramide embedded in the phosphatidylcholine membrane. This antibiotic may otherwise trigger the vacuolar membrane disintegration depending on its interaction with a peripheral protein critical for the biogenesis of this organelle. Our studies are currently in progress to clarify the mechanism underlying the vacuole disruption by PMB.

ACKNOWLEDGEMENTS

This work was supported in part by a Grant-in-Aid for Scientific Research (C) (No. 20580083) from Japan Society for the Promotion of Science.

1 Vaara, M. Analytical and preparative high-performance liquid chromatography of the papain-cleaved derivative of polymyxin B. *J. Chromatogr.* **441,** 423–430 (1988).
2 Hancock, R. E. Peptide antibiotics. *Lancet* **349,** 418–422 (1997).
3 Boguslawski, G. Effects of polymyxin B sulfate and polymyxin B nonapeptide on growth and permeability of the yeast *Saccharomyces cerevisiae*. *Mol. Gen. Genet.* **199,** 401–405 (1985).
4 Moneib, N. A. *In-vitro* activity of commonly used antifungal agents in the presence of rifampin, polymyxin B and norfloxacin against *Candida albicans*. *J. Chemother.* **7,** 525–529 (1995).
5 Schwartz, S. N., Medoff, G., Kobyashi, G. S., Kwan, C. N. & Schlessinger, D. Antifungal properties of polymyxin B and its potentiation of tetracycline as an antifungal agent. *Antimicrob. Agents Chemother.* **2,** 36–46 (1972).
6 Ogita, A., Nagao, Y., Fujita, K. & Tanaka, T. Amplification of vacuole-targeting fungicidal activity of antibacterial antibiotic polymyxin B by allicin, an allyl sulfur compound from garlic. *J. Antibiot.* **60,** 511–518 (2007).
7 Ogita, A., Matsumoto, K., Fujita, K., Usuki, Y., Hatanaka, Y. & Tanaka, T. Synergistic fungicidal activities of amphotericin B and *N*-methyl-*N*′-dodecylguanidine: a constituent of polyol macrolide antibiotic niphimycin. *J. Antibiot.* **60,** 27–35 (2007).
8 Nakayama, K., Yamaguchi, T., Doi, T., Usuki, Y., Taniguchi, M. & Tanaka, T. Synergistic combination of direct plasma membrane damage and oxidative stress as a cause of antifungal activity of polyol macrolide antibiotic niphimycin. *J. Biosci. Bioeng.* **94,** 207–211 (2002).
9 Usuki, Y., Matsumoto, K., Inoue, T., Yoshioka, K., Iio, H. & Tanaka, T. Structure-activity relationship studies on niphimycin, a guanidylpolyol macrolide antibiotic. Part 1: the role of the *N*-methyl-*N*′-alkylguanidinium moiety. *Bioorg. Med. Chem. Lett.* **16,** 1553–1556 (2006).
10 Ogita, A., Fujita, K., Taniguchi, M. & Tanaka, T. Enhancement of the fungicidal activity of amphotericin B by allicin, an allyl-sulfur compound from garlic, against the yeast *Saccharomyces cerevisiae* as a model system. *Planta Med.* **72,** 1247–1250 (2006).
11 Lindsay, D. S. & Blagburn, B. L. Antiprotozoan. Antiprotozoan drugs. In *Veterinary Pharmacology and Therapeutics* (ed Adams, H. R.) 969–983 (Iowa State University Press, Amsterdam, 1995).
12 Westley, J. W. Chemical transformations of polyether antibiotics. In *Polyether Antibiotics: Naturally Occurring Acid Ionophores* Chemistry Vol 2 (ed Westley, J. W.) 51–87 (Marcel Dekker Inc., New York, 1983).
13 Haney, M. E. Jr. & Hoehn, M. M. Monensin, a new biologically active compound. I. Discovery and isolation. *Antimicrob. Agent Chemother.* **7,** 349–352 (1967).
14 Butaye, P., Devriese, L. A. & Haesebrouck, F. Antimicrobial growth promoters used in animal feed: effects of less well known antibiotics on Gram-positive bacteria. *Clinic Microbiol. Rev.* **16,** 175–188 (2003).
15 Takahashi, M., Shibata, M. & Niki, E. Estimation of lipid peroxidation of live cells using a fluorescent probe, diphenyl-1-pyrenylphosphine. *Free Radic. Biol. Med.* **31,** 164–174 (2001).
16 Ogita, A., Fujita, K., Taniguchi, M. & Tanaka, T. Dependence of synergistic fungicidal activity of Cu^{2+} and allicin, an allyl sulfur compound from garlic, on selective accumulation of the ion in the plasma membrane fraction via allicin-mediated phospholipid peroxidation. *Planta Med.* **72,** 875–880 (2006).

17 Conradt, B., Shaw, J., Vida, T., Emr, S. & Wickner, W. *In vitro* reactions of vacuole inheritance in *Saccharomyces cerevisiae*. *J. Cell Biol.* **119,** 1469–1479 (1992).
18 Ohsumi, Y. & Anraku, Y. Active transport of basic amino acids driven by a proton motive force in vacuolar membrane vesicles of *Saccharomyces cerevisiae*. *J. Biol. Chem.* **256,** 2079–2082 (1981).
19 Tabuchi, M. *et al*. Vacuolar protein sorting in fission yeast: cloning, biosynthesis, transport, and processing of carboxypeptidase Y from *Schizosaccharomyces pombe*. *J. Bacteriol*. **179,** 4179–4189 (1997).
20 Vida, T. A. & Emr, S. D. A new vital stain for visualizing vacuolar membrane dynamics and endocytosis in yeast. *J. Cell Biol*. **128,** 779–792 (1995).
21 Arnold, T. M., Forrest, G. N. & Messember, K. J. Polymyxin antibiotics for Gram-negative infections. *Am. J. Health Syst. Pharm.* **64,** 819–826 (2007).
22 Liu, C. & Hermann, T. E. Characterization of ionomycin as a calcium ionophore. *J. Biol. Chem.* **253,** 5892–5894 (1978).
23 Reed, P. W. & Lardy, H. A. A23187: a divalent cation ionophore. *J. Biol. Chem.* **247,** 6970–6977 (1972).
24 Ogita, A. *et al*. Synergistic fungicidal activity of Cu^{2+} and allicin, an allyl sulfur compound from garlic, and its relation to the role of alkyl hydroperoxide reductase 1 as a cell surface defense in *Saccharomyces cerevisiae*. *Toxicology* **215,** 205–213 (2005).
25 Mitani, M., Yamanishi, T., Miyazaki, Y. & Otake, N. Salinomycin effects on mitochondrial ion translocation and respiration. *Antimicrob. Agents Chemother.* **9,** 655–660 (1976).
26 Machida, K., Tanaka, T., Fujita, K. & Taniguchi, M. Farnesol-induced generation of reactive oxygen species *via* indirect inhibition of mitochondrial electron transport chain in the yeast *Saccharomyces cerevisiae*. *J. Bacteriol*. **180,** 4460–4465 (1998).
27 Machida, K. & Tanaka, T. Farnesol-induced generation of reactive oxygen species dependent on mitochondrial transmembrane potential hyperpolarization mediated by F_0F_1-ATPase in yeast. *FEBS Lett.* **462,** 108–112 (1999).
28 Wickner, W. Yeast vacuoles and membrane fusion pathways. *EMBO J.* **21,** 1241–1247 (2002).
29 Zinser, E., Sperka-Gottlieb, C. D., Fasch, E. V., Kohlwein, S. D., Paltauf, F. & Daum, G. Phospholipid synthesis and lipid composition of subcellular membranes in the unicellular eukaryote *Saccharomyces cerevisiae*. *J. Bacteriol*. **173,** 2026–2034 (1991).
30 Hecktberger, P., Zinser, E., Saf, R., Hummel, K., Paltauf, F. & Daum, G. Characterization, quantification, and subcellular localization of inositol-containing sphingolipids of the yeast, *Saccharomyces cerevisiae*. *Eur. J. Biochem.* **225,** 641–649 (1994).

The Journal of Antibiotics (2009) 62, 89–93

www.nature.com/ja

ORIGINAL ARTICLE

Discovery of anti-varicella zoster virus activity of polyether antibiotic CP-44161

Yukiko Yamagishi[1,5], Chihoko Ueno[1,5], Akemi Kato[1,5], Hirohito Kai[1], Hiromi Sasamura[1], Motoi Ueno[1], Bunji Sato[1], Akihiko Fujie[1], Takashi Fujii[2], Motohiro Hino[3] and Eisaku Tsujii[4]

In search for new anti-varicella zoster virus (VZV) compounds with new mechanism of action, we applied a DNA hybridization assay (dot blot method) for screening. Using this method, we screened microbial products and found the polyether compound CP-44161 from the culture broth of an actinomycete strain. CP-44161 was previously reported as an anticoccidal agent, but there has been no claim of its antiviral activities. CP-44161 showed strong anti-VZV activity against pOka strain by plaque reduction assay. Moreover, CP-44161 showed lower cytotoxicity than other antiviral polyethers, such as monensin and nigericin. Its better safety margin and strong anti-VZV properties make it a good candidate for a new anti-VZV agent.
The Journal of Antibiotics (2009) **62,** 89–93; doi:10.1038/ja.2008.19; published online 23 January 2009

Keywords: antiviral; CP-44161; dot blot; polyether; varicella zoster virus

INTRODUCTION

Varicella zoster virus (VZV) is a member of the Herpesviridae family that causes two distinct clinical syndromes. Primary infection is manifested as varicella (chickenpox). After the primary VZV infection, latent infection is established in the sensory nerve ganglia. Reactivation of latent VZV results in a localized eruption known as herpes zoster (shingles). Herpes zoster develops in approximately 30% of people over a lifetime. The risk of disease increases with age, and also frequently occurs in immunocompromised patients, especially those with human immunodeficiency virus (HIV) infection. Complications of herpes zoster in immunocompetent hosts include postherpetic neuralgia (PHN), encephalitis, myelitis, cranial nerve palsies and peripheral nerve palsies. PHN, a persistent pain syndrome occurring after the resolution of the zoster rash, is the most challenging complication.[1]

Standard antiviral drugs currently used in the treatment of VZV infections include acyclovir (ACV), valaciclovir (VACV, the oral prodrug of ACV), famciclovir (the oral prodrug of penciclovir) and vidarabine (Ara-A).[2] A live attenuated VZV vaccine was originally developed as the 'chickenpox vaccine' to prevent varicella. Recently, a new VZV vaccine was developed for protection against herpes zoster.[1]

Despite a number of recent therapeutic advancements, there remains an urgent need to develop a new class of therapy, especially novel anti-VZV agent with a strong potency against VZV and with a different mechanism of action from nucleoside analogs, because current anti-VZV drugs exhibit lower potency against VZV than herpes simplex virus (HSV). In addition, they had some problems, such as cross-resistance and mutagenicity, which are inevitable consequences of nucleoside analogs.

To discover a new candidate as an anti-VZV agent, we applied VZV DNA dot blot hybridization assay[3] for screening anti-VZV compounds. Using this system, we screened anti-VZV agent among 34 000 microbial fermentation samples and found AS1720807 as a new anti-VZV compound. AS1720807 was the same as CP-44161, a polyether compound that was first reported as an anticoccidal compound from *Dactylosporangium salmoneum* FD 25647 (=IFO 14103) (Figure 2; Celmer *et al.*[4] and Tone *et al.*[5]).

In this paper, we describe the strong anti-VZV activities of CP-44161 *in vitro* in comparison to existing anti-VZV agents and other polyethers that were reported to have antiviral activities.

MATERIALS AND METHODS

Cells and virus

Human malignant melanoma cell line (MeWo) was obtained from the American Type Culture Collection (ATCC; Rockville, MD, USA). Cells were grown and maintained in Eagle's minimal essential medium supplemented with 10% heat-inactivated fetal bovine serum, 0.075% $NaHCO_3$ and 100 U ml^{-1} penicillin and 100 μg ml^{-1} streptomycin sulfate. Cells were grown at 37 °C in an atmosphere of 5% CO_2.

[1]Fermentation Research Labs, Astellas Pharma Inc., Ibaraki, Japan; [2]Kikuchi Research Center, The Chemo-Sero-Therapeutic Research Institute, Kyokushi, Japan; [3]Fermentation and Biotechnology Labs, Astellas Pharma Inc., Kiyosu-shi, Japan and [4]Pharmacology Research Labs, Astellas Pharma Inc., Osaka, Japan
[5]These authors contributed equally to this work.
Correspondence: Dr Y Yamagishi, Fermentation Research Labs, Astellas Pharma Inc., 5-2-3 Tokodai, Tsukuba-shi, Ibaraki 300-2698, Japan.
E-mail: yukiko.yamagishi@jp.astellas.com
Received 3 September 2008; accepted 5 December 2008; published online 23 January 2009

VZV pOka strain and clinically isolated VZV YS strain[6] were kindly provided by Dr T Suzutani (Fukushima Medical University). Cell-associated virus pools of VZV were produced by passing the virus for 48 h in MeWo cells, then trypsinizing the cells and resuspending the cells in the media containing 10% DMSO before freezing at −80 °C. Quantification of viral titers of stocks by the plaque assay and viral replication studies of VZV were performed in MeWo cells.

Reagents and antiviral compounds

Adenine 9-β-D-arabinofuranoside (Ara-A), monensin, nigericin, DMSO and 3-(4,5-dimethylthiazol-2-yl)-2,5,-diphenyltetrazolium bromide (MTT) were obtained from Sigma (St Louis, MO, USA). ACV was purchased from GlaxoSmithKline (Tokyo, Japan). Bromovinyl arauracil (BV-araU) was kindly provided by Yamasa Corporation (Chiba, Japan). All compounds were dissolved in DMSO and then diluted with cell culture medium to yield 0.1% DMSO.

Screening method for anti-VZV compound

To quantify VZV DNA synthesis directly, we modified the VZV-DNA dot blot hybridization procedure described previously.[3] MeWo cells were grown to confluence in F-225 plastic bottles and then infected with the VZV pOka strain (1.8×10^4 plaque forming units (PFU) per flask). After 8 h incubation, cells were trypsinized and resuspended in the 96-well micro-titer plates. After 1 h incubation, media in the presence or absence of various concentrations of the test compounds were added. After 36 h incubation, individual wells were harvested by removing the cell culture medium and replacing it with a buffer consisting of 0.125 mg ml^{-1} RNase A, 0.5 mg ml^{-1} proteinase K, 0.05% SDS and 10 mM Tris-HCl (pH 7.5). After 3 h incubation at 50 °C, 10× SSC (1.5 M sodium chloride and 0.15 M sodium citrate) and 0.3 M NaOH were added and then neutralized by 1.0 M ammonium acetate. The samples were transferred to a nylon membrane (Roche Diagnostics, Tokyo, Japan) with a Bio-Dot SF Microfiltration Apparatus (Bio-Rad Laboratories, Tokyo, Japan). Filters were hybridized with VZV thymidine kinase (TK) DNA probe labeled by the digoxigenin (DIG) DNA labeling kit (Roche Diagnostics). Hybridization procedure was performed according to the manufacturer's protocol. DIG-labeled VZV DNA was detected by DIG Luminescent Detection kit (Roche Diagnostics) and the intensity of the spots was quantified by image analysis.

Plaque reduction assay

The antiviral effects of compounds against VZV were determined by plaque reduction assay. MeWo cells were grown to confluence in 24-well tissue culture plates and then infected with the VZV pOka strain or YS strain (40 PFU per well). After 1 h incubation, media containing various concentrations of the compounds or 0.1% DMSO were added. After 3 days, the cells were stained with 1.0% crystal violet in 70% EtOH, and the number of viral plaques was counted.

Cytotoxicity assay

The cytotoxicity of compounds against growing host MeWo cells (2×10^4 cells per well in 96-well tissue culture plates) was determined with the MTT assay as the procedure described previously.[7]

RESULTS

Screening for anti-VZV compound by DNA dot blot assay

Dot blot method has been shown to be a very sensitive and efficient method to detect VZV DNA from clinical specimens.[3] However, there has been no report of isolating anti-VZV compound using this method. We applied the non-isotopic detection system by using the DIG-labeled VZV TK probe in this method (Figure 1) and simplified the process of DNA purification for facilitating the screening procedure.

Next, to evaluate this method as a tool for screening new anti-VZV compounds, we compared the sensitivity of this method for anti-VZV drug to a conventional plaque reduction assay. As shown in Table 1, this method was as sensitive as the plaque assay; however, it could be completed in 36 h, which means that it could halve the assay period compared with the plaque assay. Moreover, its short assay period and direct detection of viral DNA gave us another benefit of drug screening. We found that this method reduced the assay noise of coexisting materials in microbial fermentation samples, such as inhibitors of viral adsorption and cytotoxic compounds.

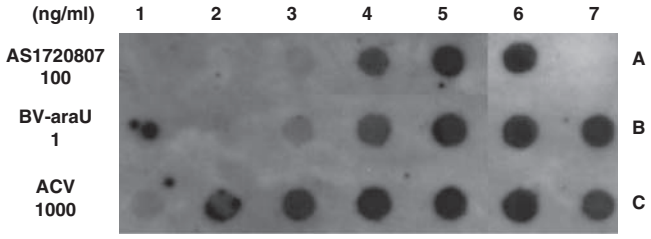

Figure 1 Dot blot screening for anti-VZV compounds. VZV DNA levels in the presence or absence of AS1720807 (lanes 1A–5A, top dose 100 ng ml^{-1} with doubling dilution) were determined by the dot blot method. VZV-infected cells with BV-araU (lanes 1B–5B, top dose 1 ng ml^{-1} with doubling dilution) and ACV (lanes 1C–5C, top dose 1000 ng ml^{-1} with doubling dilution). Controls were performed for uninfected cells (7A), VZV-infected cells without drug treatment (lanes 6A–6C). Lane 7B represents 50% inhibition and lane 7C represents 75% inhibition control.

Table 1 Sensitivity comparison between the dot blot method and plaque reduction assay

Compound	*Dot blot*	*Plaque*
	EC_{50}[a] (μg ml^{-1})	*EC_{50}[a] (μg ml^{-1})*
CP-44161	0.015	0.0051
BV-araU	0.00055	0.00041
ACV	0.95	2.7
Ara-A	1.1	1.8

[a]EC_{50} was the concentration that inhibited 50% of VZV replication in MeWo cells. Values represent the mean of three independent experiments.

Then we applied this method for screening anti-VZV compounds from microbial products. Among 34 000 microbial fermentation samples, we found a sample, which was an extract of fermentation broth of actinomycete strain no. 642788, that showed very strong anti-VZV activity. Using bioassay-guided preparation, we isolated the active substance as a powder and named it AS1720807.

Fermentation and isolation of AS1720807 (CP-44161)

Strain no. 642788, a producer strain of AS1720807, is an actinomycete strain that was isolated from soil sample collected in Malaysia. Strain no. 642788 was identified as *Dactylosporangium* sp. by morphological characteristics and phylogenic analysis of 16S rRNA gene sequence. The homology value between 642788 and IFO 14103 (D86938) was 99.0% (1436/1451) (data not shown).

A slant culture of strain was inoculated into a 225-ml Erlenmeyer flask containing 60 ml of a seed medium composed of soluble starch 1.0%, yeast extract 0.4%, gellan gum 0.5%, agar 0.1%, calcium chloride 0.0004%, pH 7.0 and cultured for 5 days at 30 °C. The seed culture (2.4 ml) was then inoculated into 500-ml Erlenmeyer flasks containing 120 ml of the production medium composed of soluble starch 2.0%, yeast extract 0.4%, allophane 1.0%, pH 7.0 and cultured for 5 days at 30 °C.

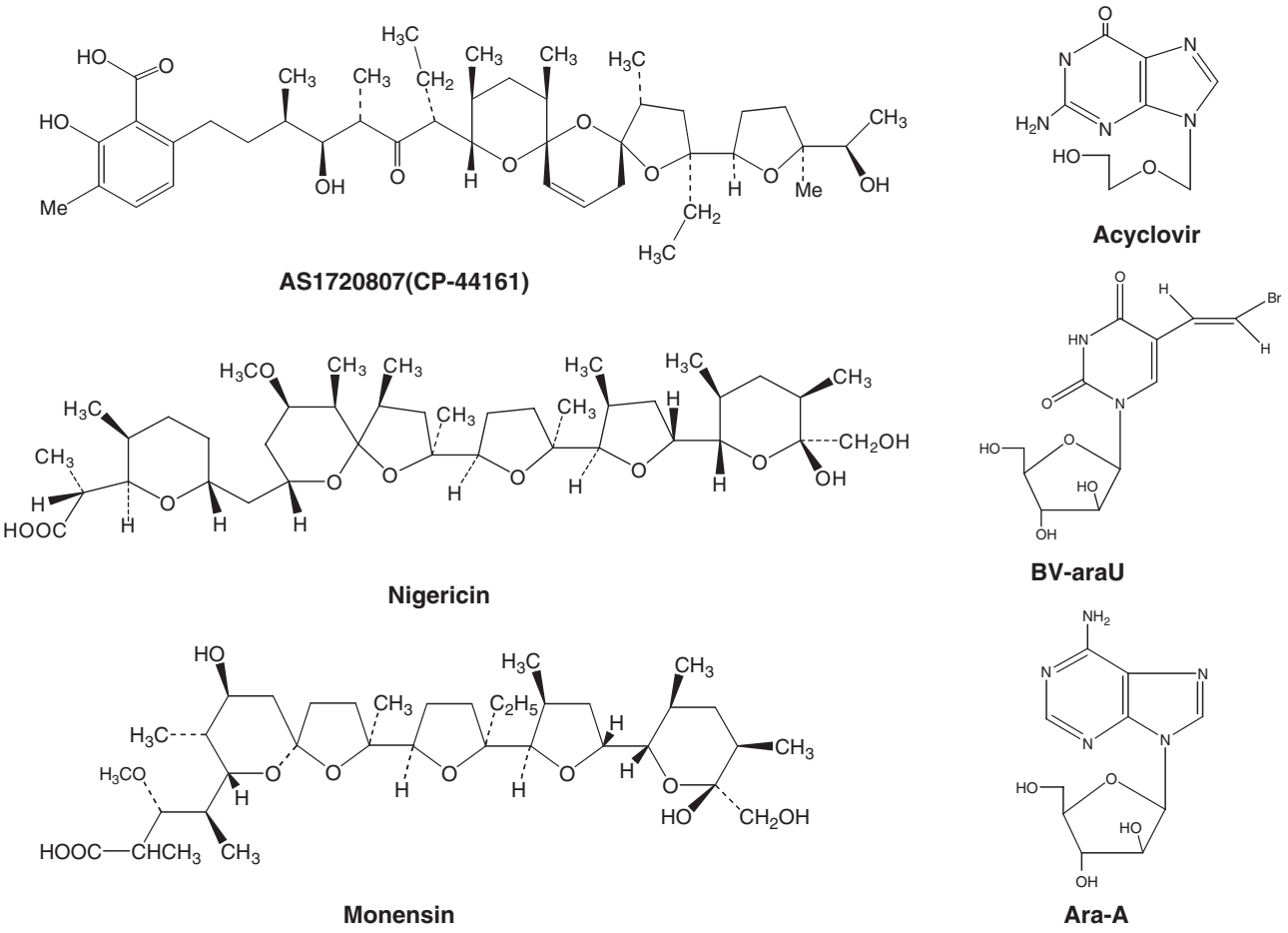

Figure 2 Structures of AS1720807 (CP-44161) and related compounds.

The broth was extracted with equal volume of Me_2CO. The extract was applied on a DIAION HP-20 column and eluted with Me_2CO, and concentrated. The concentrate was applied on a MicroBead SilicaGel 5D column, and eluted with 3:1 (v/v) of *n*-hexane-EtOAc. The active fractions were applied on a Daiso-gel SP-120-40/60-C4 column and eluted with 65% CH_3CN containing 5.0 mM sodium phosphate buffer, pH 7.5. The pooled fractions were extracted with diethyl ether and concentrated under reduced pressure to obtain AS1720807 as a white powder.

By physico-chemical analysis, the structure of AS1720807 was determined as CP-44161 (Figure 2; Celmer *et al.*[4] and Tone *et al.*[5]), a polyether previously reported as an anticoccidal compound (data not shown).

The following biological experiments were conducted with AS1720807 as CP-44161.

Anti-VZV activities of CP-44161

Antiviral activities of CP-44161 against the VZV pOka strain and clinically isolated YS strain were determined by plaque reduction assay. CP-44161 inhibited VZV replication in a dose-dependent manner (Figure 3). As shown in Table 2, the results gave an EC_{50} (concentration producing 50% inhibition) value against the pOka and YS strains for CP-44161 of 0.0051 and 0.015 μg ml^{-1} compared with an EC_{50} value for ACV of 2.7 and 2.9 μg ml^{-1} and for Ara-A of 1.8 and 5.7 μg ml^{-1} at 72 h, respectively. The results showed that CP-44161 had strong anti-VZV activity compared with current anti-VZV agents, ACV and Ara-A.

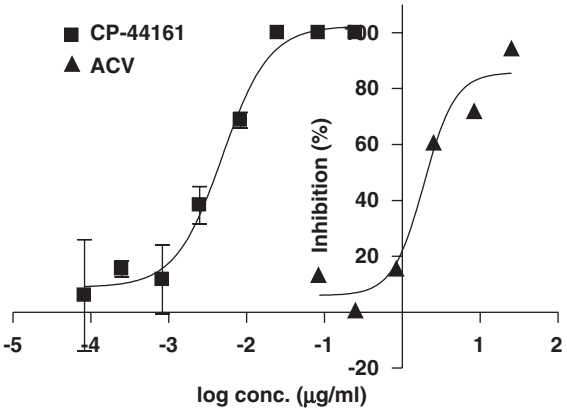

Figure 3 Dose-dependent anti-VZV activity of CP-44161 and ACV as measured by the plaque reduction assay. Data are presented as the mean ± standard deviation of triplicate experiments.

Anti-VZV activity and cellular toxicity of CP-44161 and other polyethers

Higher concentration (up to 1.0 μg ml^{-1}) of CP-44161 was necessary to exhibit cytotoxicity in host MeWo cells. As CP-44161 was a

Table 2 Anti-VZV activities and cellular toxicity of CP-44161

Compound	VZV pOka	VZV YS	MeWo
	EC_{50}[a] ($\mu g\,ml^{-1}$)	EC_{50}[a] ($\mu g\,ml^{-1}$)	CC_{50}[b] ($\mu g\,ml^{-1}$)
CP-44161	0.0051	0.015	0.39
ACV	2.7	2.9	>25
Ara-A	1.8	5.7	9

[a]Antiviral activity was determined by the plaque assay. EC_{50} was the concentration that inhibited 50% of VZV replication in MeWo cells.
[b]Cytotoxic effect was determined by the MTT assay. CC_{50} was the concentration that showed 50% cytotoxic effects in MeWo cells.
Values represent the mean of three independent experiments.

Table 3 Anti-VZV activity and cellular toxicity of CP-44161 and other polyethers

Compound	VZV pOka	MeWo	Selectivity index[c]
	EC_{50}[a] ($\mu g\,ml^{-1}$)	CC_{50}[b] ($\mu g\,ml^{-1}$)	
CP-44161	0.0051	0.39	76
Monensin	0.0071	0.01	1.4
Nigericin	0.0011	0.01	9.1

Values represent the mean of three independent experiments.
[a]Antiviral activity was determined by the plaque assay. EC_{50} was the concentration that inhibited 50% of VZV replication in MeWo cells.
[b]Cytotoxic effect was determined by the MTT assay. CC_{50} was the concentration that showed 50% cytotoxic effects in MeWo cells.
[c]The selectivity index (SI) was calculated as CC_{50}/EC_{50}.

polyether, we also compared anti-VZV activity and cytotoxicity with other polyether compounds, nigericin and monensin, which were reported to have anti-HSV activities.[8–10] As shown in Table 3, nigericin and monensin showed strong anti-VZV activities, but they also exhibited strong cytotoxicity against host MeWo cells. As shown in Table 3, CP-44161 had a relatively higher selectivity index (ratio of 50% cytotoxic concentration to 50% inhibitory concentration against VZV replication) compared with other polyethers.

DISCUSSION

The dot blot hybridization has been used to help diagnose several viral infections,[11,12] Seidlin *et al.*[3] also developed this method for the detection of VZV DNA from clinical specimens. Dot blot method has been shown to be a very sensitive and efficient method to detect VZV replication; however, there has been no report of its application in drug screening for antiviral compounds. First, we introduced the non-isotopic detection system into dot blot method, and compared this method with a conventional plaque reduction assay in terms of its usefulness for drug screening and found some advantages; for example, short assay period and reduction of assay noise. Short assay period reduced the noise of coexisting cytotoxic compounds, and direct detection of viral DNA excluded pseudo-positive results that were sometimes observed in the plaque reduction assay.

By using this method to screen anti-VZV compounds, we found and isolated AS1720807 (CP-44161) from one of the microbial fermentation samples produced by *Dactylosporangium* sp. no. 642788. CP-44161 was previously reported as an anticoccidal agent, but there has been no claim of its antiviral activities. Next, we demonstrated that CP-44161 exhibited anti-VZV activity by the plaque reduction assay. CP-44161 inhibited viral replication *in vitro* in a dose-dependent manner. CP-44161 had more potent anti-VZV activities than clinically used agent, against not only laboratory strain but also clinical isolate.

As is well known, antibacterial mechanism of polyether antibiotics against Gram-positive bacteria is based on their inhibitory effect on the biological membrane ion transport.[13] For some virus (for example, influenza virus), the low pH environment of the endosome triggers fusion of the virion envelope with cellular membranes.[14,15] Nakamura *et al.*[16] showed the inhibitory effects of polyethers on HIV replication. Regarding the anti-herpes virus activities, nigericin and its derivative nigericinol, which have potassium ionophore activities, were reported to have anti-HSV-1 and 2 activities *in vitro*.[8] Another polyether monensin, which has a sodium ionophore activity, inhibited HSV-1 (ref. 9,10) and human cytomegalovirus replication[17] *in vitro*. Pleiotropic antiviral actions of monensin were reported. Johnson *et al.*[9] and Ghosh-Choudhury *et al.*[18] showed that monensin blocked late stages in the post-translational processing of the viral glycoproteins of HSV-1 and HSV-2.

In summary, we established an efficient *in vitro* screening system using DNA dot blot assay for anti-VZV compounds from crude microbial fermentation samples. Using this system, we isolated CP-44161, which had strong anti-VZV activity with lower cytotoxicity than other polyethers. Other polyethers, nigericin and monensin, also exhibited antiviral activities against VZV, but they also exhibited strong cytotoxicity against host cells. Nakamura *et al.*[16] estimated the relative cytotoxicities of the polyethers against host cells of HIV. They showed that nigericin and lasalocid had a higher selectivity index than monensin. The results presented here were considered reasonable because the structure of CP-44161 was similar to lasalocid.

The mechanism by which CP-44161 inhibits VZV replication and the reason of its lower cytotoxicity are currently unknown. Lower cytotoxicity and strong anti-VZV properties of CP-44161 make it a good candidate for a new anti-VZV agent. Further experimental studies concerning its antiviral activity *in vivo* and the mode of action are under investigation.

ACKNOWLEDGEMENTS

We thank Dr S Takase for NMR spectra measurement of CP-44161, Dr Neelam Shahab (SIRIM Rerhad, Malaysia) and Mr H Muramatsu for the culture of actinomycetes strain no. 642788, and Mr T Zenkoh, Dr K Sudo and Dr K Maki for helpful discussions.

1 Kimberlin, D. W. & Whitley, R. J. Varicella-zoster vaccine for the prevention of herpes zoster. *N. Engl. J. Med.* **356,** 1338–1343 (2007).
2 De Clercq, E. Recent highlights in the development of new antiviral drugs. *Curr. Opin. Microbiol.* **8,** 552–560 (2005).
3 Seidlin, M. *et al.* Detection of varicella-zoster virus by dot-blot hybridization using a molecularly cloned viral DNA probe. *J. Med. Virol.* **13,** 53–61 (1984).
4 Celmer, W. D. *et al.* Polycyclic ether antibiotic produced by new species of *Dactylosporangium*, in United States Patent 4081532. Pfizer Inc., New York, NY, USA (1976).
5 Tone, J. *et al.* Abstract, 18th ICACC Meeting, Atlanta, Georgia (1978).
6 Sakuma, T. Strains of varicella-zoster virus resistant to 1-beta-D-arabinofuranosyl-E-5-(2-bromovinyl)uracil. *Antimicrob. Agents Chemother.* **25,** 742–746 (1984).
7 Denizot, F. & Lang, R. Rapid colorimetric assay for cell growth and survival. Modifications to the tetrazolium dye procedure giving improved sensitivity and reliability. *J. Immunol. Methods* **89,** 271–277 (1986).
8 Grabley, S. *et al.* Secondary metabolites by chemical screening 17. Nigericinol derivatives: synthesis, biological activities, and modeling studies. *J. Med. Chem.* **35,** 939–944 (1992).
9 Johnson, D. C. & Spear, P. G. Monensin inhibits the processing of herpes simplex virus glycoproteins, their transport to the cell surface, and the egress of virions from infected cells. *J. Virol.* **43,** 1102–1112 (1982).
10 Kousoulas, K. G., Bzik, D. J. & Person, S. Effect of the ionophore monensin on herpes simplex virus type 1-induced cell fusion, glycoprotein synthesis, and virion infectivity. *Intervirology* **20,** 56–60 (1983).

11 Brandsma, J. & Miller, G. Nucleic acid spot hybridization: rapid quantitative screening of lymphoid cell lines for Epstein–Barr viral DNA. *Proc. Natl Acad. Sci. USA* **77,** 6851–6855 (1980).
12 Berninger, M. *et al*. An assay for the detection of the DNA genome of hepatitis B virus in serum. *J. Med. Virol.* **9,** 57–68 (1982).
13 Harold, F. M. & Baarda, J. R. Effects of nigericin and monactin on cation permeability of *Streptococcus faecalis* and metabolic capacities of potassium-depleted cells. *J. Bacteriol.* **95,** 816–823 (1968).
14 Guinea, R. & Carrasco, L. Concanamycin A blocks influenza virus entry into cells under acidic conditions. *FEBS Lett.* **349,** 327–330 (1994).
15 Daniels, P. U. & Edwardson, J. M. Intracellular processing and transport of influenza-virus envelope proteins in Madin–Darby canine kidney cells. Effects of the carboxylic ionophores monensin and nigericin. *Biochem. J.* **252,** 693–700 (1988).
16 Nakamura, M. *et al*. Inhibitory effects of polyethers on human immunodeficiency virus replication. *Antimicrob. Agents Chemother.* **36,** 492–494 (1992).
17 Kaiser, C. J. & Radsak, K. Inhibition by monensin of human cytomegalovirus DNA replication. *Arch. Virol.* **94,** 229–245 (1987).
18 Ghosh-Choudhury, N., Graham, A. & Ghosh, H. P. Herpes simplex virus type 2 glycoprotein biogenesis: effect of monensin on glycoprotein maturation, intracellular transport and virus infectivity. *J. Gen. Virol.* **68,** 1939–1949 (1987).

The Journal of Antibiotics (2009) 62, 95–98

www.nature.com/ja

ORIGINAL ARTICLE

Anti-herpes virus activity of polyether antibiotic CP-44161 *in vivo*

Yukiko Yamagishi[1,7], Motoi Ueno[1,7], Chihoko Ueno[1,7], Akemi Kato[1], Ryuichi Kanasaki[1], Bunji Sato[1], Koji Takakura[2], Akihiko Fujie[1], Hidenori Nakajima[3], Takashi Fujii[4], Motohiro Hino[5] and Eisaku Tsujii[6]

In the previous study, we discovered a polyether antibiotic CP-44161, which was reported earlier as an anticoccidal agent, as an anti-varicella zoster virus compound. In this study, we demonstrated that CP-44161 had a very strong and broad anti-herpes virus activities against herpes simplex virus type 1 (HSV-1) and type 2 (HSV-2) *in vitro*. To determine the antiviral activity of CP-44161 *in vivo*, we examined its effect on the cutaneous HSV-2 infection model in Balb/c mice. CP-44161 showed inhibitory effect on lesion development as well as acyclovir (ACV) when the treatment was started from day 3. Meanwhile, in case the start of treatment was delayed until day 4, when ACV was no longer effective, the effectiveness of CP-44161 still remained. In this model, CP-44161 also showed inhibitory effect on the proliferation of HSV-2 DNA in dorsal root ganglia. This is the first article to report that polyether antibiotics can be effective on viral infection *in vivo*.
The Journal of Antibiotics (2009) **62,** 95–98; doi:10.1038/ja.2008.18; published online 23 January 2009

Keywords: antiviral; herpes virus; CP-44161; polyether

INTRODUCTION

There are eight human herpesvirus that cause various diseases in humans. Herpes simplex virus type 1 (HSV-1), a causative agent of cold sore and corneal herpes, HSV type 2 (HSV-2), a causative agent of genital herpes, and varicella zoster virus (VZV), a causative agent of varicella (chickenpox) and herpes zoster (shingles), belong to alphaherpesvirinae. They usually infect mucosal epithelial cells and travel along the neuron (by a process called retrograde transport) to trigeminal ganglia and then establish latent infection.[1] Most of the problems with herpesvirus infections are due to reactivation that may lead to recurrent infections. The risk of diseases increases with age, and also frequently occurs in immunocompromised hosts, such as cancer patients, transplantation patients or acquired immunodeficiency syndrome patients.[2]

Standard antiviral drugs at present used in the treatment of HSV and VZV infections include acyclovir (ACV), valaciclovir (VACV, the oral prodrug of ACV), famciclovir (the oral prodrug of penciclovir) and vidarabine (Ara-A).[3,4] Despite a number of recent therapeutic advancements, there remains an urgent need to develop a new class of therapy, especially novel anti-herpes virus agent with a strong potency against HSV-2 and VZV, because anti-herpes virus agents used at present exhibit lower potency against HSV-2 and VZV. Furthermore, as they had some problems, such as cross-resistance and mutagenicity, the development of new agents with different mechanism of action from nucleoside analogs was required.

To discover a new candidate for anti-herpes virus agent, we screened microbial fermentation samples. In the preceding article,[5] we have reported the discovery of anti-VZV activity of CP-44161 (Figure 1; refs 6, 7), from an extract of fermentation broth of *Dactylosporangium* sp. no. 642788. CP-44161, which was a polyether reported earlier as an anticoccidal compound, exhibited a strong anti-VZV activity and lower cytotoxicity than other antiviral polyethers, such as nigericin and monensin.

In this study, we showed strong and broad antiviral activities of CP-44161 against HSV-1 and HSV-2 *in vitro*. Moreover, we demonstrated the antiviral activity of CP-44161 *in vivo* on the cutaneous HSV-2 infection model in Balb/c mice.

MATERIALS AND METHODS

Cells and viruses

African green monkey kidney cell line, Vero (CCL-81), was obtained from the American Type Culture Collection (ATCC; Rockville, MD, USA). Cells were grown and maintained in Eagle's minimal essential medium supplemented with 10% heat-inactivated fetal bovine serum (FBS), 0.075% $NaHCO_3$, 100 U ml^{-1} penicillin and 100 μg ml^{-1} streptomycin sulfate. Cells were grown at 37 °C in an atmosphere of 5% CO_2.

Herpes simplex virus type 1 (VR-3 strain) was kindly provided by Dr T Suzutani (Fukushima Medical University) and HSV-2 (186 strain)[8] was kindly provided by Dr Y Nishiyama (Nagoya University). Vero cells were

[1]Fermentation Research Labs, Astellas Pharma Inc., Tokodai, Tsukuba-shi, Ibaraki, Japan; [2]Pharmacology Research Labs, Astellas Pharma Inc., Miyukigaoka, Tsukuba-shi, Ibaraki, Japan; [3]Molecular Medicine Research Labs, Astellas Pharma Inc., Tokodai, Tsukuba-shi, Ibaraki, Japan; [4]Kikuchi Research Center, The Chemo-Sero-Therapeutic Research Institute, Kyokushi, Kikuchi-shi, Kumamoto, Japan; [5]Fermentation and Biotechnology Labs, Astellas Pharma Inc., Nakagawara, Kiyosu-shi, Aichi, Japan and [6]Pharmacology Research Labs, Astellas Pharma Inc., Kashima, Yodogawa-ku, Osaka, Japan
[7]These authors contributed equally to this work.
Correspondence: Dr Y Yamagishi, Fermentation Research Labs., Astellas Pharma Inc., 5-2-3, Tokodai, Tsukuba-shi, Ibaraki, 300-2698, Japan.
E-mail: yukiko.yamagishi@jp.astellas.com
Received 2 October 2008; accepted 5 December 2008; published online 23 January 2009

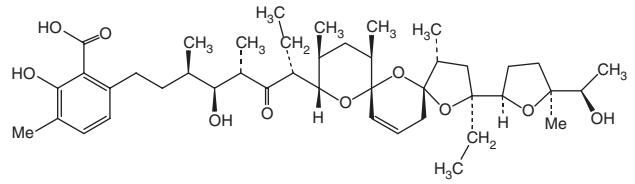

Figure 1 The structure of CP-44161.

used to produce virus pools, quantification of viral titers of stocks by the plaque assay. Viral replication studies of HSV were also performed in Vero cells.

Reagents and antiviral compounds

CP-44161 was prepared from a culture broth of *Dactylosporangium* sp. no. 642788 as described in our earlier report.[5]

Adenine 9-β-D-arabinofuranoside (Ara-A), DMSO and 3-(4,5-dimethylthiazol-2-yl)-2,5,-diphenyltetrazolium bromide (MTT) were obtained from Sigma (St Louis, MO, USA). ACV was purchased from GlaxoSmithKline (Tokyo, Japan). All compounds were dissolved in DMSO and then diluted with cell culture medium to yield 0.1% DMSO.

In vitro antiviral assays

The antiviral effects of compounds were determined by plaque reduction assay. Vero cells were grown to confluence in 24-well tissue culture plates and then infected with HSV-1 VR-3 strain or HSV-2 186 strain (40 plaque forming units (PFU) per well). After 1 h incubation, media containing 1.5% agarose in the presence or absence of various concentrations of the compounds were added. After 2 days, the cells were stained overnight with 0.01% neutral red and the number of viral plaques was counted.

Cytotoxicity assay

The cytotoxicity of compounds against growing Vero cells (5×10^3 cells per well in 96-well tissue culture plates) for 48 h was determined with an MTT assay as the procedure described earlier.[9]

In vivo studies

All animal experimental procedures were approved by the Animal Experiment Committee of Fujisawa Pharmaceutical Co. Ltd., the company that is now known as Astellas Pharma Inc.

Antiviral effect on cutaneous HSV infection in Balb/c mice

Seven-week-old female Balb/c mice (Charles River Laboratories, Yokohama, Tokyo, Japan) were used. Each group of animals, controls or treated, contained 10 mice.

Mice were anaesthetized with pentobarbital (50 mg kg^{-1}, i.p.), and then the mid-flank and right foot were clipped and depilated with a chemical depilatory, Hair Remover Milkycream (Kanebo Co. Ltd., Tokyo, Japan). Three days later, HSV-2 (3×10^3 PFU in 10 µl) was inoculated on the shin of the right hind paw.

For topical treatments of CP-44161, 3% olive oil solution was formulated. The olive oil without CP-44161 was used as the control. Drug treatment of animals began 3 or 4 days post-infection, and drugs were applied twice a day up to 8 days post-infection with a sterile cotton swab. ACV was dissolved in physiological saline and was administered orally at a dose of 100 mg kg^{-1}.

Beginning 1 day after infection, the inoculated site was evaluated and scored daily for 8 days: 0, no visible change in the inoculation or surrounding tissue; 1–2, one or two small vesicles on the inoculation site; 3–4, many vesicles on the inoculation or surrounding tissue; 5–6, mild zosteriform; 7–8, severe zosteriform.

Quantification of HSV DNA in the dorsal root ganglia

Seven-week-old female Balb/c mice (Charles River Laboratories, Yokohama, Japan) were infected as described above. Drug treatment of animals began 3 days after infection, and drugs were applied twice a day for the subsequent 3 days. Each group of animals, controls or treated, contained nine mice.

Five days post-infection, the dorsal root ganglia (DRG) were dissected from decapitated mice, immediately frozen by dry ice and stored at −80 °C until assay. Total DNA in the tissue was extracted with DNeasy tissue kit (Qiagen, Tokyo, Japan) according to a manufacturer's protocol.

The determination of HSV-2 DNA in the total DNA was quantified by real-time PCR using an ABI prism 7900HT sequence detection system (Applied Biosystems, Tokyo, Japan). Primers were designed for the detection of HSV-2 thymidine kinase (TK) gene. The sequences of the primers were as follows: TK (forward), 5′-ggctcctcatatcgggggggg-3′; TK (reverse), 5′-cgcggaacagggcaaacagc-3′. PCR was performed using the SYBR-green technology. The PCR program consists of activation step at 95 °C for 10 min and 40 cycles of denaturation at 94 °C for 0.5 min, annealing and extension at 67 °C for 1 min; HSV-2 genome was used as a standard. On each amplification curve, the threshold cycle was determined and used for the quantification of DNA using the ABI prism 7900 software.

Table 1 Antiviral activities against HSV-1,2 and cellular cytotoxicity of CP-44161

Compound	*HSV-1 VR-3* EC_{50} (µg ml^{-1})[a]	*HSV-2 186* EC_{50} (µg ml^{-1})[a]	*Vero* CC_{50} (µg ml^{-1})[b]
CP-44161	0.025	0.018	0.58
ACV	0.025	1.5	>50
Ara-A	1.9	5.6	25

Values provided in this table represent the mean of three independent experiments.
[a]Antiviral activity was determined by plaque assay. EC_{50} was the concentration that inhibited 50% of HSV replication in Vero cells.
[b]Cytotoxic effect was determined by MTT assay. CC_{50} was the concentration that showed 50% cytotoxic effects in Vero cells.

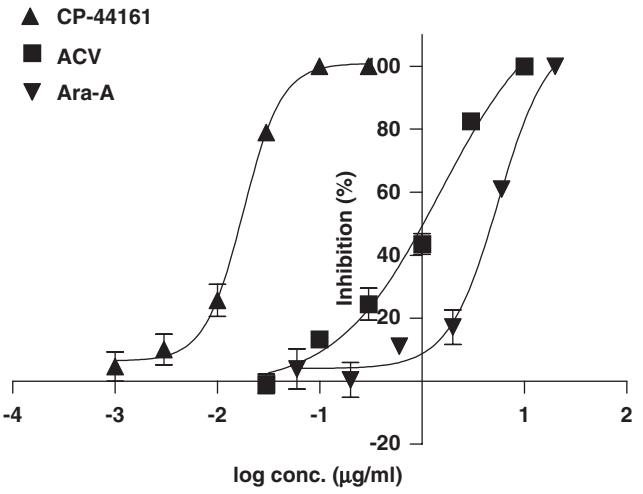

Figure 2 Dose-dependent antiviral activity of CP-44161 against HSV-2. Data are presented as the mean ± standard deviation of triplicate experiments.

Statistical analysis

Statistical significance was estimated according to *t*-tests using GraphPad Prism 4 software (GraphPad Software Inc.). A *P*-value of <0.05 was judged significant.

RESULTS

Antiviral activities of CP-44161 against HSV-1 and HSV-2

We obtained antiviral activities of CP-44161 against HSV-1 VR-3 strain and HSV-2 186 strain in plaque reduction assay. As shown in Table 1 and Figure 2, CP-44161 inhibited the replication of HSV-1 and HSV-2 in a dose-dependent manner. Of particular interest is the anti-HSV-2 activity (Figure 2). CP-44161 gave an EC_{50} value of 0.018 µg ml^{-1} compared with an EC_{50} value of 1.5 µg ml^{-1} for ACV

and of 5.6 μg ml^{-1} for Ara-A at 48 h. These results showed that CP-44161 had stronger anti-HSV-2 activity than those of ACV and Ara-A, which are in clinical use.

Antiviral effect of CP-44161 on cutaneous HSV-2 infections in Balb/c mice

Next, we tried to evaluate the antiviral activity of CP-44161 *in vivo* on the cutaneous HSV-2 infection model in Balb/c mice.

In the preliminary experiment, we found that mice cutaneously infected with HSV-2 showed lesion, but the lesion score began to decrease after day 8 in the control group. Therefore, the therapeutic effect was judged at day 8. As the oral bioavailability of CP-44161 was poor (data not shown), we evaluated antiviral activity of CP-44161 *in vivo* using the topical ointment. CP-44161 was administered topically with 3% olive oil solution (equivalent to 30 mg kg^{-1}). ACV was administered orally at a dose of 100 mg kg^{-1}.

In this model, the lesion started to develop on the skin on day 4 (Figures 3a and b). When the treatment was started from day 3, both CP-44161 and ACV significantly suppressed lesion development in the skin of mice with equivalent efficacy on day 8 (Figure 3c, $P<0.01$), but the olive oil control was ineffective in preventing lesion formation. Unlike the case of the treatment started from day 3, when the treatment was started from day 4, ACV was no longer able to inhibit the development of skin lesions. However, CP-44161 showed a significant effect in equivalent efficacy of the results that was started from day 3 (Figure 3c, $P<0.01$). These results indicated that CP-44161 could be given after the development of symptoms when ACV was no longer effective.

Effect of CP-44161 on HSV-2 DNA in the DRG

In the above cutaneous infection model, we ascertained the antiviral effect of CP-44161 *in vivo* by lesion score. To elucidate whether CP-44161 could inhibit viral proliferation *in vivo*, we quantified the HSV-2 DNA in DRG. We modified the method for the detection of HSV TK gene by using real-time PCR instead of the PCR analysis.[10]

In the preliminary experiment, we found that HSV proliferation in DRG peaked at day 5. Therefore, the therapeutic effect was judged at day 5. As shown in Figure 4, 3% ointment of CP-44161 significantly inhibited the replication of HSV-2 DNA in DRG (Figure 4, $P<0.01$). It was administered from day 3 to day 5. On day 5, DRG were dissected from treated mice, and the amount of HSV-2 DNA was quantified. When we made a comparison of the effect between CP-44161 and ACV on the same condition, CP-44161 exhibited an equivalent efficacy to the oral treatment of ACV (100 mg kg^{-1}) (data not shown).

DISCUSSION

We demonstrated earlier that the polyether compound CP-44161, discovered from one of the microbial fermentation samples produced by *Dactylosporangium* sp. no. 642788, showed anti-VZV activities.[5]

In this study, we first demonstrated that CP-44161 exhibited a broad anti-herpes virus activity against alphaherpesvirinae, such as HSV-1 and HSV-2, *in vitro* in a dose-dependent manner (Table 1 and Figure 2). CP-44161 inhibited replications of HSV-1 and HSV-2, similar to other polyethers, such as nigericin and monensin (data not shown). Especially in terms of anti-HSV-2 activity, this compound exhibited stronger potency than anti-HSV agents used at present, ACV and Ara-A (Figure 2).

Next we demonstrated that CP-44161 exhibited anti-herpes virus activity *in vivo*. Owing to its poor oral bioavailability, we evaluated antiviral activity of CP-44161 topically. As the solvent for CP-44161,

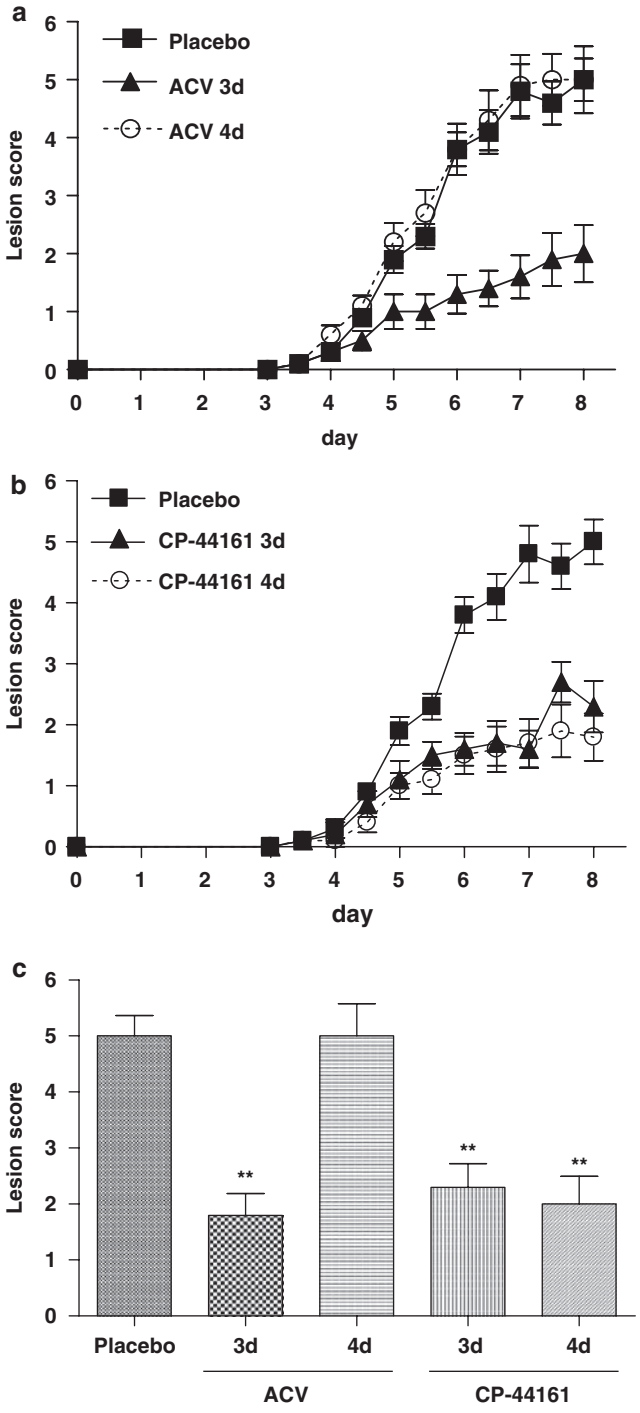

Figure 3 Effects of treatment with CP-44161 and ACV on the development of skin lesions on cutaneous HSV infection in Balb/c mice. Mice were inoculated with 3×10^3 PFU of HSV-2 strain 186 on the right hind paw on day 0. (**a**) ACV (100 mg kg^{-1}) was administered orally twice a day from 3 or 4 days after HSV-2 inoculation. Placebo (saline) was administered orally twice a day from 3 days after HSV-2 inoculation. (**b**) CP-44161 (3% ointment) was administered topically twice a day from 3 or 4 days after HSV-2 inoculation. Placebo (olive oil) was administered topically twice a day from 3 days after HSV-2 inoculation. (**c**) Lesion score on day 8. Data points represent the average score of 10 mice per group ± s.e.

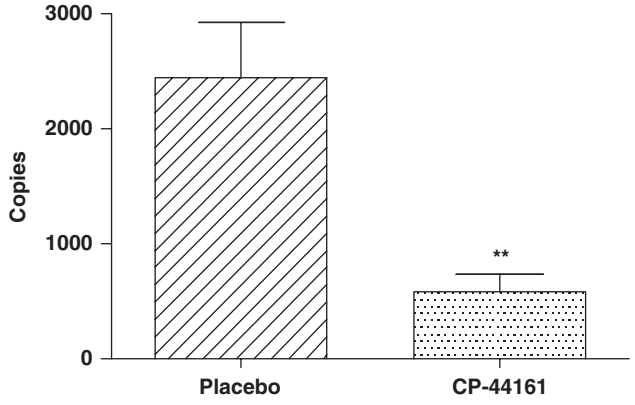

Figure 4 Effects of treatment with CP-44161 on the levels of HSV-2 gene in the dorsal root ganglia (DRG) on cutaneous HSV infection in Balb/c mice. Mice were inoculated with 3×10^3 PFU of HSV-2 strain 186 on the right hind paw on day 0. CP-44161 (3% ointment) and placebo (olive oil) was administered topically twice a day from 3 days after HSV-2 inoculation. On day 5, DRG were dissected and DNA was extracted. The copy number of HSV-2 in DRG was quantified by real-time PCR. Data points represent the average score of 9 mice per group ± s.e.

olive oil was selected, as CP-44161 was dissolved in olive oil completely and the olive oil formulation gave us the best antiviral effect (data not shown). Topical treatment of cutaneous HSV infection has the advantages of convenience and target site selection along with the prospect for maintenance of high local dose rates. However, in herpes zoster, topical monotherapy with ACV is less effective at preventing virus shedding than oral therapy and has little effect on symptoms.[11] So we selected oral administration of ACV.

The development of a zosteriform rash in this Balb/c mouse model is analogous to the final step in the development of a recrudescent lesion, which might occur after reactivation of latent virus.[12] In this system, virus traveled from the inoculation site, where virus replicated primarily, to the sensory nervous system and then returned to the skin, resulting in the zosteriform rash. When we started the treatment from day 3, after the onset of lesion development on the skin, both CP-44161 (3% ointment) and ACV (100 mg kg^{-1}) showed significant effects in lesion score, with equivalent efficacy on day 8 (Figure 3c). However, CP-44161 was effective even if the start of the treatment delayed, when ACV was no longer effective. Early treatment with antiviral agents, such as ACV and vidarabine, needs to shorten the skin lesions and complications related to herpes zoster.[13] In clinical practice, the start of administration of VACV limited within the first 72 h after the onset of symptoms. These results indicated that CP-44161 could be given over 72 h after the onset; that is, the recalcitrant cases against ACV.

Then we demonstrated that CP-44161 could inhibit viral proliferation *in vivo* by the quantified detection of the HSV-2 DNA in DRG. The results in Figure 4 confirmed that CP-44161 showed significant inhibition of the replication of HSV-2 DNA in DRG. The result indicated that the inhibition on the proliferation of HSV-2 in DRG may be responsible for the inhibition of zosteriform development of this compound.

Tissue culture studies have demonstrated antiviral activity of polyethers against a wide range of viruses.[14–17] In terms of the *in vivo* antiviral activities of polyethers, monensin, narasin, septamycin and nigericin were effective in treating an infection of transmissible gastroenteritis virus in piglets at doses of 0.1–100 mg kg^{-1} (ref. 18). In Bulgaria, a preparation containing a nigericin derivative (named Pandavir) was used topically as an anti-herpes drug.[19] However, the mechanism of antiviral activities *in vivo* has not been characterized. Here, we showed antiviral activity of polyether on murine model for the first time. This enabled us to analyze the mechanism of action of polyethers *in vivo* easily. Further experimental studies concerning the mode of action of CP-44161 *in vitro* and *in vivo* are under investigation.

According to this study, our data indicated that CP-44161 might be a good candidate for a new anti-herpes virus agent. It could be used on not only HSV but also VZV and also might have a potential against post-herpetic neuralgia.

ACKNOWLEDGEMENTS

We thank Mr R Enomoto for technical advice on Balb/c mice model and Dr K Sudo and Dr K Maki for helpful discussions.

1 Whitley, R. J. & Roizman, B. Herpes simplex virus infections. *Lancet.* **357,** 1513–1518 (2001).
2 Wutzler, P. Antiviral therapy of herpes simplex and varicella-zoster virus infections. *Intervirology* **40,** 343–356 (1997).
3 Littler, E. The past, present and future of antiviral drug discovery. *Idrugs* **7,** 1104–1112 (2004).
4 De Clercq, E. Recent highlights in the development of new antiviral drugs. *Curr. Opin. Microbiol.* **8,** 552–560 (2005).
5 Yamagishi, Y. *et al.* Discovery of anti-varicella zoster virus activity of polyether antibiotic CP-44161. *J. Antibiot.* **62,** 89–93 (2009).
6 Celmer, W. D. *et al. Polycyclic Ether Antibiotic Produced by New Species of Dactylosporangium in United States Patent 4081532* (Pfizer Inc.: New York, NY, USA, 1976).
7 Tone, J. *et al.* 18th ICACC Meeting, Atlanta, Georgia Abstract: (1978).
8 Nishiyama, Y. *et al.* Construction of a US3 lacZ insertion mutant of herpes simplex virus type 2 and characterization of its phenotype *in vitro* and *in vivo. Virology* **190,** 256–268 (1992).
9 Denizot, F., Lang, R., Rapid colorimetric assay for cell growth and survival. Modifications to the tetrazolium dye procedure giving improved sensitivity and reliability. *J. Immunol. Methods* **89,** 271–277 (1986).
10 Takasaki, I. *et al.* Allodynia and hyperalgesia induced by herpes simplex virus type-1 infection in mice. *Pain* **86,** 95–101 (2000).
11 Bridges, C. G. *et al.* The ribonucleotide reductase inhibitor (E)-2′-fluoromethylene-2′-deoxycytidine (MDL 101,731): a potential topical therapy for herpes simplex virus infection. *Antiviral Res.* **27,** 325–334 (1995).
12 Simmons, A. & Nash, A. A. Zosteriform spread of herpes simplex virus as a model of recrudescence and its use to investigate the role of immune cells in prevention of recurrent disease. *J. Virol.* **52,** 816–821 (1984).
13 Whitley, R. J. *et al.* Disseminated herpes zoster in the immunocompromised host: a comparative trial of acyclovir and vidarabine. The NIAID Collaborative Antiviral Study Group. *J. Infect. Dis.* **165,** 450–455 (1992).
14 Grabley, S. *et al.* Secondary metabolites by chemical screening. 17. Nigericinol derivatives: synthesis, biological activities, and modeling studies. *J. Med. Chem.* **35,** 939–944 (1992).
15 Johnson, D. C. & Spear, P. G. Monensin inhibits the processing of herpes simplex virus glycoproteins, their transport to the cell surface, and the egress of virions from infected cells. *J. Virol.* **43,** 1102–1112 (1982).
16 Kousoulas, K. G. *et al.* Effect of the ionophore monensin on herpes simplex virus type 1-induced cell fusion, glycoprotein synthesis, and virion infectivity. *Intervirology* **20,** 56–60 (1983).
17 Kaiser, C. J. & Radsak, K. Inhibition by monensin of human cytomegalovirus DNA replication. *Archiv. Virology* **94,** 229–245 (1987).
18 Gale, C. & Mcdougald, L. R. *Anti-Viral Method in Animals in United States Patent 3995027* (Eli Lilly and Company: Indianapolis, IN, USA, 1976).
19 Dundarov, S. *et al.* Means for virus disease cure in *Japanese Patent* 1093524 A (Bulgaria, 1989).

The Journal of Antibiotics (2009) 62, 99–104

www.nature.com/ja

ORIGINAL ARTICLE

Caboxamycin, a new antibiotic of the benzoxazole family produced by the deep-sea strain *Streptomyces* sp. NTK 937*

Claudia Hohmann[1,8], Kathrin Schneider[2,8], Christina Bruntner[1], Elisabeth Irran[2], Graeme Nicholson[3], Alan T Bull[4], Amanda L Jones[5], Roselyn Brown[5], James EM Stach[5], Michael Goodfellow[5], Winfried Beil[6], Marco Krämer[7], Johannes F Imhoff[7], Roderich D Süssmuth[2] and Hans-Peter Fiedler[1]

Caboxamycin, a new benzoxazole antibiotic, was detected by HPLC-diode array screening in extracts of the marine strain *Streptomyces* sp. NTK 937, which was isolated from deep-sea sediment collected in the Canary Basin. The structure of caboxamycin was determined by mass spectrometry, NMR experiments and X-ray analysis. It showed inhibitory activity against Gram-positive bacteria, selected human tumor cell lines and the enzyme phosphodiesterase.
The Journal of Antibiotics (2009) **62,** 99–104; doi:10.1038/ja.2008.24; published online 23 January 2009

Keywords: benzoxazole antibiotic; fermentation; isolation; marine *Streptomyces*; structural elucidation

INTRODUCTION

A set of 600 actinomycetes isolated from marine sediments from various sites in the Atlantic and Pacific Oceans were screened using our HPLC-diode array technology for the production of bioactive secondary metabolites. It is becoming increasingly clear that actinomycetes isolated from marine habitats are a rich source of new natural products, including drug candidates.[1–5] Extracts from the culture filtrate of strain NTK 937 showed a prominent peak in the HPLC-diode array analysis that had an unusual UV-visible spectrum, albeit it was similar to that of nataxazole from our HPLC-UV-Vis database which contains 867 entries, mostly antibiotics.[6] Nataxazole, a new member of the benzoxazole family of antibiotics, was extracted from terrestrial *Streptomyces* sp. Tü 6176.[7] Nataxazole has a structure similar to that of benzoxazoles UK-1[8] and AJI9561,[9] which were derived from *Streptomyces* strains, and were shown to have potent anti-tumor properties. The similarity of the UV-visible spectrum of the metabolite produced by strain NTK 937 to nataxazole underlines its structural relationship to benzoxazoles; the new compound was named caboxamycin (**1**) composed from the strain's collection site, the Canary Basin and the benzoxazole scaffold of its structure, which is shown in Figure 1. Herein, we report on the taxonomy of the producing strain, the fermentation, isolation and structural elucidation of caboxamycin and its biological activities.

RESULTS

Taxonomy of the producing strain

The chemical and morphological properties of strain NTK 937 were consistent with its classification in the genus *Streptomyces*.[10] The organism formed an extensively branched substrate mycelium, straight spore chains on the aerial mycelium, contained hexa- and octa-hydrogenated menaquinones with nine isoprene units as the predominate isoprenologues, and gave whole-cell hydrolysates rich in LL-diaminopimelic acid. Comparison of an almost complete 16S rRNA sequence of strain NTK 937 with corresponding sequences of *Streptomyces* type strains showed that it formed a distinct phyletic line in the *Streptomyces* 16S rRNA gene tree.

Screening, fermentation and isolation

When grown in the 20-liter fermentor strain NTK 937 reached a maximal biomass of 12 mg dry weight per ml after 5 days of incubation. Production of **1** started at 72 h, reaching a maximal yield of 15 mg l^{-1} after incubation for 5 days. The HPLC elution profile of the corresponding culture filtrate is shown in Figure 2. **1** was isolated from the culture filtrate by separation on an Amberlite XAD-16 column; the extracts were concentrated to an aqueous residue and extracted with ethylacetate and concentrated *in vacuo* to dryness. The

[1]Mikrobiologisches Institut, Universität Tübingen, Auf der Morgenstelle, Tübingen, Germany; [2]Institut für Chemie, Technische Universität Berlin, Berlin, Germany; [3]Institut für Organische Chemie, Universität Tübingen, Auf der Morgenstelle, Tübingen, Germany; [4]Research School of Biosciences, University of Kent, Canterbury, UK; [5]School of Biology, Newcastle University, Newcastle upon Tyne, UK; [6]Institut für Pharmakologie, Medizinische Hochschule Hannover, Carl-Neuberg-Str. 1, Hannover, Germany and [7]Leibniz-Institut für Meereswissenschaften IFM-GEOMAR, Düsternbrooker, Kiel, Germany
[8]These authors contributed equally to this work.
Correspondence: Dr RD Süssmuth, Institut für Chemie, Technische Universität Berlin, Straße des 17. Juni 124, 10623 Berlin, Germany.
E-mail: suessmuth@chem.tu-berlin.de or H-P Fiedler, Mikrobiologisches Institut, Universität Tübingen, Auf der Morgenstelle 28, 72076 Tübingen, Germany.
E-mail: hans-peter.fiedler@uni-tuebingen.de
*Art. No. 48 in 'Biosynthetic Capacities of Actinomycetes'. Art. No. 47: See ref. 7
Received 25 July 2008; accepted 17 December 2008; published online 23 January 2009

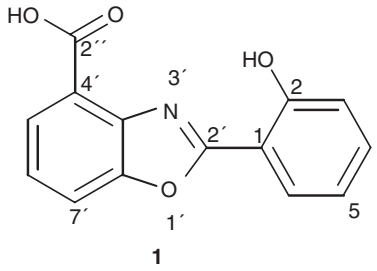

1

Figure 1 Structure of caboxamycin (**1**).

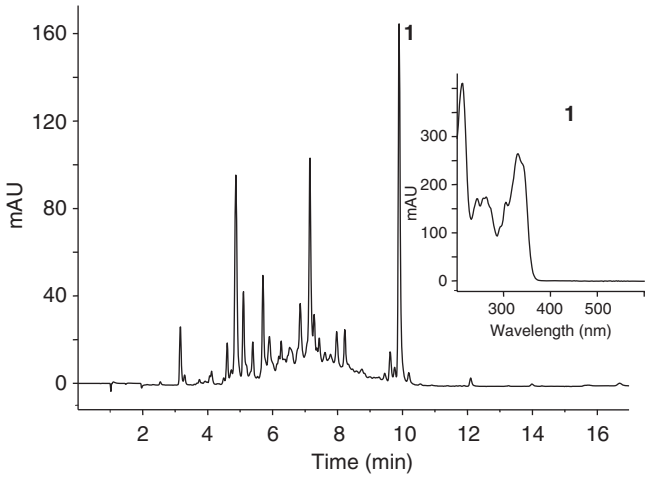

Figure 2 HPLC analysis of a culture filtrate from *Streptomyces* sp. NTK 937 at a fermentation time of 120 h, monitored at 310 nm, and UV-visible spectrum of caboxamycin (**1**), retention time 9.9 min.

crude product was purified by chromatography on a diol-modified silica gel column followed by chromatography on a Sephadex LH-20 and Toyopearl HW-40S column. **1** was obtained as a white, yellow-fluorescent powder after concentrated to dryness.

Structural elucidation

The mass spectrum derived from the HPLC-ESI-MS chromatograms revealed the molecular mass for **1** [$(M+H)^+$=256.0]. The exact molecular mass was determined by high-resolution ESI-FT-ICR-MS as 256.06010 Da [$(M+H)^+$] (**1**), this corresponds to the molecular formulae $C_{14}H_9NO_4$ (**1**) [$(M+H)^+_{theor}$=256.06043; Δm=1.29 p.p.m.]. The ESI-FTICR-MS measurement of **1** showed an additional molecular mass of 564.02409 Da [(M-3H+Fe+H)$^+$]. This corresponds well with the molecular formula $C_{28}H_{16}N_2O_8Fe$ [$(2M-3H+Fe+H)^+_{theor}$ =564.02506; Δm=1.72 p.p.m.] and suggests that the compound is able to complex metal ions. The physico-chemical properties of **1** are summarized in Table 1.

The ^{1}H-NMR-spectrum of **1** showed seven signals in the aromatic region between 8.2 and 7 p.p.m. and one broad signal at 11.8 p.p.m. ^{13}C-NMR and DEPT spectra revealed the presence of seven aromatic CH groups and seven quaternary carbons between 170 and 110 p.p.m. The correlation of ^{1}H-NMR-signals to the corresponding C-atoms was determined in a Heteronuclear Multiple Quantum Coherence NMR experiment. Seven signals were found in accordance with the DEPT spectrum. Compared to the molecular formula, $C_{14}H_9N_1O_4$, two protons should be bound to heteroatoms (OH or NH), one of which giving a broad signal at 11.8 p.p.m. in the ^{1}H-NMR-spectrum.

Table 1 Physico-chemical properties of caboxamycin (1)

	1
Appearance	White powder
Molecular weight	255
Molecular formula	$C_{14}H_9N_1O_4$
ESI-FT-ICR MS ($m\,z^{-1}$)	
Found	256.06010 $(M+H)^+$
Calcd	256.06043 $(M+H)^+$
UV λ_{max}^{MeOH} [nm] (ε [$cm^2\,mmol^{-1}$])	212 (20), 243 (8.16), 257 (sh, 8.16), 263 (8.37), 273 (sh, 7.35), 292 (sh, 5.51), 305 (sh, 7.76), 331 (11.43), 342 (sh, 10.82)
IR ν_{max} (cm^{-1})	3466, 3088, 3046, 3006, 2956, 2920, 2850, 2676, 2570, 1690, 1633, 1591, 1546, 1486, 1433, 1296, 1264, 1247, 1239, 1183, 1155, 1065, 875, 752, 740, 724

The structure was fully elucidated using COSY and HMBC spectra. The ^{1}H-^{1}H-COSY experiment revealed two spin systems, one of which showed correlations from H-4 to H-6 and the other one from H-10 to H-13 (Figure 3). The structure was fully elucidated using the HMBC spectrum; structure consists of two constituents, a salicylic acid and a hydroxy-anthranilic acid connected by a ring closure between the carboxylic acid group of the salicylic acid and the hydroxyl- and amin-groups of the hydroxy-anthranilic acid (Figure 1). The correlations from H-5′ to C-2′′, C-3′a and C-7′, from H-6′ to C-4′ and C-7′a and from H-7′ to C-3′a and C-5′, shown in Figure 3, together with the chemical shifts of C-3′a, 138.7 p.p.m. and C-7′a, 149.5 p.p.m., prove the presence of a hydroxy-anthranilic acid, especially for the positions of the nitrogen-, the oxygen-atoms and of the carboxylic acid group at C-3′a. The presence of a salicylic acid moiety was proven by the connectivities from H-3 to C-1 and C-5, from H-4 to C-2 and C-6, from H-5 to C-1 and C-3 and from H-6 to C-2′, C-2 and C-4 (Figure 3). Comparing the NMR data obtained for **1**, summarized in Table 2, to the NMR data of known metabolites (Table 2) with a similar structure; for example, AJI9561[11] (Figure 4), verifies the structure of **1**. Moreover, parallel to NMR studies, crystallization experiments were performed with a single crystal obtained for compound **1**. Subsequent X-ray structural determination fully confirmed the structure of compound **1** (Figure 3).

Biological activity

Caboxamycin (**1**) showed antibiotic activity against the Gram-positive bacteria *Bacillus subtilis* (IC_{50}=8 μM), *Staphylococcus lentus* (IC_{50}=20 μM) and the yeast *Candida glabrata* (IC_{50}=117 μM). Also the biofilm formation of *Staphylococcus xylosus* was weakly inhibited. A significant activity was present against the phytopathogenic bacteria *Xanthomonas campestris* (IC_{50}=43 μM) and *Ralstonia solanacearum* (IC_{50}=176 μM) and against the opportunistic pathogen *Staphylococcus epidermidis* (IC_{50}=43 μM). The corresponding data for chloramphenicol (positive control prokaryotes) were: *Bacillus subtilis* (IC_{50}=9 μM), *Staphylococcus lentus* (IC_{50}=14 μM), *Xanthomonas campestris* (IC_{50}=6 μM), *Ralstonia solanacearum* (IC_{50}=75 μM), *Staphylococcus epidermidis* (IC_{50}=7 μM) and for cycloheximide (positive control eukaryotes): *Candida glabrata* (IC_{50}=4 μM).

The cytotoxic effect of caboxamycin (**1**) was tested in different tumor cell lines. It showed a moderate growth inhibitory activity (IC_{50}: 28.6–29.4 μM) towards gastric adenocarcinoma (AGS), hepato-

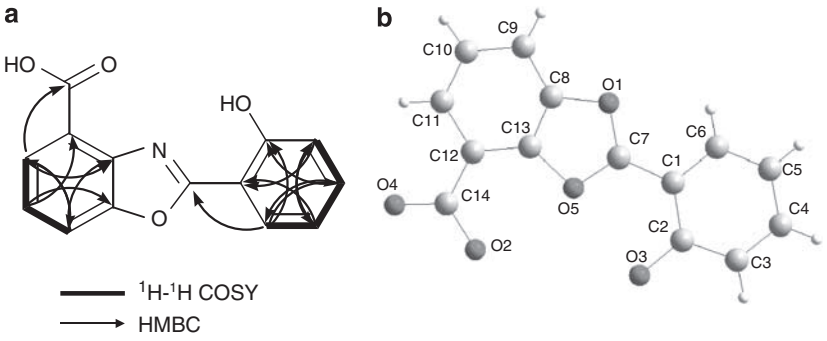

Figure 3 Selected 2D NMR correlations (**a**) and X-ray structure (**b**) of caboxamycin (**1**).

Table 2 ^{1}H and ^{13}C NMR spectral data of caboxamycin (1) and AJI9561 (3) [11] in DMSO-d_6

	1 in DMSO-d_6		*3 in DMSO-d_6*	
No.	*δ (^{1}H) [p.p.m.] J in Hz*	*δ (^{13}C) [p.p.m.]*	*δ (^{1}H) [p.p.m.] J in Hz*	*δ (^{13}C) [p.p.m.]*
1		109.7	—	120.5
2		158.4	—	150.4
3	7.12 d (8.13)	117.3	7.06 d (8.0)	121.1
4	7.53 m	134.4	7.36 t (8.0)	131.8
5	7.07 t (7.23)	119.9	6.85 d (8.0)	128.7
6	8.00 d (7.61)	127.4		140.8
2′		163.6		161.5
3′a		138.7		139.9
4′		121.8		118.7
5′	7.97 d (7.74)	127.2	8.37 d (7.6)	125.9
6′	7.54 m	125.3	7.59 t (7.6)	125.3
7′	8.07 d (8.00)	115.3	7.88 d (7.6)	113.9
7′a		149.5		151.2
2″		165.6		162.8
3″ a				141.4
4″				122.3
5″			8.21 d (8.0)	127.3
6″			7.58 d (8.0)	124.8
7″			7.94 d (8.0)	115.3
7″ a				151.7
Me			2.86 s	21.3
OH			12.91 brs	
COOH			11.7 br	

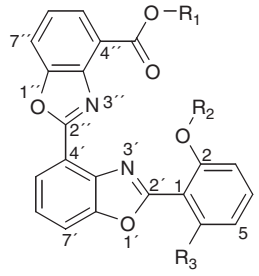

2:UK-1:$R_1 = CH_3$; $R_2 = R_3 = H$
3:AJI9561:$R_1 = R_2 = H$; $R_3 = CH_3$
4:Nataxazole:$R_1 = CH_3$; $R_2 = H$; $R_3 = CH_3$
5:Me-UK-1:$R_1 = R_2 = CH_3$; $R_3 = H$
6:DeMe-UK-1:$R_1 = R_2 = R_3 = H$

Figure 4 Structures of benzoxazole metabolites from *Streptomyces* strains.

Table 3 Growth inhibitory activity ($\mu g\,ml^{-1}$) of caboxamycin (1) and UK-1 (2) against selected human tumor cell lines

Cell line	***1***		***2***	
	GI_{50}	*TGI*	*GI_{50}*	*TGI*
AGS	7.5	>10[a]	0.8	1.9
Hep G2	7.4	>10[b]	0.085	2.4
MCF7	7.3	>10[c]	0.65	3.5

Abbreviations: GI_{50}, 50% growth inhibition; TGI, 100% growth inhibition.
[a]72% inhibition at 10 $\mu g\,ml^{-1}$.
[b]70% inhibition at 10 $\mu g\,ml^{-1}$.
[c]80% inhibition at 10 $\mu g\,ml^{-1}$.

cellular carcinoma (Hep G2) and breast carcinoma cells (MCF7). UK-1 (**2**) was more potent than **1** (Table 3).

Caboxamycin (**1**) is a weak inhibitor of bovine brain PDE (IC_{50}=148 μM) and only slightly inhibited human PDE-4B2 (IC_{50}=1.46 mM).

DISCUSSION

The benzoxazole core structure of caboxamycin (**1**) is part of the natural products UK-1 (**2**) from *Streptomyces* sp. 517-02,[8] AJI9561 (**3**) from *Streptomyces* sp. AJI9561[9] and nataxazole (**4**) from *Streptomyces* sp. Tü 6176.[7] **2**∼**4** showed potent cytotoxic activities against various tumor cell lines whereas growth inhibition was not observed against Gram-positive or Gram-negative bacteria, or against yeasts and fungi. Furthermore, two derivatives of UK-1, Me-UK-1 (**5**) and DeMe-UK-1 (**6**), were prepared by methylation with methyl iodide and alkaline hydrolysis, respectively;[12] their structures are shown in Figure 4. Interestingly, **6** exhibited anti-bacterial activity[13] and **5** anti-fungal activity.[14]

In the last decade efforts have been made to understand the selective cytotoxic activity of UK-1 (**2**) towards cancer cells versus bacteria and fungi, and for this purpose various synthetic derivates have been prepared (Figure 5) and their biological activities evaluated and compared.[15–17] Reynolds *et al.*[18] investigated the metal ion coordination by **2**. It was shown that **2** bound divalent metal ions and DNA in a divalent metal ion-dependent manner. It also bound to double-stranded DNA 10 times more tightly in the presence of Mg^{2+} and inhibited human topoisomerase II.[16]

It was demonstrated that the synthetic benzoxazole derivative **7**, which is the methyl ester of **1**, retained the selectivity of the natural product against cancer cells and therefore represents a minimum structural pharmacophore.[14] The synthetic derivative **8**, which constitutes the methyl ether of **1** and **9**, which represents the decarboxylated **1**, did not exhibit any cytotoxic or anti-bacterial activities.[15] It

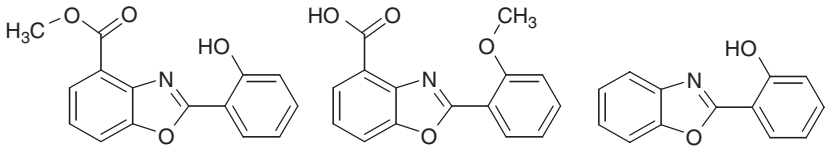

7 **8** **9**

Figure 5 Structures of synthetic benzoxazole derivatives.[14]

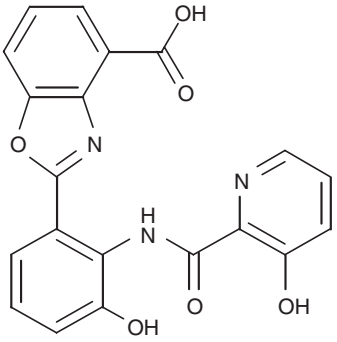

10

Figure 6 Structure of antibiotic A33853.

was shown that an appropriate substituent in position 4′ of the benzoxazole core is important for an efficient Mg^{2+}-binding ability. The described cytotoxic activity of the described natural product **1** and the observation of an iron-intermediate with ESI-FT-ICR-MS are in accordance with these results. UK-1 displays cytotoxic activity against certain solid tumor-derived cell lines.[15] Caboxamycin is less potent than UK-1. Therefore the interaction between **2** and the Mg^{2+} ion may be stronger than that of **1**. Synthetic derived **1** has been described as an intermediate in the synthesis of benzoxazole carboxamides, but its biological activity has not been evaluated.[19] The streptomycete metabolite **1** and the evaluation of its biological activity add an element to the investigations of synthetic derivatives of the natural product UK-1 (**2**).

A further benzoxazole natural product related to UK-1 family is antibiotic A-33853 (**10**) which is produced by a *Streptomyces* strain;[20] its structure is shown in Figure 6. Although benzoxazoles **2–6** are composed of two molecules, hydroxy-anthranilic acid and one salicylic acid, which form two ring closures resulting in the bis(benzoxazole) structure, **10** consists of two molecules, hydroxy-anthranilic acid and one 3-hydroxy-picolinic acid, which build one benzoxazole and one amide bond. Interestingly, **10** showed anti-bacterial activity against penicillin-resistant *Staphylococcus* and *Streptococcus* strains, and anti-viral and anti-trichomonal activities *in vitro*.[20] Unfortunately, data are not available on the cytotoxic activity and the metal-binding ability of **10**, hence it is not possible to consider the contributions of the various structural elements to the biological activity.

Among biological activities of caboxamycin (**1**) the inhibition of phosphodiesterases are notable. Phosphodiesterases are essential regulators of cyclic nucleotide signalling with diverse physiological functions. PDE-4-selective inhibitors have therapeutic potential for treating major diseases, such as asthmatic inflammation and chronic obstructive pulmonary disease[21,22] and several PDE-4 inhibitors have reached the clinical trial of phases II and III status.[22] The PDE-4B enzyme is widely expressed in human inflammatory cells, negatively regulates a wide range of pro-inflammatory and immune cells[21,23] and appears to be involved in the production of the tumor necrosis factor TNF-α and other cytokines promoting the inflammatory response.[22] Therefore, by inhibiting the PDE-4B enzyme, inflammatory response is blocked or strongly reduced.

The results pointed out, that caboxamycin has a 10-fold stronger inhibitory effect to the mixture of the three bovine PDE isoforms (IC_{50}=148 μM) than on the human PDE-4B2 (IC_{50}=1.46 mM). This might be based on significantly stronger inhibition of PDE-2 and PDE-10 by caboxamycin than PDE-4. Despite this weak inhibition, the effect is notable because the effect against other phosphodiesterases possibly may be much stronger than the measured effects against the selection of enzymes tested. In addition, structural modifications of the caboxamycin molecule may yield molecules demonstrating much stronger effects. Structural modification according to the binding properties to human PDE-4B2 already has successfully been carried out with other PDE-4 inhibitors.[22]

METHODS

Producing organism and taxonomy

Strain NTK 937 was isolated from an Atlantic Ocean deep-sea sediment core collected in 2001 at the southern edge of the Saharan debris flow near the Canary Islands (27°02′392N, 18°29′022W) at a depth of 3814 m. Isolations were made from the turbidite fraction of the core (0–38 cm from surface) which was deposited approximately 1,000 years ago, but derived from older (approximately 200 000 years) previously deposited sediment from further upslope.[11]

Strain NTK 937 was examined using a combination of genotypic and phenotypic procedures known to produce data of value in the delineation of *Streptomyces* species.[24,25]

Fermentation and isolation

Batch fermentations of strain NTK 937 were carried out in a 20-liter fermentor equipped with a turbine impeller system (b20; B.Braun, Melsungen, Germany) in a complex medium consisting of mannitol 20 g and soybean meal 20 g in 1 l tap water; pH was adjusted to 7.5 prior to sterilization. The fermentor was inoculated with 5% by volume of a shake flask culture grown in a seed medium at 27 °C in 500 ml-Erlenmeyer flasks with a single baffle for 72 h on a rotary shaker at 120 r.p.m. The fermentation was carried out for 5 days with an aeration rate of 0.5-volume air/volume/minute and agitation at 250 r.p.m.

Hyphlo Super-cel (2%) was added to the fermentation broth, which was separated by multiple sheet filtration into culture filtrate and mycelium. The culture filtrate was applied to an Amberlite XAD-16 column (resin volume 800 ml) and the resin washed with H_2O and H_2O–MeOH (8:2); caboxamycin (**1**) was eluted with 100% MeOH and concentrated *in vacuo* to an aqueous residue. The concentrate was extracted three times with ethylacetate, and the organic extracts combined and concentrated *in vacuo* to dryness. The crude product was dissolved in MeOH and applied to a diol-modified silica gel column (40×2.5 cm; LiChroprep Diol, Merck, Darmstadt, Germany). **1** was separated using a linear gradient of cyclohexane–DCM–MeOH and was eluted with DCM–10% MeOH at a flow rate of 420 ml h^{-1}. Further purification was achieved by chromatography on Sephadex LH-20 using MeOH–DCM (2:1) and Toyopearl HW-40S with MeOH (each column 90×2.5 cm) at a flow rate of 30 ml h^{-1}.

HPLC-DAD analyses

The chromatographic system consisted of a HP 1090M liquid chromatograph equipped with a diode-array detector and a HP Kayak XM 600 ChemStation (Agilent Technologies, Waldbronn, Germany). Multiple wavelength monitoring was performed at 210, 230, 260, 280, 310, 360, 435 and 500 nm, and UV-visible spectra were measured from 200 to 600 nm. A 10-ml aliquot of the fermentation broth was centrifuged, and the supernatant adjusted to pH 4 and extracted with the same volume of EtOAc. After centrifugation, the organic layer was concentrated to dryness *in vacuo* and resuspended in 1 ml MeOH. Here, 10 µl aliquots of the samples were injected onto an HPLC column (125×4.6 mm) fitted with a guard-column (20×4.6 mm) filled with 5-µm Nucleosil-100 C-18 (Maisch, Ammerbuch, Germany). The samples were analyzed by linear gradient elution using 0.1% ortho-phosphoric acid as solvent A and MeCN as solvent B at a flow rate of 2 ml min^{-1}. The gradient was from 0 to 100% for solvent B in 15 min with a 2-min hold at 100% for solvent B.

Structural elucidation

LC-MS experiments were performed on an Applied Biosystems QTrap 2000 (Applied Biosystems, Darmstadt, Germany) coupled to an Agilent 1100 HPLC system (Agilent). High-resolution ESI-FT-ICR mass spectra were recorded on an APEX II FTICR mass spectrometer (4.7 T, Bruker-Daltonics, Bremen, Germany) and NMR experiments on a DRX 500 NMR spectrometer (Bruker, Karlsruhe, Germany) equipped with a BBI probe head with z gradients.

Biological activity

Anti-microbial assays were performed as described earlier.[26] The following strains were used: *Staphylococcus epidermidis* (DSM 20044), *Pseudomonas syringae* pvar. *aptata* (DSM 50252), *Pseudomonas fluorescens* (NCIMB 10586), *Xanthomonas campestris* (DSM 2405), *Ralstonia solanacearum* (DSM 9544) and *Candida glabrata* (DSM 6425).

Biofilm formation with *Staphylococcus xylosus* (DSM 20267) was analyzed by a crystal violet staining assay[27] in 96-well microtiter plates with the following modifications: cells were cultivated at 37 °C instead of 30 °C; the brain heart medium (BHI) was replaced by the trypticase soy yeast extract medium (30 g l^{-1} Bacto tryptic soy broth and 3 g l^{-1} yeast extract), the cell density at 600 nm of the initial bacterial suspension was 0.01 and EtOH was used instead of glacial acetic acid for solubilization of the incorporated dye.

The inhibitory action of caboxamycin (**1**) on the growth of tumor cells was tested according to NCI guidelines[28] with the human tumor cell lines AGS (gastric adenocarcinoma), MCF7 (breast adenocarcinoma) and Hep G2 (hepatocellular carcinoma). Aliquots of cell suspensions (5×10^3 cells) were placed in 96-well microtiter plates in 0.2 ml culture medium (RPMI-1640 with 10% fetal calf serum) and incubated in a humidified atmosphere of 5% CO_2 in air. After 24 h caboxamycin (**1**) (0.1 ~ 10 µg ml^{-1}) and UK-1 (**2**) (0.1 ~ 10 µg ml^{-1}) as positive control were added to the cells and the cells cultivated for additional 48 h. The cell count was surveyed by protein determination with sulforhodamine B. From the resulting concentration–activity curves, the GI_{50} (concentration at which half of the cells were inhibited in their growth) and TGI (concentration at which a total inhibition of cell growth was observed) values were obtained.

Analysis of the effect of **1** on human recombinant cAMP-specific phosphodiesterase (PDE-4B2) was carried out with final concentrations of the substance of 488 µM (125 µg ml^{-1}) in 50 mM Tris-HCl buffer (pH 7.5) containing 8.3 mM $MgCl_2$, 1.7 mM EGTA and 10 mU recombinant human cAMP-specific PDE 4B2 (Merck Bioscience 524736-10U, Darmstadt, Germany) in a volume of 20 µl per well. The reaction was started with 20 µl of 40 µM cAMP (Sigma A9501, Taufkirchen, Germany) dissolved in 50 mM Tris-HCl (pH 7.5) containing 8.3 mM $MgCl_2$ and 1.7 mM EGTA. After an incubation period of 30 min at 30 °C the reaction was stopped and the AMP concentration was quantified with the PDELight HTS cAMP Phosphodiesterase Assay Kit (Lonza, LT07-600, Wuppertal, Germany) according to the instructions of the supplier. The luminescence was measured using the microtiter plate reader Infinite M200 (Tecan, Crailsheim, Germany) with 0.1 s integration time. For inhibition of the PDE, 100 µM of Rolipram (4-[3-(Cyclopentyloxy)-4-methoxyphenyl]-2-pyrrolidinone) (Merck Bioscience Cat.No. 557330) were used as a positive control. The effect of **1** on PDE activity from bovine brain (a mixture of three isoforms PDE-2, PDE-4 and PDE-10) was tested accordingly. 10 mM Tris-HCl buffer (pH 7.4) was used containing 1 mU (1 µl) of 3,5-cyclic-nucleotide-specific PDE from bovine brain (Sigma P9529)[29] in a total volume of 20 µl, and the reaction was started with 20 µl of 40 µM cAMP (Sigma A9501) solution in 10 mM Tris-HCl pH 7.4.

ACKNOWLEDGEMENTS

This work was supported by Boehringer-Ingelheim Pharma GmbH (Biberach, Germany), the European Commission (project ACTINOGEN, 6th framework, Grant LSHM-CT-2004-005224). We thank the crew of the RRS Charles Darwin for collecting deep-sea samples and Dr DG Masson (National Oceanography Centre, Southampton, UK) for access to the sediment cores, Mr G Grewe, Universität Tübingen for assistance in fermentations, Mrs A Erhard, IFM-GEOMAR for technical support and Agilent Technologies (Waldbronn, Germany) for HPLC-software support.

1 Jensen, P. R., Mincer, T. C., Williams, P. G. & Fenical, W. Marine actinomycete diversity and natural product discovery. *Antonie van Leeuwenhoek*. **87,** 43–48 (2005).
2 Fiedler, H.-P. *et al.* Marine actinomycetes as a source of novel secondary metabolites. *Antonie van Leeuwenhoek*. **87,** 37–42 (2005).
3 Fenical, W. & Jensen, P. R. Developing a new resource for drug discovery: marine actinomycete bacteria. *Nature Chem. Biol*. **2,** 666–673 (2006).
4 Lam, K. S. Discovery of novel metabolites from marine actinomycetes. *Curr Opin Microbiol* **9,** 245–251 (2006).
5 Bull, A. T. & Stach, J. E. M. Marine actinobacteria: new opportunities for natural product search and discovery. *Trends Microbiol*. **15,** 491–499 (2007).
6 Fiedler, H.-P. Biosynthetic capacities of actinomycetes. 1. Screening for novel secondary metabolites by HPLC and UV-visible absorbance libraries. *Nat. Prod. Lett.* **2,** 119–128 (1993).
7 Sommer, P. S. M. *et al*. Nataxazole, a new benzoxazole derivative with antitumor activity produced by *Streptomyces* sp. Tü 6176. *J. Antibiot.* **61,** 683–686 (2008).
8 Ueki, M. *et al*. UK-1, a novel cytotoxic metabolite from *Streptomyces* sp. 517-02. I. Taxonomy, fermentation, isolation, physico-chemical and biological properties. *J. Antibiot.* **46,** 1089–1094 (1993).
9 Sato, S. *et al*. AJI9561, a new cytotoxic benzoxazole derivative produced by *Streptomyces* sp. *J. Antibiot.* **54,** 102–104 (2001).
10 Manfio, G. P., Zakrezewska-Czerwinska, J., Atalan, E. & Goodfellow, M. Towards minimal standards for the description of *Streptomyces* species. *Bioteckhnologia* **7–8,** 242–253 (1995).
11 Stach, J. E. M. *et al.* Statistical approaches for estimating actinobacterial diversity in marine sediments. *Appl. Environm. Microbiol*. **69,** 6189–6200 (2003).
12 Shibata, K., Kashiwada, M., Ueki, M. & Taniguchi, M. UK-1, a novel cytotoxic metabolite from *Streptomyces* sp. 517-02. II. Structural elucidation. *J. Antibiot.* **46,** 1095–1100 (1993).
13 Ueki, M. & Taniguchi, M. UK-1, a novel cytotoxic metabolite from *Streptomyces* sp. 517-02. III. Antibacterial action of demethyl UK-1. *J. Antibiot.* **50,** 788–790 (1997).
14 Ueki, M., Shibata, K. & Taniguchi, M. UK-1, a novel cytotoxic metabolite from *Streptomyces* sp. 517-02. IV. Antifungal action of methyl UK-1. *J. Antibiot.* **51,** 883–885 (1998).
15 Kumar, D., Jacob, M. R., Reynolds, M. B. & Kerwin, S. M. Synthesis and evaluation of anticancer benzoxazoles and benzimidazoles related to UK-1. *Bioorg. Med. Chem.* **10,** 3997–4004 (2002).
16 Wang, B. B., Maghami, N., Goodlin, V. L. & Smith, P. J. Critical structural motif for the catalytic inhibition of human topoisomerase II by UK-1 and analogs. *Bioorg. Med. Chem. Lett.* **14,** 3221–3226 (2004).
17 Huang, S.-T., Hsei, I.-J. & Chen, C. Synthesis and anticancer evaluation of bis(benzimidazoles), bis(benzoxazoles), and benzothiazoles. *Bioorg. Med. Chem.* **14,** 6106–6119 (2006).
18 Reynolds, M. B., DeLuca, M. R. & Kerwin, S. M. The novel bis(benzoxazole) cytotoxic natural product UK-1 is a magnesium ion-dependent DNA binding agent and inhibitor of human topoisomerase II. *Bioorg. Chem.* **27,** 326–337 (1999).
19 Fairfax, D. J. & Yang, Z. Benzoxazolecarboxamides for treating CINV and IBS-D and their preparation and pharmaceutical compositions. *US Pat. Appl.* 20,060,183,769, August 17 (2006).
20 Michel, K. H., Boeck, L. D., Hoehn, M. M., Jones, N. D. & Chaney, M. O. The discovery, fermentation, isolation, and structure of antibiotic A33853 and its tetraacetyl derivative. *J. Antibiot.* **37,** 441–445 (1984).
21 Giembycz, M. Phosphodiesterase-4 inhibitors and the treatment of asthma. *Drugs* **59,** 192–212 (2000).
22 Houslay, M., Schafer, P. & Zhang, K. Phosphodiesterase-4 as a therapeutic target. *Drug Discov. Today* **11,** 1503–1519 (2005).
23 Manning, C. *et al.* Suppression of human inflammatory cell function by subtype-selective PDE4 inhibitors correlates with inhibition of PDE4A and PDE4B. *Brit. J. Pharmacol*. **128,** 1393–1398 (1999).
24 Williams, S. T., Goodfellow, M. & Alderson, G. Genus *Streptomyces* Waksman and Henrici 1943, 339^{AL}. In: S. T. Williams *et al*. (eds). *Bergey's Manual of Systematic Bacteriology*, Vol. 4. Williams & Wilkins: Baltimore. pp 2452–2492 (1989).

25 Xu, C. *et al.* Neutrotolerant acidophilic *Streptomyces* species isolated from acidic soils in China: *Streptomyces guanduensis* sp. nov., *Streptomyces paucisporus* sp. nov., *Streptomyces rubidus* sp. nov. and *Streptomyces yanglinensis* sp. nov. *Int. J. Syst. Evol. Microbiol.* **56,** 1109–1115 (2006).
26 Lang, G., Wiese, J., Schmaljohann, R. & Imhoff, J. F. New pentaenes from the sponge-derived marine fungus *Penicillium rugulosum*: structure determination and biosynthetic studies. *Tetrahedron* **63,** 11844–11849 (2007).
27 Chavant, P., Gaillard-Martinie, B., Talon, R., Hebraud, M. & Bernardi, T. A new device for rapid evaluation of biofilm formation potential by bacteria. *J. Microbiol. Methods* **68,** 605–612 (2007).
28 Grever, M. R., Shepartz, S. A. & Chabner, B. A. The National Cancer Institute: cancer drug discovery and development program. *Semin. Oncol.* **19,** 622–638 (1992).
29 Morill, M., Thompson, S. & Stellwagen, E. Purification of a cyclic nucleotide phosphodiesterase from bovine brain using blue dextran-sepharose chromatography. *J. Biol. Chem.* **254,** 4371–4374 (1979).

The Journal of Antibiotics (2009) 62, 105–107

www.nature.com/ja

NOTE

A cell-based screening to detect inhibitors of BRAF signaling pathway

Yukihiro Asami[1,3], Mihoko Mori[1,4], Hiroyuki Koshino[2], Yasuyo Sekiyama[1,5], Takayuki Teruya[1], Siro Simizu[1], Takeo Usui[1,6] and Hiroyuki Osada[1]

The Journal of Antibiotics (2009) **62,** 105–107; doi:10.1038/ja.2008.17; published online 9 January 2009

Keywords: BRAF; cell-based assay; malformins; protein phosphatase; signal transduction

BRAF, a serine/threonine kinase, regulates the mitogen-activated protein kinase (RAS/RAF/MEK/ERK) pathway, which is involved in the transduction of mitogenic signals from the cell membrane to the nucleus. BRAF is known to be mutated in 70% of malignant melanomas. The most common BRAF mutation is V600E, and it increases the kinase activity that constitutively stimulates ERK signaling, cell proliferation and survival. The mutation is an early event for the development of melanoma and it is present in 80% of primary melanomas.[1,2] Recently, it has been reported that mutant BRAF protein is a client of Hsp90, which is required for the folding and stability of mutant BRAF. Therefore, BRAF-mutated cells are more sensitive to the Hsp90 inhibitor, compared with BRAF wild-type cells.[3] On the basis of the above-mentioned background, we established the screening system using BRAF wild-type and BRAF mutant cells to identify the BRAF pathway inhibitors from microbial metabolites.

First, we observed that ERK1/2 in wild-type BRAF cells was activated by the addition of serum or growth factors, and that ERK1/2 in BRAF-mutated cells is constitutively active (data not shown) by western blotting experiments. Next, we examined the effects of some known inhibitors—actinomycin D (RNA synthesis inhibitor), cycloheximide (protein synthesis inhibitor), paclitaxel (tubulin inhibitor), leptomycin B (CRM1 inhibitor), tunicamycin (*N*-linked glycosylation inhibitor), staurosporine (protein kinase inhibitor), trichostatin A (histone deacetylase inhibitor), SP600125 (JNK inhibitor), SB203580 (p38 inhibitor), LY294002 (PI3 kinase inhibitor), U0126 (MEK inhibitor), geldanamycin (Hsp90 inhibitor), RK-682 (tyrosine phosphatase inhibitor), tautomycin (protein phosphatase 1 and 2A inhibitor) and phoslactomycin C (protein phosphatase 2A inhibitor)—on the cell-based assay.[4,5] We found that U0126 and geldanamycin preferentially decreased the cell viability of BRAF mutant WM266-4 cells (Table 1). The selectivity ratio of CHL-1/WM266-4 was more than 10-fold. The selectivity ratios of other inhibitors were smaller than 1.0. These results suggest that this screening system is suitable for the detection of BRAF-signaling inhibitors from microbial metabolites.

In this cell-based assay, we tested 3000 microbial extracts and identified the aimed inhibitory activity in the fermentation broth of an unidentified fungus. The active compounds were identified as malformin A1, A2 and C[6–9] by electrospray ionization tandem mass spectrometry (ESI-MS/MS) and the amino-acid analysis with Marfey's reagent *N*-(3-fluoro-4,6-dinitrophenyl)-L-alaninamide (FDAA).[10,11]

Next, we investigated the effects of malformin A1, A2 and C on the growth of BRAF-mutated and wild-type cells in this assay. The IC_{50} values and selectivity ratio of BRAF-nonmutated cells/BRAF-mutated cells of malformin A1, A2 and C are shown in Table 2. Malformin A2 and C preferentially inhibited the growth of BRAF mutant WM266-4 and SK-MEL-28 cells. The selectivity ratio of malformin A1 was lower than that of malformin A2 and C. The difference of amino-acid composition of these three compounds may reflect the difference in biological activity. Structure–activity relationship of malformin derivatives must be studied in the future.

During the investigation of the molecular target, we noticed that malformins changed the cell shapes drastically (Figure 1). WM266-4 shows flat and fibroblastic morphology (Figure 1a), but most of the cells changed to round form after 3 h of treatment with malformin A1, A2 and C (Figures 1c–e).

[1]Antibiotics Laboratory and Chemical Biology Depatment, Advanced Science Institute, RIKEN, Wako, Saitama, Japan and [2]Molecular Characterization Team, Advanced Technology Support Division Advanced Science Institute, RIKEN, Wako, Saitama, Japan
Correspondence: Professor H Osada, Antibiotics Laboratory and Chemical Biology Department, Advanced Science Institute, RIKEN, 2-1 Hirosawa, Wako, Saitama 351-0198, Japan.
E-mail: hisyo@riken.jp
[3]Current address: Laboratory of Microbiology, Graduate School of Pharmaceutical Sciences, The University of Tokyo, 3-1, 7-chome, Hongo, Bunkyo-ku, Tokyo 113-0033, Japan.
[4]Current address: Laboratory of Biological Functions, Department of Drug Discovery Sciences, Kitasato Institute For Life Sciences, Kitasato University, 5-9-1, Shirokane, Minato-ku, Tokyo 108-8641, Japan.
[5]Current address: RIKEN Plant Science Center, 1-7-22 Suehiro-cho, Tsurumi-ku, Yokohama-shi 235-0045, Japan.
[6]Current address: Graduate School of Life and Environmental Sciences, University of Tsukuba, Tsukuba, Ibaraki, Japan.
Received 11 October 2008; accepted 19 November 2008; published online 9 January 2009

It was reported that microcystins and oscillamides, other cyclic peptide compounds, inhibit the protein phosphatases.[12,13] Furthermore, tautomycin, a potent inhibitor of protein phosphatase 1 and 2A, also changed the cell morphology of WM266-4 cells as malformin did (Figure 1b). These results suggest that malformins change cell morphology through protein phosphatase inhibition. To test this possibility, we next investigated the phosphorylation level of vimentin in malformin-treated NIH3T3 cells because it has been known that protein phosphatase 1 and 2A inhibitors induce vimentin overphosphorylation *in situ*.[14,15] To determine whether the phosphorylation sites on vimentin were changed on treatment with malformins, we used site-specific phosphorylated vimentin antibodies, 4A4 and MO82

Table 1 Effect of test compounds on BRAF mutated and wild-type melanoma cell lines

	IC_{50} (μM)		
Compound	*WM266-4 (BRAF mutant)*	*CHL-1 (BRAF wild)*	*Ratio (CHL-1/WM266-4)*
Actinomycin D	0.6	0.04	0.07
Cycloheximide	3.6	0.3	0.08
Paclitaxel	0.2	0.004	0.02
Leptomycin B	0.0016	0.00074	0.46
Tunicamycin	6.0	1.2	0.2
Staurosporine	0.25	0.03	0.12
Trichostatin A	0.05	0.08	1.6
SP600125	50.0	5.5	0.11
SB203580	25.0	40.0	1.6
LY294002	20.0	60.0	3.0
U0126	2.5	30.0	12.0
Geldanamycin	0.04	2.0	50.0
RK-682	67.9	135.9	2.1
Tautomycin	0.07	0.07	1.0
Phoslactomycin C	3.5	4.5	1.3

The concentrations of compounds needed to inhibit the cell growth in 50% of that in WM266-4 and CHL-1 cells were determined as IC_{50}. The selectivity of the inhibition was calculated as the ratio of the IC_{50} value of test compounds treated in CHL-1 cells divided by that in WM266-4 cells.

Table 2 Malformins preferentially inhibited the growth of BRAF-mutated melanoma cell lines

	IC_{50} (μM)			Ratio	
Compound	*WM266-4*	*SK-MEL-28*	*CHL-1*	*(CHL-1/ WM266-4)*	*(CHL-1/ SK-MEL-28)*
Malformin A1	0.05	0.36	0.64	1.2	1.8
Malformin A2	0.83	0.68	5.81	7.0	8.5
Malformin C	0.26	0.08	0.87	3.3	10.9

The concentrations of malformin A1, A2 and C needed to inhibit the cell growth in 50% of that in WM266-4, SK-MEL-28 and CHL-1 cells were determined as IC_{50}. The selectivity of the inhibition was calculated as the ratio of the IC_{50} value of malformin A1-, A2- and C-treated CHL-1 cells divided by that in WM266-4 or SK-MEL-28 cells.

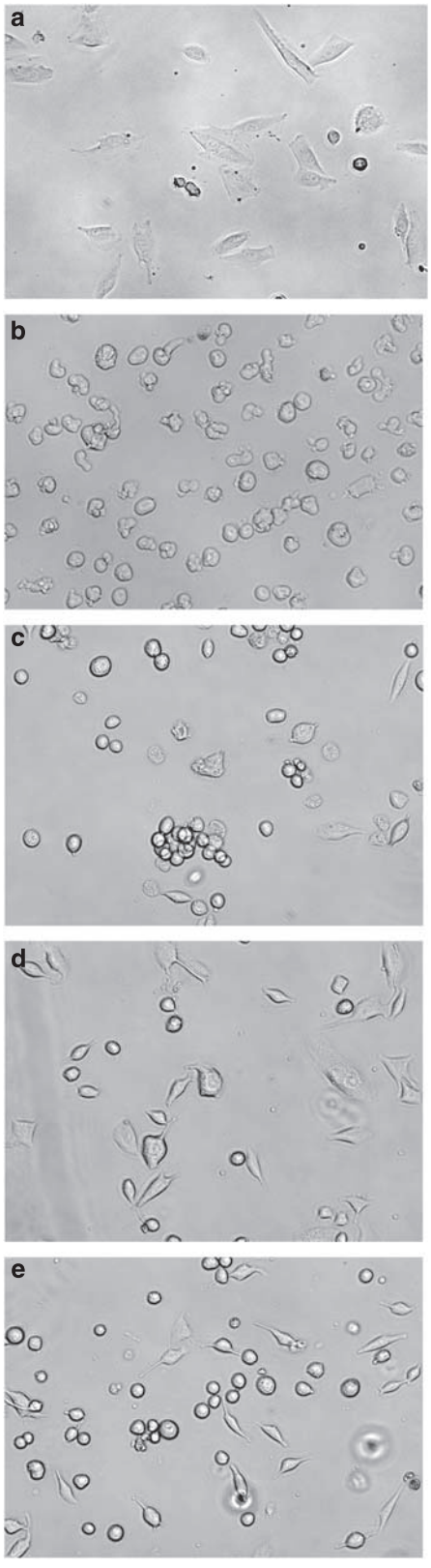

Figure 1 Malformins induced the morphological change in WM266-4 cells. The WM266-4 cells were suspended at a density of 3.0×10^4 cells ml^{-1}. Cell suspension was added to wells of six-well plate (2000 μl per well). Microplates were placed in a CO_2 incubator (air containing 5% CO_2 at 37 °C) for 18 h and morphological change of the cells was observed at 3 h after treatment with the test compounds. (**a**) 1% DMSO, (**b**) 40 μM tautomycin, (**c**) 10 μM malformin A1, (**d**) 20 μM malformin A2 and (**e**) 20 μM malformin C.

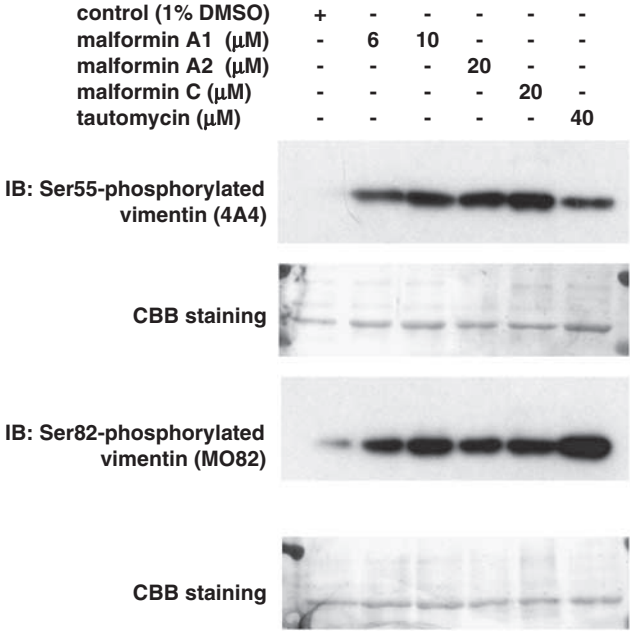

Figure 2 Malformins induced the vimentin phosphorylation of NIH3T3 cells. NIH3T3 cells were treated for 4 h with various concentrations of malformin A1, A2, C and tautomycin. After treatment, the cells were harvested, and immunoblotting was performed. IB: antibodies used for immunoblotting. CBB staining: Coomassie Brilliant Blue solution used for the detection of total vimentin. 1% DMSO treatment (lane 1); 6 μM malformin A1 (lane 2); 10 μM malformin A1 (lane 3); 20 μM malformin A2 (lane 4); 20 μM malformin C (lane 5); 40 μM tautomycin (lane 6).

antibodies that recognize phosphorylation at Ser55 and Ser82, respectively.[15] Tautomycin treatment induced the phosphorylation of Ser55 (4A4) and Ser82 (MO82) of vimentin. Likewise, malformin A1, A2 and C also induced phosphorylation of vimentin at Ser55 and Ser82 in NIH3T3 cells for 4 h incubation (Figure 2). These results suggest that malformin A1, A2 and C may affect protein phosphatases directly or indirectly *in situ*.

There were several reports on the biological activity of malformins,[16–18] but this is the first observation that malformins affected protein phosphorylation of vimentin. Recently, malformin C induced the phosphorylation of cdc2.[19] Our finding is consistent with previous reports.[19–21] Further intensive studies on malformins may shed light on the pivotal events in the BRAF pathway of tumor cells.

ACKNOWLEDGEMENTS

This work was supported in part by a Grant-in-Aid from the Ministry of Education, Culture, Sports, Science and Technology of Japan and by the Chemical Biology Project (RIKEN). YA was supported by the Special Postdoctoral Researchers Program. We thank Dr H Kakeya for valuable suggestions.

1 Davies, H. *et al*. Mutations of the BRAF gene in human cancer. *Nature* **417,** 949–954 (2002).
2 Brummer, T., Martin, P., Herzog, S., Misawa, Y., Daly, R. J. & Reth, M. Functional analysis of the regulatory requirements of B-Raf and the B-Raf(V600E) oncoprotein. *Oncogene* **5,** 6262–6276 (2006).
3 Grbovic, O. M. *et al*. V600E B-Raf requires the Hsp90 chaperone for stability and is degraded in response to Hsp90 inhibitors. *Proc. Natl Acad. Sci. USA* **103,** 57–62 (2006).
4 Cell culture conditions; WM266-4 (ATCC Number: CRL-1675), SK-MEL-28 (ATCC Number: HTB-72) and CHL-1 cells (ATCC Number: CRL-9446) were cultured in DMEM (Dulbecco's Modified Eagle's Medium) containing 10% fetal calf serum and 30 μg/ml of penicillin and 42 μg/ml of streptomycin in 5% CO_2 in an incubator at 37 °C. A Cell-Based Assay conditions; WM266-4, SK-MEL-28 and CHL-1 cells were seeded on 96-well microplates (1.0×10^4 cells per well), respectively. Test compounds were dissolved in methanol at appropriate concentrations and were treated for 72 h at 37 °C in a 5% CO_2 atmosphere. Cell proliferation assays were carried out by the WST-8™ (Nacalai Tesque, Kyoto, Japan) protocol. The absorbance (A450) of each well was measured by a Wallac 1420 multilabel counter (Amersham Biosciences, Piscataway, NJ).
5 Asami, Y., Kakeya, H., Okada, G., Toi, M. & Osada, H. RK-95113, a new angiogenesis inhibitor produced by *Aspergillus fumigatus*. *J. Antibiot.* **59,** 724–728 (2006).
6 Takahashi, N. & Curtis, R. W. Isolation & characterization of malformin. *Plant. Physiol.* **36,** 30–36 (1961).
7 Sugawara, F., Kim, K. W., Uzawa, J., Yoshida, S., Takahashi, N. & Curtis, R. W. Structure of malformin A_2, reinvestigation of phytotoxic metabolites produced by aspergillus niger. *Tetrahedron Lett.* **31,** 4337–4340 (1990).
8 Kim, K. W., Sugawara, F., Yoshida, S., Murofushi, N., Takahashi, N. & Curtis, R. W. Structure of malformin A, a phytotoxic metabolite produced by *Aspergillus niger*. *Biosci. Biotechnol. Biochem.* **57,** 240–243 (1993).
9 Anderegg, R. J., Biemann, K., Büchi, G. & Cushman, M. Malformin C, a new metabolite of *Aspergillus niger*. *J. Am. Chem. Soc.* **98,** 3365–3370 (1976).
10 Malformin A1: $[\alpha]^{25}_{D}$ −2.9 (*c* 0.073, MeOH); FAB-MS *m/z* 530 $[M+H]^+$; ESI-MS *m/z* 530 $[M+H]^+$; ESI-MS/MS on $[M+H]^+$ (CE 50 eV) *m/z* 530.4 (100%), 502.5 (22.4%), 417.1 (29.9%), 372.1 (27.1%), 318.1 (11.2 %), 304.1 (23.4%), 258.7 (26.2%), 231.1 (42.1%), 212.9 (18.7%), 199.5 (23.4%), 185.5 (11.2%); HR FAB-MS calcd. for $C_{23}H_{40}N_5O_5S_2$ $[M+H]^+$ 530.2471, found: 530.2528; molecular formula: $C_{23}H_{39}N_5O_5S_2$; Amino acid anlysis (ratio): L-Val(1), D-Leu(1), L-Ile(1). Malformin A2: $[\alpha]^{25}_{D}$ +1.7 (*c* 0.039, MeOH); FAB-MS *m/z* 516 $[M+H]^+$; ESI-MS *m/z* 516 $[M+H]^+$; ESI-MS/MS on $[M+H]^+$ (CE 50 eV) *m/z* 516.4 (100%), 488.2 (26%), 471.4 (29%), 417.0 (41%), 403.0 (14%), 372.2 (32%), 304.2 (45%), 259.0 (25.0%), 231.0 (47.0%), 213.0 (25.0%), 185.0 (28.0%); HR FAB-MS calcd. for $C_{22}H_{38}N_5O_5S_2$ $[M+H]^+$ 516.2314, found: 516.2309; molecular formula: $C_{22}H_{37}N_5O_5S_2$; Amino acid analysis (ratio): L-Val(2), D-Leu(1). Malformin C: $[\alpha]^{25}_{D}$ −1.5 (*c* 0.20, MeOH); FAB-MS *m/z* 530 $[M+H]^+$; ESI-MS *m/z* 530 $[M+H]^+$; ESI-MS/MS on $[M+H]^+$ (CE 50 eV) *m/z* 530.4 (100%), 502.2 (15.9%), 485.4 (19.0%), 417.2 (31.7%), 372.2 (28.6%), 318.2 (15.9%), 304.2 (30.2%), 259.2 (21.4%), 230.8 (36.5%), 213.4 (12.7%), 199.2 (11.9%), 185.2 (18.3%); HR FAB-MS calcd. for $C_{23}H_{40}N_5O_5S_2$ $[M+H]^+$ 530.2471, found: 530.2536; molecular formula: $C_{23}H_{39}N_5O_5S_2$; Amino acid analysis (ratio): L-Val(1), L-Leu(1), D-Leu(1).
11 Marfey, P. Determination of D-amino acids. II. Use of a bifunctional reagent, 1,5-difluoro-2,4-dinitrobenzene. *Carlsberg. Res. Commun.* **49,** 591–596 (1984).
12 MacKintosh, C., Beattie, K. A., Klumpp, S., Cohen, P. & Codd, G. A. Cyanobacterial microcystin-LR is a potent and specific inhibitor of protein phosphatases 1 and 2A from both mammals and higher plants. *FEBS Lett.* **264,** 187–192 (1990).
13 Sano, T., Usui, T., Ueda, K., Osada, H. & Kaya, K. Isolation of new protein phosphatase inhibitors from two cyanobacteria species, Planktothrix spp. *J. Nat. Prod.* **64,** 1052–1055 (2001).
14 Usui, T., Marriott, G., Inagaki, M., Swarup, G. & Osada, H. Protein phosphatase 2A inhibitors, phoslactomycins. Effects on the cytoskeleton in NIH/3T3 cells. *J. Biochem.* **125,** 960–965 (1999).
15 Tsujimura, K., Ogawara, M., Takeuchi, Y., Imajoh-Ohmi, S., Ha, M. H. & Inagaki, M. Visualization and function of vimentin phosphorylation by cdc2 kinase during mitosis. *J. Biol. Chem.* **269,** 31097–31106 (1994).
16 Koizumi, Y. & Hasumi, K. Enhancement of fibrinolytic activity of U937 cells by malformin A1. *J. Antibiot.* **55,** 78–82 (2002).
17 Bannon, P. G., Dawes, J. & Dean, R. T. Malformin A prevents IL-1 induced endothelial changes by inhibition of protein synthesis. *Thromb. Haemost.* **72,** 482–483 (1994).
18 Herbert, J. M. *et al*. Malformin-A1 inhibits the binding of interleukin-1 beta (IL1 beta) and suppresses the expression of tissue factor in human endothelial cells and monocytes. *Biochem. Pharmacol.* **48,** 1211–1217 (1994).
19 Hagimori, K., Fukuda, T., Hasegawa, Y., Ōmura, S. & Tomoda, H. Fungal malformins inhibit bleomycin-induced G2 checkpoint in Jurkat cells. *Biol. Pharm. Bull* **30,** 1379–1383 (2007).
20 Kracht, M., Heiner, A., Resch, K. & Szamel, M. Interleukin-1-induced signaling in T-cells. Evidence for the involvement of phosphatases PP1 and PP2A in regulating protein kinase C-mediated protein phosphorylation and interleukin-2 synthesis. *J. Biol. Chem.* **268,** 21066–21072 (1993).
21 Janosch, P. *et al*. The Raf-1 kinase associates with vimentin kinases and regulates the structure of vimentin filaments. *FASEB J.* **14,** 2008–2021 (2000).

The Journal of Antibiotics (2009) 62, 109–111

www.nature.com/ja

NOTE

Effect of lactoferricin on fluoroquinolone susceptibility of uropathogenic *Escherichia coli*

Catia Longhi, Massimiliano Marazzato, Maria Pia Conte, Valerio Iebba, Serena Schippa, Lucilla Seganti and Antonella Comanducci

The Journal of Antibiotics (2009) **62,** 109–111; doi:10.1038/ja.2008.22; published online 23 January 2009

Keywords: *Escherichia coli*; fluoroquinolones; lactoferricin B; MIC; resistance

Members of the *Enterobacteriaceae* family are mainly involved in the etiology of urinary tract infections, and *Escherichia coli* is by far the most common microorganism isolated from about 50% of all nosocomial and 90% of outpatients' urinary tract infections.[1] Quinolones are effective antibacterial agents that are commonly used as antimicrobials in the management of urinary tract infections, owing to which the rates of antimicrobial resistance among *E. coli* strains have increased greatly during the past two decades.[1,2] Bacteria are able to develop resistance by point mutations in chromosomal genes codifying DNA gyrase and topoisomerase IV targeted by quinolones.[3] Other mechanisms involve mutations affecting the accumulation of fluoroquinolones in the bacterial cell, such as the expression of outer membrane proteins and alteration in the lipopolysaccharide.[3] Furthermore, plasmid-mediated resistance has also been identified: *qnr* gene products capable of protecting DNA gyrase and AAC(6′)-Ib-cr, a variant aminoglycoside acetyltransferase, providing enzymatic antibiotic inactivation.[3]

The emergence of bacterial strains exhibiting resistance against conventional antibiotics has encouraged the search for novel antimicrobial strategies. Among the compounds that are currently under investigation for their therapeutic potential are a number of antimicrobial peptides.[4] The positively charged antimicrobial peptide lactoferricin B (Lfcin B), a 25-amino-acid peptide released from the N-terminal part of bovine lactoferrin (Lf) by gastric pepsin cleavage, has recently received attention due to its broad host defense properties against bacteria, fungi and parasites.[5,6] Lfcin B is active toward Gram-positive and Gram-negative species, including *E. coli*. This peptide contains many hydrophobic and positively charged residues, which enable its interaction with negatively charged biological membranes. In *E. coli*, depolarization and large effects on the integrity of cytoplasmic membrane have been shown.[6,7]

Lf and Lfcin B have been shown to be effective synergistic agents when used in combination with antibiotics.[6] Among Gram-negative bacteria, Lf enhances the sensitivity of *Pseudomonas aeruginosa* to chloramphenicol,[8] of *Stenotrophomonas maltophilia* to rifampin,[9] of *Salmonella enterica* to erythromycin[10] and of *E. coli* to novobiocin.[11] Lfcin B has been shown to act synergistically with erythromycin,[12] and a synergistic growth-inhibitory activity by bovine Lf lysate and gentamicin toward *E. coli* was observed.[13]

In this study, we primarily analyzed the susceptibility of uropathogenic *E. coli* strains to fluoroquinolones. As *E. coli* fluoroquinolone resistance has been associated with reductions in virulence traits and shifts from the phylogenetic group B2 toward groups A, B1 or D,[2] we then compared antibiotic resistance with the strains belonging to phylogenetic groups and with the occurrence of some capsular determinants that can be considered as cell protection genes. In succession, to gain insight into the interference of natural peptides with susceptibility to fluoroquinolones, we examined whether Lfcin B could influence the activity of norfloxacin and ciprofloxacin toward these strains.

E. coli strains were isolated from the urine of subjects attending a private medical practice at BIOS s.p.a. Microbiology Laboratory and Hospital, Umberto I BIT 05 Microbiology Laboratory, and identified using standard methods. The strains were stored in 15% glycerol at −80 °C and subcultured in Brain Hearth Infusion broth (Oxoid, Rome, Italy) at pH 6.8 for further analysis. *E. coli* ATCC 25922 was used as the bacterial reference strain.

The phylogenetic grouping of *E. coli* strains was determined by PCR. The three candidate genes were *chuA* 279-bp, *yjaA* 211-bp and an anonymous DNA fragment designated TSPE42 152-bp. The phylogroup classification (A, B1, B2, D) was made on the basis of the presence of specific PCR-amplified fragments according to Kanamaru *et al.*[14]

E. coli were screened by PCR for cell protection genes associated with three capsule groups. The tested genes were *kpsMT*K1 (153 bp), *kpsMT* II (272bp) and *kpsMT*K5 (159 bp). Primer sequences, PCR mixtures and conditions were as published by Johnson and Stell.[15]

Antimicrobial susceptibility tests were carried out according to the National Committee for Clinical Laboratory Standards guidelines[16] for the antibiotics cephalotin, cefotaxime, amoxicillin, gentamicin,

Department of Public Health Sciences, Sapienza University, Rome, Italy
Correspondence: Professor L Seganti, Department of Public Health Sciences, Microbiology Section, Sapienza University, P.le Aldo Moro 5, Rome 00185, Italy.
E-mail: lucilla.seganti@uniroma1.it
Received 25 July 2008; accepted 4 December 2008; published online 23 January 2009

ciprofloxacin, norfloxacin, nitrofurantoin and co-trimoxazole, by the automated microdilution method Vitek2 (Biomérieux, Rome, Italy).

Norfloxacin and ciprofloxacin, used in minimal inhibition concentration assays, were purchased from Sigma-Aldrich (Milan, Italy). Lfcin B (FKCRRWQWRMKKLGAPSITCVRRAF) was synthesized by GenScript Corporation (Piscataway, NJ, USA). The chemicals were dissolved in double-distilled water and stored at $-20\,^{\circ}C$ until used.

The minimal inhibitory concentrations (MICs) of the drugs were determined using a standard microdilution technique in 1.0% Bacto Peptone Water (DIFCO Lab, Detroit, MI, USA), pH 6.8, with a log-phase inoculum of 1×10^4 CFU ml^{-1}. Polystyrene 96-well plates (Nunc, Rochester, NY, USA) were incubated at 37 °C up to 24 h. After incubation, the optical density was determined in each well at 590 nm. The MIC was defined as the lowest concentration of the drug at which bacterial growth was inhibited. All tests were carried out in triplicate and the results were averaged.

Synergy testing was performed to determine the *in vitro* ciprofloxacin and norfloxacin interactions with Lfcin B by the fractional inhibitory concentration (FIC) index.[17] The FIC index calculation was performed according to Vorland *et al.*:[12] synergy was defined as the condition when the FIC index was <0.5, partial synergism as when $0.5<\mathrm{FIC}<1$, indifference as when $1<\mathrm{FIC}<4$, and antagonism as when the FIC index was >4. Checkerboard test results represented the average of triplicate testing for each isolate.

Fifty-four *E. coli* strains isolated from the urine samples of clinical and community UTI patients were submitted to antimicrobial susceptibility tests performed routinely for Gram-negative bacteria. The results obtained were evaluated according to clinical criteria as the percentage of sensitive, intermediate or resistant strains. Among the isolates examined, a noticeable resistance to most of the drugs tested was observed (results not shown), and the prevalence averaged around 22.2% for norfloxacin and ciprofloxacin. In Table 1, the susceptibility of *E. coli* isolates exhibiting resistance to fluoroquinolones, of sensitive isolates and of the ATCC 25922 reference strain, as well as the presence of cell protection genes codifying for the expression of extracellular capsule polysaccharides and phylogenetic grouping, is reported. *E. coli* strains sensitive to fluoroquinolones exhibited MIC values 2–8-fold higher than those of the ATCC 25922 reference strain. Three quinolone-susceptible *E. coli* strains belonged to the phylogenetic group B2 and one to group D, whereas, among the resistant ones, three, four and five strains belonged to A, B2 and D groups, respectively. The three cell protection genes tested—*kpsMT*K1, *kpsMT* II, *kpsMT*K5—were randomly distributed in both quinolone-susceptible and -resistant strains; *kpsMT* II capsule gene was the most frequent.

Then trials were performed to assess the MICs of the peptide Lfcin B toward the growth of *E. coli* isolates. Lfcin B was serially twofold diluted, starting from the concentration of 50 down to 0.097 μg ml^{-1}. The results obtained showed that 12.5 μg ml^{-1} was the dose capable of completely inhibiting bacterial growth in all strains tested and 3.12 μg ml^{-1} corresponded to the sub-inhibiting concentration, because at this concentration, after 24-h incubation at 37 °C, no decrease in the optical density, as compared with Lfcin B-untreated controls, was observed.

To determine Lfcin B–fluoroquinolone interactions, the FIC index was evaluated for each strain by combining different concentrations of norfloxacin, ciprofloxacin and Lfcin B. Table 2 summarizes the synergy data. The combination of Lfcin B with the quinolones had synergistic or partial synergistic effects toward both resistant and sensitive strains. Synergy was associated with a decrease of two or more dilutions of MIC values and was observed for both quinolones in two resistant strains. Partial synergism was associated with a decrease up to two dilutions of MICs: ciprofloxacin showed partial synergism with Lfcin B against six *E. coli* isolates (two susceptible and four resistant strains) whereas norfloxacin showed partial synergism against four isolates (one susceptible and three resistant strains). Indifference between the antibacterial agents used and Lfcin B was observed in the remaining uropathogenic *E. coli* tested and in the reference strain, whereas antagonism was never detected. Hence, in response to this association, most of the strains showed a variation in MIC values: synergistic effect was observed for both drugs in 12.5% of strains, whereas partial synergism was observed for ciprofloxacin in 37.5% of strains and for norfloxacin in 20% of strains.

In agreement with literature data,[1] the results from this investigation showed that, in a noticeable percentage of uropathogenic *E. coli*

Table 1 Susceptibility to fluoroquinolones of *E. coli* strains and distribution of phylogenetic groups and *kpsMT*K1, *kpsMT*II and *kpsMT*K5 capsule genes

Strains s,[a] r[b]	*MIC (μg ml^{-1}) ciprofloxacin*	*MIC (μg ml^{-1}) norfloxacin*	*Phylogenetic group*	kpsMT*K1*	kpsMT*II*	kpsMT*K5*
ATCC 25922	0.05	0.05	B2	–	+	+
C86 s	0.78	0.78	B2	+	+	–
O39 s	0.39	0.19	B2	+	+	–
C38 s	3.12	3.12	B2	–	+	+
C43 s	0.39	0.39	D	+	–	–
C58 r	50	12.5	B2	–	+	+
O12 r	25	12.5	D	+	+	+
C24 r	50	100	D	–	+	+
C25 r	12.5	100	D	–	+	+
C20 r	50	25	B2	+	+	–
C31 r	50	50	A	+	–	–
C69 r	100	100	B2	+	+	+
C87 r	50	50	D	–	+	+
C104 r	100	100	B2	–	+	+
C111 r	50	50	A	–	–	–
C134 r	50	50	A	–	–	–
O25 r	200	200	D	+	+	–

Fluoroquinolone susceptibility: [a]sensitive strain, [b]resistant strain.

Table 2 FIC index and interaction of fluoroquinolones in combination with Lactoferricin B towards *E. coli* strains

Strains s[a], r[b]	Ciprofloxacin		Norfloxacin	
	FIC index	Interaction	FIC index	Interaction
ATCC 25922	1.5	Indifference	1.5	Indifference
C86 s	0.7	Partial synergism	0.7	Partial synergism
O39 s	0.7	Partial synergism	1.5	Indifference
C38 s	1.5	Indifference	1.5	Indifference
C43 s	1.5	Indifference	1.5	Indifference
C58 r	0.3	Synergism	0.4	Synergism
O12 r	0.9	Partial synergism	0.9	Partial synergism
C24 r	0.7	Partial synergism	0.6	Partial synergism
C25 r	0.6	Partial synergism	1.5	Indifference
C20 r	1.5	Indifference	1.5	Indifference
C31 r	1.5	Indifference	1.5	Indifference
C69 r	1.5	Indifference	1.5	Indifference
C87 r	0.7	Partial synergism	0.8	Partial synergism
C104 r	1.5	Indifference	1.5	Indifference
C111 r	1.5	Indifference	1.5	Indifference
C134 r	0.4	Synergism	0.4	Synergism
O25 r	1.5	Indifference	1.5	Indifference

Abbreviation: FIC, fractional inhibitory concentration.
Fluoroquinolone susceptibility: [a]sensitive strain, [b]resistant strain.

isolates, a high level of resistance to fluoroquinolones was present. However, the investigation of *E. coli* phylogroups and cell protection genes related to pathogenicity failed to individuate phylogenetic traits or capsule genes associated with fluoroquinolone resistance. Data obtained with synergy tests showed that the cationic peptide Lfcin B used alone had a powerful inhibiting effect toward all uropathogenic *E. coli* isolates investigated, and that in 50% of the strains examined the combination of Lfcin B with fluoroquinolones determined a decrease of the MICs (synergism or partial synergism).

The overall results achieved on interaction between Lfcin B and fluoroquinolones in both *E. coli*-susceptible and -resistant strains are possibly due to the membrane-disorganizing nature of this peptide,[6,7] which leads not only to increased permeability through the bacterial cell wall but also to the dissipation of the proton-motive force, resulting in decreased activity of ATP-dependent multi-drug efflux pumps.[6] At sub-inhibiting concentrations, Lfcin B may affect the access/efflux of drugs, thus modifying the quinolone concentrations required to inhibit growth.

Furthermore, the results obtained allow the assumption that Lfcin B could act on *E. coli* strains, independently from their resistance or susceptibility to fluoroquinolones, causing different events: a synergistic or semi-synergistic action with consequent decrease of MIC values, or indifference. The fluoroquinolones exert their inhibitory action by forming a stable complex with the DNA and the target enzyme.[18] Thus, a clarification of the behavior shown by both sensitive and resistant *E. coli* strains in combination experiments can be related to both altered quinolone uptake and mutational events in different enzyme regions holding amino acids involved in the interaction with fluoroquinolones. A silent mutation in drug susceptibility could still influence the kind of interaction between the drugs and the enzyme: this could be the case of the sensitive strains C86 and O39, in which the response to the association of fluoroquinolones with Lfcin B is semi-synergistic with a consequent decrease of MIC values. Moreover, the presence of movable resistance DNA gyrase protective genes, such as *qnr*A, *qnr*B, *qnr*S and/or AAC(6′)-IB-cr,[3] in the *E. coli* strains could also influence the response to fluoroquinolones–Lfcin B association. To better understand the mechanisms of interaction between Lfcin B and these drugs, resulting in synergism, a molecular analysis of the major genes implicated in resistance will be required.

Interestingly, experimental data in mice showed that oral administration of Lf and derivative peptides is effective in reducing infection and inflammation at the level of the urinary tract, through the transfer of Lf or its peptides to the site of infection via renal secretion,[19] suggesting that Lfcin B–fluoroquinolone association might represent an approach to control the growth of uropathogenic *E. coli*.

Taken together, these results could be of interest as the association of fluoroquinolones with the antibacterial peptide Lfcin B could allow the use of these therapeutic agents at lower concentrations for a reasonable number of *E. coli* strains. Moreover, this association could allow extending the prescription of drugs that otherwise should be discarded because of the increased resistance of bacteria to them worldwide.[1–3]

ACKNOWLEDGEMENTS

This work was supported by grants from MIUR to Dr L Seganti and S Schippa.

1 Nickel, J. C. Urinary tract infections and resistant bacteria. *Rev. Urol.* **9,** 78–80 (2007).
2 Moreno, E. *et al*. Quinolone, fluoroquinolone and trimethoprim/sulfamethoxazole resistance in relation to virulence determinants and phylogenetic background among uropathogenic *Escherichia coli*. *J. Antimicrob. Chemother.* **57,** 204–211 (2006).
3 Robicsek, A., Jacoby, G. A. & Hooper, D. C. The worldwide emergence of plasmid-mediated quinolone resistance. *Lancet Infect. Dis.* **6,** 629–640 (2006).
4 Jenssen, H., Hamill, P. & Hancock, R. E. Peptide antimicrobial agents. *Clin. Microbiol. Rev.* **19,** 491–511 (2006).
5 Valenti, P., Berlutti, F., Conte, M. P., Longhi, C. & Seganti, L. Lactoferrin functions: current status and perspectives. *J. Clin. Gastroenterol.* **38,** 127–129 (2004).
6 Gifford, J. L., Hunter, H. N. & Vogel, H. J. Lactoferricin: a lactoferrin-derived peptide with antimicrobial, antiviral, antitumor and immunological properties. *Cell Mol. Life Sci.* **62,** 2588–2598 (2005).
7 van der Kraan, M. I. *et al*. Ultrastructural effects of antimicrobial peptides from bovine lactoferrin on the membranes of *Candida albicans* and *Escherichia coli*. *Peptides* **26,** 1537–1542 (2005).
8 Fowler, C. E., Soothill, J. S. & Oakes, L. MICs of rifampicin and chloramphenicol for mucoid *Pseudomonas aeruginosa* strains are lower when human lactoferrin is present. *J. Antimicrob. Chemother.* **40,** 877–879 (1997).
9 Qamruddin, A. O., Alkawash, M. A. & Soothill, J. S. Antibiotic susceptibility of *Stenotrophomonas maltophilia* in the presence of lactoferrin. *Antimicrob. Agents Chemother.* **49,** 4425–4426 (2005).
10 Naidu, A. S. & Arnold, R. R. Lactoferrin interaction with *Salmonellae* potentiates antibiotic susceptibility *in vitro*. *Diagn. Microbiol. Infect Dis.* **20,** 69–75 (1994).
11 Sanchez, M. S. & Watts, J. L. Enhancement of the activity of novobiocin against *Escherichia coli* by lactoferrin. *J. Dairy Sci.* **82,** 494–499 (1999).
12 Vorland, L. H. *et al*. Interference of the antimicrobial peptide lactoferricin B with the action of various antibiotics against *Escherichia coli* and *Staphylococcus aureus*. *Scand. J. Infect. Dis.* **31,** 173–177 (1999).
13 Chen, P. W., Ho, S. P., Shyu, C. L. & Mao, F. C. Effects of bovine lactoferrin hydrolysate on the *in vitro* antimicrobial susceptibility of *Escherichia coli* strains isolated from baby pigs. *Am. J. Vet. Res.* **65,** 131–137 (2004).
14 Kanamaru, S. *et al*. Subtyping of uropathogenic *Escherichia coli* according to the pathogenicity island encoding uropathogenic-specific protein: comparison with phylogenetic groups. *Int. J. Urol.* **13,** 754–760 (2006).
15 Johnson, J. R. & Stell, A. L. Extended virulence genotypes of *Escherichia coli* strains from patients with urosepsis in relation to phylogeny and host compromise. *J. Infect. Dis.* **72,** 181–261 (2000).
16 National Committee for Clinical Laboratory Standards. *Methods for Dilution Antimicrobial Susceptibility Tests for Bacteria that Grow Aerobically.* 3rd edn. (Villanova, PA, 1993).
17 Moody, J. A. Synergy testing. Broth microdilution checkerboard and broth macrodilution methods. in *Clinical microbiology procedures handbook*, vol. 1 (ed Isenberg, H.D.) pp 5.18 1–14 (ASM Press, Washington, 1992).
18 Madurga, S., Sánchez-Céspedes, J., Belda, I., Vila, J. & Giralt, E. Mechanism of binding of fluoroquinolones to the quinolone resistance-determining region of DNA gyrase: towards an understanding of the molecular basis of quinolone resistance. *Chembiochem.* **9,** 2081–2086 (2008).
19 Haversen, L. A., Engberg, I., Baltzer, L., Dolphin, G., Hanson, L. A. & Mattsby-Baltzer, I. Human lactoferrin and peptides derived from a surface-exposed helical region reduce experimental *Escherichia coli* urinary tract infection in mice. *Infect. Immun.* **68,** 5816–5823 (2000).

The Journal of Antibiotics (2009) 62, 113–116

www.nature.com/ja

NOTE

Synthesis and antimicrobial activity of ciprofloxacin and norfloxacin permanently bonded to polyethylene glycol by a thiourea linker

Gábor Pintér[1], Pál Horváth[1], Sándor Bujdosó[1], Ferenc Sztaricskai[1], Sándor Kéki[2], Miklós Zsuga[2], Szilvia Kardos[3], Ferenc Rozgonyi[3] and Pál Herczegh[1]

The Journal of Antibiotics (2009) **62,** 113–116; doi:10.1038/ja.2008.26; published online 16 January 2009

Keywords: antibacterial; fluoroquinolone; permanent bond; polyethylene glycol; telechelic

C_2-symmetric (divalent) biologically active molecules are an extensively studied field, as certain substances possessing a B-linker-B type structure (where B represents a bioactive molecule) have promising biological properties.[1] The synthesis and investigation of the dimers of the highly antibacterial quinolonecarboxylic acids were also carried out. However, the norfloxacin dimers linked with an alkyl chain, described by Coppel *et al.*,[2] were very slightly active. Later Kerns *et al.*[3–5] synthesized the C_2-symmetric and mixed dimers of ciprofloxacin and norfloxacin using 1,4-phenylenebis-methylene and 2-butene-1,4-diyl linkers. These derivatives possessed comparable activity with that of the monomers and, in a few cases, higher MIC values were found against certain drug-resistant strains.

Polyethylene glycol (PEG), a cheap and nontoxic telechelic polymer diol of amphiphilic character is soluble both in water and organic solvents; therefore, it is often used as a carrier for drug molecules.

Bioactive molecules linked covalently to PEG possess favorable pharmacodynamic properties due to high water solubility and lipophilicity of the polymer, and PEGylation usually results in an enhanced biological stability and the products are less immunogenic. The PEGylated drug conjugates are primarily used in a 'releasable' form (that is, in a form linked by means of bondings unstable in a biological milieu).

In contrast, in the permanently bonded form, the drug molecule is attached to the polymer with covalent bondings stable in a biological milieu. The permanently bonded form is also advantageous, as numerous drug molecules introduced to therapy contains PEG in such a linkage. Related compounds are the PEGylated derivative of the bovine adenosyl deaminase enzyme ADAGEN,[6] the PEGylated L-asparagine-containing ONCASPAR,[7] PEG-INTRON,[8] which contains PEGylated interferon, and NEULASTA[9] carrying a PEGylated granulocyte-colony stimulating factor. Incorporation of the monofunctional PEG chain(s) to these protein-type bioactive molecules resulted in decreasing immunogenity of the parent compound, as well as in the increase of the circulation half-life time and the stability. There are few reports on permanently bonded drugs, but those compounds exhibit low biological activity.[10]

Ciprofloxacin was encapsulated in PEG-coated, long-circulating sustained-release liposomes.[11,12] It is to be noted that Carraher *et al.*[13] reported the synthesis and biological activity of ciprofloxacin covalently bonded to organotin polymers of **1** and **2**. Norfloxacin was also attached to methacrylate polymers.[14]

The goal of this work was to investigate the antimicrobial effect of the quinolonecarboxylic acid dimers prepared with a PEG linker, and to study the effect of PEGylation on the antibacterial activity.

To investigate the separate effect of the PEGylation and dimerization of **1** and **2** on the antimicrobial effect, both the mono- and bifunctional PEG derivatives of the antimicrobial agents were prepared.

Monomethoxy-PEG ($MW_{average}$=1132 Da) and PEG ($MW_{average}$=1382 Da) were converted[15] into the monoamino (**3**) and diamino (**4**) derivatives, whose treatment with thiophosgene gave the corresponding mono- and diisothiocyanates **5** and **6**, respectively (Scheme 1).The reaction of **4** and **6** with ciprofloxacin and norfloxacin under mild conditions (Scheme 1) led to the PEG-conjugates (**7**, **8**, **9**, **10**), whose structures were proved by matrix-assisted laser desorption/ionization (MALDI) mass spectrometry and NMR spectroscopy. (Figure 1 represents the MALDI-time of flight (TOF) mass spectrum of **6** and **9**). Thiourea and its derivatives cannot be hydrolyzed by

[1]Department of Pharmaceutial Chemistry, University of Debrecen, Debrecen, Hungary; [2]Department of Applied Chemistry, University of Debrecen, Debrecen, Hungary and [3]Institute of Medicinal Microbiology, Semmelweis University, Budapest, Hungary
Correspondence: Dr P Herczegh, Department of Pharmaceutial Chemistry, University of Debrecen, PO Box 70, Debrecen H-4010, Hungary.
E-mail: herczeghp@gmail.com
Received 20 October 2008; accepted 18 December 2008; published online 16 January 2009

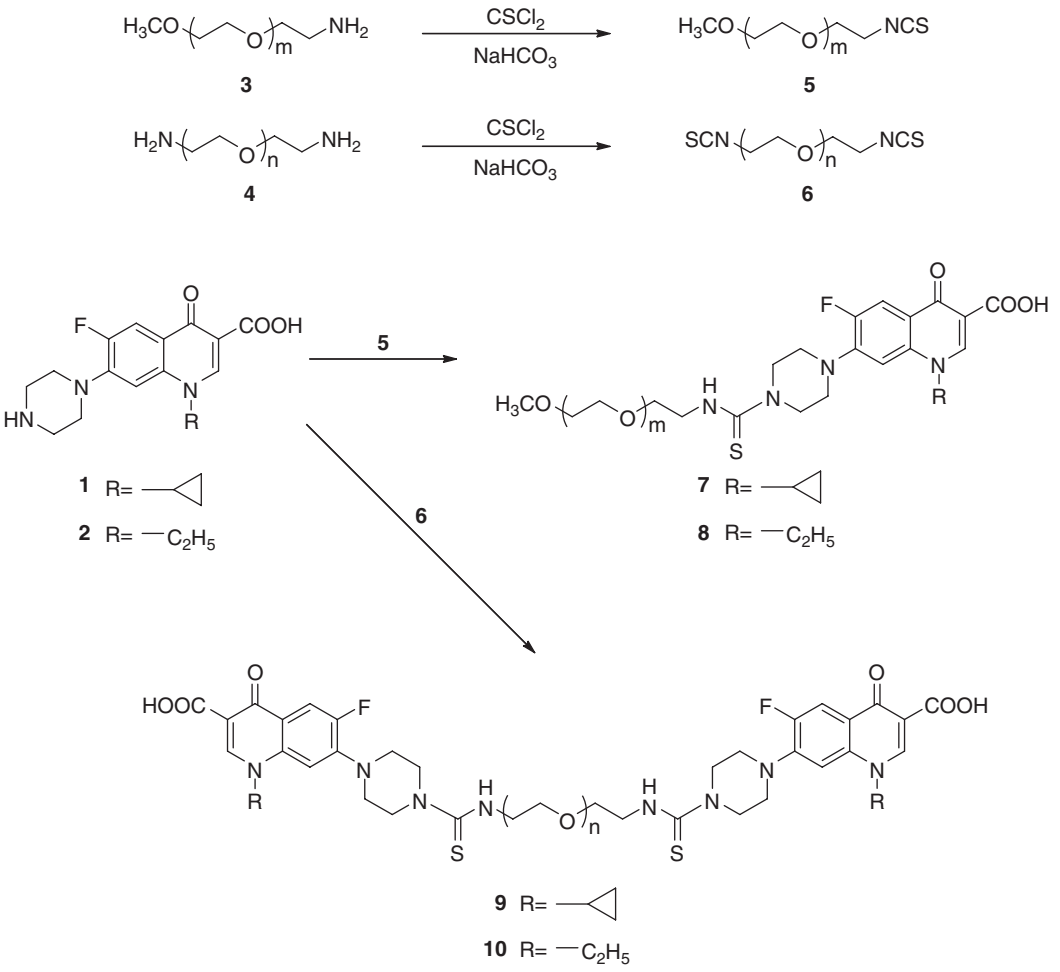

Scheme 1 Formation of PEG-isothiocyanates and synthesis of PEGylated quinolonecarboxylic acid derivatives.

ureases of different origin[16,17] or they are inhibitors of these enzymes.[18] Therefore, the permanently bonded drug conjugates containing a thiourea-linking moiety are expected as stable molecules under biological conditions. Consequently, the prepared permanently bonded drug conjugates do not correspond to a delivery system, but represent original macromolecules carrying bioactive endgroups.

The data in Table 1 show the MIC values of our substances toward several bacterial strains. As PEGylation increases the molecular mass aproximately 5–6 times, the change in the activity expressed in $\mu mol\,l^{-1}$ is more informative than the concentrations given in $\mu g\,ml^{-1}$.

The PEG conjugates possessed weak activity, or were inactive against the Gram-positive *Staphylococci*, with the exception of the dimeric ciprofloxacin **9** against strains **a** and **b** (in 7.5 $\mu mol\,l^{-1}$). Nevertheless, **1** and **2** were also inefficient toward half of the Gram-positive strains investigated. At the same time, against *Bacillus subtilis*, the ciprofloxacin derivatives **7** and **9** have similar activity than the parent compounds (in 2.6 and 1.8 µmol, respectively).

PEGylation emerged with more attractive results in the case of the Gram-negative bacterial strains. The PEG derivatives **7** and **9** had molar MIC values against *Escherichia coli*, *Pseudomonas aeruginosa* and *Enterobacter cloacae* similar to those of ciprofloxacin and norfloxacin, and the norfloxacyl compound **10** was also reasonably efficient against *E. coli* (**g**). PEGylation decreased the activity of norfloxacin more than that of ciprofloxacin. On the other hand, on comparison of the microbial effect of **1** and **2** with that of the monovalent and dimeric derivatives (i.e., to **7** and **9**, and to **8** and **10**, respectively) against Gram-negative strains, no significant changes were observed. Consequently, we may conclude that (at least in the case of the MW=1500 PEG) dimerization of **1** and **2** does not significantly influence the biological activity against Gram negatives.

As permanent covalent PEGylation does not affect the molar MIC values observed for certain microorganisms, it is believed that compounds **7–10** could be sufficient examples for the further investigation of the influence of PEGylation on antimicrobial activity.

In summary, it was observed that bonding of ciprofloxacin and norfloxacin to PEG with a permanent covalent linkage leads to an insignificant decrease in the molar activity of some of the products against certain Gram-negative bacteria. This fact opens the way to the synthesis of another stable polymer-antibiotic chimera, which may have better antimicrobial activity than that of the parent compounds.

EXPERIMENTAL SECTION

General methods

Unless otherwise stated, the starting materials and solvents were purchased from commercial sources (Sigma-Aldrich, St Louis, MO, USA or Fluka, Buchs, Switzerland) and used as received. All solvents were distilled before use. CH_2Cl_2 was distilled from P_2O_5 and stored over 4 Å molecular sieves. Triethylamine was distilled from KOH before use. ^1H NMR spectra were recorded at 360.13 MHz

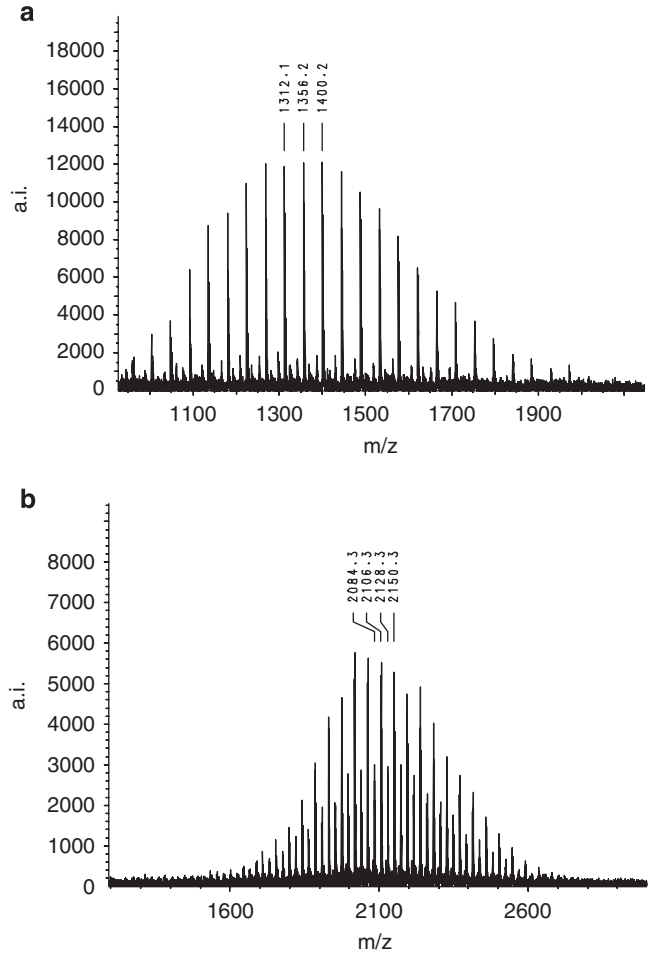

Figure 1 MALDI-TOF mass spectrum of **6** (spectrum a) and **9** (spectrum b).

with a Bruker WP-360 SY spectrometer, using DMSO-d_6 as solvent and tetramethylsilane as internal standard. Mass spectra were recorded with a Bruker Biflex-III MALDI-TOF mass spectrometer. For column chromatography, Merck silica gel (Kieselgel 60), 0.063–0.200 mm (70–230 mesh) was used. TLC was performed on Kieselgel 60 F_{254} (Merck), using CH_2Cl_2—MeOH solvent system as eluent.

Spots were visualized by irradiation under UV lamp, and/or by spraying with an ammonium-molibdenate/sulfuric acid solution and heating. Evaporations were carried out under diminished pressure at 35–40 °C (bath temperature).

Monomethoxy-isothiocyanato-PEG (5)

To a solution of 60 ml of 0.54 M sodium hydrogencarbonate in water, a solution of thiophosgene (0.520 ml, 6.08 mmol) in dichloromethane (60 ml) was added. The mixture was stirred vigorously and a solution of **3** (3.0 g, 2.73 mmol) in dichloromethane (100 ml) was added dropwise for 1 h. After 15 min, the aqueous phase was extracted with CH_2Cl_2 (2×100 ml). Evaporation of the combined organic phases resulted in 2.87 g of **5** (93%). The structure and purity were proved by the MALDI spectrum.

MS (MALDI-TOF) $MW_{average}$=1153.2 Da $(M+Na)^+$. Calculated for $C_{50}H_{99}O_{24}NS$ 1129.6.

Diisothiocyanato-PEG (6)

It was obtained from the diamino-PEG with the method applied for **5** using 2 equivalents of $CSCl_2$ and $NaHCO_3$. Yield: 92%.

MS (MALDI-TOF) $MW_{average}$=1356.2 Da $(M+Na)^+$. Calculated for $C_{58}H_{112}O_{27}N_2S_2$ 1332.7.

Preparation of thiocarbamoyl-PEG derivatives of 1 and 2 (7–10)

Typical procedure (for 9)

1 HCl (0.154 g, 0.42 mmol) and triethylamine (0.116 ml, 0.84 mmol) were dissolved in dry CH_2Cl_2 (35 ml), then 0.201 g (0.14 mmol) of **6** was added and the mixture was allowed to react for 3 days at room temperature. The product was purified by column chromatography on silica gel using an 85:15 CH_2Cl_2—MeOH solvent system as eluent. Yield: 67 mg (23%).

MS (MALDI-TOF) $MW_{average}$=2106.3 Da $(M+Na)^+$, 2128.3 Da $(M-H+2Na)^+$. Calculated for $C_{96}H_{156}O_{35}N_8S_2F_2$ 2083.0.

^{1}H NMR (360 MHz, DMSO-d_6) δ 8.67 (2H, s, quinolone C*H*), 7.92 (2H, d, *J*=13.3, aromatic), 7.55 (2H, d, *J*=7.4, aromatic), 4.02–4.04 (4H, m, −CH_2-NH-C=S), 3.80–3.86 (2H, m, cyclopropyl C*H*), 3.34–3.71 (m, polymer -CH_2-CH_2-O-, piperazine), 1.22–1.37 (8H, m, cyclopropyl methylene).

Compound 7

1 HCl (0.089 g, 0.24 mmol) and triethylamine (66 µl, 0.84 mmol) were dissolved in dry CH_2Cl_2 (35 ml), then 0.19 g (0.16 mmol) of **5** was added and the procedure described for **9** was used. Yield: 55 mg (23%).

MS (MALDI-TOF) $MW_{average}$=1527.6 Da $(M+Na)^+$, 1549.6 Da $(M-H+2Na)^+$. Calculated for $C_{69}H_{121}O_{28}N_4SF$ 1504.8.

^{1}H NMR (360 MHz, DMSO-d_6) δ 8.66 (1H, s, quinolone C*H*), 7.91 (1H, d, *J*=13.3, aromatic), 7.55 (1H, d, *J*=7.4, aromatic), 4.02–4.06 (2H, m, −CH_2-NH-C=S), 3.78–3.88 (1H, m, cyclopropyl C*H*), 3.34–3.71 (m, polymer -CH_2-CH_2-O-, piperazine), 3.24 (3H, s, H_3C-O-CH_2-CH_2-O-), 1.22-1.35 (4H, m, cyclopropyl methylene).

Compound 8

5 (0.196 g, 0.17 mmol) was dissolved in dry CH_2Cl_2 (50 ml) and **2** (0.081 g, 0.25 mmol) was added. Using the general method, 48 mg of **8** was resulted (20%).

MS (MALDI-TOF) $MW_{average}$=1428.1 Da $(M+Na)^+$, 1450.1 Da $(M-H+2Na)^+$. Calculated for $C_{64}H_{113}O_{26}N_4SF$ 1404.7.

^{1}H NMR (360 MHz, DMSO-d_6) δ 8.95 (1H, s, quinolone C*H*), 7.94 (1H, d, *J*=13.3, aromatic), 7.18 (1H, d, *J*=7.4, aromatic), 4.59 (2H, q, *J*=7.1, H_3C-CH_2-N), 4.00–4.06 (2H, m, -CH_2-NH-C=S), 3.27-3.71 (m, polymer -CH_2-CH_2-O-, piperazine), 3.24 (3H, s, H_3C-O-CH_2-CH_2-O-), 1.42 (3H, t, CH_3-CH_2-N).

Compound 10

6 (0.196 g, 0.13 mmol) was dissolved in dry CH_2Cl_2 (50 ml) and **2** (0.118 g, 0.37 mmol) was added, and the reaction mixture was stirred for 3 days at room temperature. The product was purified by column chromatography on silica gel using a 85:15 CH_2Cl_2—MeOH solvent system as eluent. Yield: 48 mg (18%).

MS (MALDI-TOF) $MW_{average}$=2082.5 Da $(M+Na)^+$, 2104.5 Da $(M-H+2Na)^+$. Calculated for $C_{94}H_{156}O_{35}N_8S_2F_2$ 2059.0.

^{1}H NMR (360 MHz, DMSO-d_6) δ 8.95 (1H, s, quinolone C*H*), 7.94 (1H, d, *J*=13.3, aromatic), 7.18 (1H, d, *J*=7.4, aromatic), 4.59 (4H, q, *J*=7.1, H_3C-CH_2-N), 4.02–4.06 (4H, m, -CH_2-NH-C=S), 3.27–3.71 (m, polymer -CH_2-CH_2-O-, piperazine), 1.42 (3H, t, CH_3-CH_2-N).

Biological assays

The efficacy of the prepared antimicrobials was determined with the broth microdilution method according to the NCCLS guideline.[19] Bacterial strains were grown on 5% bovine blood agar plates at 35 °C overnight. Appropriate numbers of colonies were suspended in physiological saline to reach the density of 0.5 McFarland for inoculation.

Stock solutions of different concentrations of the substances were prepared in either distilled water or H_2O and methanol (1:1) or H_2O and DMSO (1:1), respectively, depending on the solubility of the given preparation. These were twofold serially diluted from 256 to 0.5 µg ml^{-1} in cation-adjusted Mueller–Hinton broth, then 100 µl of each dilution was transferred into microplate holes. Inoculation was carried out with 10 µl of each bacterial suspension.

Table 1 MICs of quinolonecarboxylic acid derivatives (μmol l^{-1})

Test microorganismus	*MIC (μmol l^{-1})*					
	Ciprofloxacin hydrochloride 1	*Norfloxacin 2*	*Mono-ciprofloxacyl-PEG 7*	*Mono-norfloxacyl-PEG 8*	*Bis-ciprofloxacyl-PEG 9*	*Bis-norfloxacyl-PEG 10*
Staphylococcus aureus[a]	1.3	6.2	42.2	>166.4	7.5	>125.4
Staphylococcus aureus[b]	1.3	6.2	84.4	>166.4	7.5	>125.4
Staphylococcus aureus[c]	>696.3	>801.2	>168.9	>166.4	>120.3	>125.4
Staphylococcus haemolyticus[d]	43.5	400.6	>168.9	>166.4	>120.3	>125.4
Staphylococcus epidermidis[e]	1.3	3.1	84.4	>166.4	15.0	>125.4
Staphylococcus epidermidis[f]	>696.3	>801.2	>168.9	>166.4	>120.3	>125.4
Escherichia coli[g]	1.3	1.5	0.6	10.4	3.7	3.9
Pseudomonas aeruginosa[h]	1.3	1.5	10.5	>166.4	3.7	62.7
Klebsiella[i]	174.0	801.2	>168.9	>166.4	>120.3	>125.4
Bacillus subtilis[j]	1.3	1.5	2.6	20.8	1.8	15.6
Enterobacter cloacae[k]	1.3	1.5	2.6	41.6	1.8	31.3
Acinetobacter baumannii[l]	174.0	>801.2	>168.9	>166.4	>120.3	>125.4

[a]ATTC 29213 (methicillin susceptible).
[b]ATTC 33591 (methicillin resistant).
[c]13797 (methicillin, ciprofloxacin resistant).
[d]13654 (ciprofloxacin resistant).
[e]ATTC 25299 (methicillin susceptible).
[f]12333 (methicillin resistant, mecA gene positive).
[g]ATTC 25992.
[h]NCTC 10006.
[i]4660 (2005) (ESBL).
[j]ATCC 6633.
[k]11213 (2005).
[l]ATCC 6018.

Incubation was performed at 35 °C for 18 h and determination of the MIC was made with naked eyes on a mirror.

Solvents were also tested for inhibition of bacterial growth, and none of them exerted bacteriostatic effect at the concentration used.

ACKNOWLEDGEMENTS

This work was supported by the Hungarian Academy of Sciences and the National Scientific Research Found Grants no.: OTKA T042512, T046186, T046744 and RET-06/2004.

1 Bérubé, G. Natural and synthetic biologically active dimeric molecules: anticancer agents, anti-HIV agents, steroid derivatives and opioid antagonists. *Curr. Med. Chem.* **13,** 131–154 (2006).
2 Coppel, R., Deady, L., Loria, P., Olden, D. & Turnidge, J. Synthesis and antibacterial activity of some bisquinones. *Aust. J. Chem.* **49,** 255–259 (1996).
3 Kerns, R. J. *et al.* Piperazinyl-linked fluoroquinolone dimers possessing potent antibacterial activity against drug-resistant strains of *Staphylococcus aureus*. *Bioorg. Med. Chem. Lett.* **13,** 1745–1749 (2003).
4 Kerns, R. J. *et al.* Structural requirements of piperazinyl-linked fluoroquinolone dimers for activity against drug-resistant strains of *Staphylococcus aureus*. *Bioorg. Med. Chem. Lett.* **13,** 2109–2112 (2003).
5 Kerns, R. J., Rybak, M. J. & Cheung, C. M. Susceptibility studies of piperazinyl–cross-linked fluoroquinolone dimers against test strains of Gram-positive and Gram-negative bacteria. *Diagn. Microbiol. Infect. Dis.* **54,** 305–310 (2006).
6 Hershfield, M. S. Adenosine deaminiase deficiency: clinical expression, molecular basis, and therapy. *Semin. Hematol.* **35,** 291–298 (1998).
7 Kurtzberg, J. Asparaginase. in *Cancer Medicine.* 4th edn (eds Holland Jr J.F., Bast Jr R.C., Morton D.L., Frei III E., Kufe D.W., & Weichselbaum R.R.) 1027 (Lippinscott Williams and Wilkins, V.I, Section XVI, Chemotherapeutic Agents, Baltimore, MD, 1997).
8 Grace, M. *et al.* Structural and biologic characterization of pegylated recombinant *IFN*- alpha 2b. *IFN Cytokine Res.* **21,** 1103–1115 (2001).
9 Holmes, F. A. *et al.* Blinded, randomized, multicenter study to evaluate single administration pegfilgrastim once per cycle versus daily filgrastim as an adjunct to chemotherapy in patients with high-risk stage II or stage III/IV breast cancer. *J. Clin. Oncol.* **20,** 727–731 (2002).
10 Greenwald, R. B., Pendri, A. & Bolikal, D. Highly water soluble taxol derivatives: 7-polyethylene glycol carbamates and carbonates. *J. Org. Chem.* **60,** 331–336 (1995).
11 Bakker-Woudenberg, I. J. M., ten Kate, M. T., Guo, L., Working, P. & Mouton, J. W. Improved efficacy of ciprofloxacin administered in polyethylene glycol-coated liposomes for treatment of *Klebsiella pneumoniae* pneumonia in rats. *Antimicrob. Agents Chemother.* **45,** 1487–1492 (2001).
12 Bakker-Woudenberg, I. J. M., ten Kate, M. T., Guo, L., Working, P. & Mouton, J. W. Ciprofloxacin in polyethylene glycol-coated liposomes: efficacy in rat models of acute or chronic *Pseudomonas aeruginosa* infection. *Antimicrob. Agents Chemother.* **46,** 2575–2581 (2002).
13 Naoshima, Y., Nagao, K., Carraher, C. E., Zhao, A. & Siegmann-Louda, D. W. Bacterial activity of organotin polymers derived from ciprofloxacin, cephalexin, norfloxacin, and acyclovir. *Polym. Mater. Sci. Eng.* **90,** 534–536 (2004).
14 Dizman, A. & Mathias, L. J. Synthesis, characterization, and antibacterial activities of novel methacrylate polymers containing norfloxacin. *Biomacromolecules* **6,** 514–520 (2005).
15 Mongondry, P., Bonnans-Plaisance, C., Jean, M. & Tassin, J. F. Mild synthesis of amino-poly(ethylene glycol)s. application to steric stabilization of clays. *Macromol. Rapid Commun.* **24,** 681–685 (2003).
16 Dixon, N. E., Riddles, P. W., Gazzola, C., Blakeley, R. L. & Zerner, B. Jack bean urease (EC 3.5.1.5). V. On the mechanism of action of urease on urea, formamide, acetamide, *N*-methylurea, and related compounds. *Can. J. Biochem.* **58,** 1335–1344 (1980).
17 Clemens, A. L., Lee, B.-Y. & Horwitz, M. A. Purification, characterization, and genetic analysis of *Mycobacterium tuberculosis* urease, a potentially critical determinant of host- pathogen interaction. *J. Bacteriol.* **177,** 5644–5652 (1995).
18 Nagata, K., Satoh, H., Iwahi, T., Shimoyama, T. & Tamura, T. Potent inhibitory action of the gastric proton pump inhibitor lansoprazole against urease activity of *Helicobacter pylori*: unique action selective for *H.* pylori cells. *Antimicrob. Agents Chemother.* **37,** 769–774 (1993).
19 National Committee for Clinical Laboratory Standards. *Performance Standards for Antimicrobial Susceptibility Testing.* 12th Informational Supplement M100 – S12. (NCCLS, Wayne, PA, USA, 2002).

The Journal of Antibiotics (2009) 62, 117

www.nature.com/ja

ERRATUM

Modification of the antibiotic olivomycin I at the 2′-keto group of the side chain. Novel derivatives, antitumor and topoisomerase I-poisoning activity

Anna N Tevyashova, Eugenia N Zbarsky, Jan Balzarini, Alexander A Shtil, Lyubov G Dezhenkova, Vladimir M Bukhman, Victor B Zbarsky and Maria N Preobrazhenskaya

The Journal of Antibiotics (2009) **62,** 117; doi:10.1038/ja.2009.3

Correction to: *The Journal of Antibiotics* (2009) **62**, 37–41; doi:10.1038/ja.2008.7

Due to a typesetting error, the name of the second author in the above paper was published incorrectly. The correct name of this author is Eugenia N Olsufyeva.

Our typesetters would like to apologize for this mistake.